TVVR 12/5001
ISSN-1101-9824

Modeling Wave, Currents, and Sediment Transport in Ystad Bay

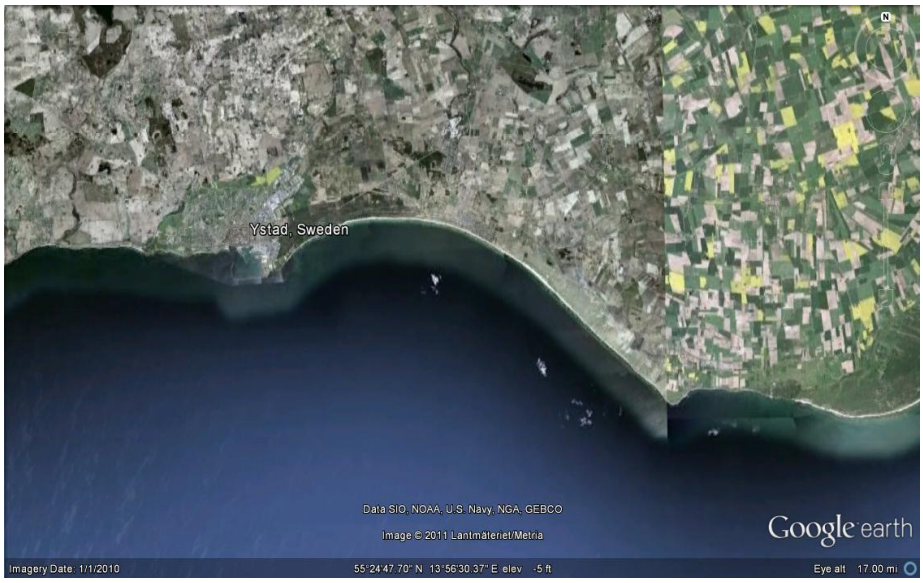

Sediment transport patterns and their implications for topographic change in the Ystad Bay

Seyed Abbas Hosseini Sadabadi

Division of Water Resources Engineering
Lund University, 2011

TVVR 12/5001
ISSN-1101-9824

Modeling Wave, Currents, and Sediment Transport in Ystad Bay

Sediment transport patterns and their implications for topographic change in the Ystad Bay

Key Words: Ystad Bay, EBED Model, SWAN, Modelling Wave, Sediment Transport

SEYED ABBAS HOSSEINI SADABADI

Dedicated to My Parents

16/02/2012

Lund, Sweden

Acknowledgments

This thesis project would not have been possible without the support of many people. I hereby wish to express my gratitude to my supervisor, Prof. Magnus Larson who was abundantly helpful and offered invaluable assistance, support and guidance. Special thanks also to Dr. Pham Thanh Nam for the great assistance with the application of the EBED-modified model. I would also like to convey special thanks to the Faculty of Hydraulics Engineering, Delft University, Holland, particularly professor Rosh Ranasinghe and doctoral students, Matthieu de Schipper and Sierd Devries for helping me through the SWAN application. I also appreciate Professor Hans Hanson's helpful comments during my thesis. My thanks go to Åforsk Company for financial support during my visit to the Delft University, the Netherlands and finally I would like to thank the Department of Water Resources Engineering at Lund University for providing me with the 24 hour access to the computer lab.

Seyed Abbas Hosseini Sadabadi

Abstract

Coastal areas around the world are being shaped by many natural phenomena, as well as by man-induced activities. Hydrodynamic phenomena such as wind-generated waves, extreme storms and seasonal tides cause a continued change in topography and the natural sediment formation in the nearshore zone as a result of erosion and accumulation. Therefore, the nature of the nearshore zone and its protection through different structures and activities is of great importance for coastal engineers and project managers.

In the recent decades, numerical modelling has been an engineering tool for the simulation of waves and sediment transport in coastal waters and bays. Nowadays, there are a number of developed models in terms of simulating nearshore hydrodynamics and sediment transport. The results of these models in practical applications have been validated and shown to be in good agreement with observations. However, due to the complexity of morphological phenomena in coastal waters, especially in the nearshore regions, these models usually deal with some specific processes and are limited by time and space scales.

The main objective of this study is employ two advanced numerical models, SWAN and EBED (modified) model to determine the sediment transport patterns and their implications for topographic changes due to waves and currents in the Ystad Bay, Skåne, Sweden. This work was performed with emphasis on different time scales and various types of wave conditions.

In order to derive a sediment pattern for the Ystad Bay, a preliminary study of the background data for the Ystad Bay was performed. The SWAN and the EBED-modified model were numerically implemented to calculate the wave field in the bay for the wave conditions from 2004 to 2010 for both extreme situations and for long-term representative conditions, and the simulation results were illustrated afterwards. Furthermore, the EBED-modified model was applied to derive two-dimensional current fields. A numerical model developed by Nam (2010) was subsequently implemented to calculate the sediment transport with focus on longshore transport.

The simulation results from the application of the numerical models show that waves from south and southwest, which have the long fetches for Ystad Bay, will cause erosion in the western parts of the bay and accretion along the lower southeastern part of the bay. These results are in a good agreement with observations. However, the sediment transport model should be improved to include cross-shore transport in the future.

Contents

1 Introduction

1.1 Background

Coastal areas are variously faced with wide range of hydrodynamic processes such as wind-induced waves, currents, and tides. Coastal structures, including breakwaters, sea walls and beach nourishments (a soft structure), also have significant influences on the natural sediment balance in the nearshore zones. The hydrodynamic conditions together with the coastal structures change the sediment balance and the beach topography resulting in erosion and accretion within the beach area. Applying numerical models in order to understand and predict the beach evolution is highly useful and helpful in achieving an evolution that is desirable with regard to human activities at the coast.

Figure 1. Sediment formation around Grevelingen dam, the Netherlands (Deltawerken, 2010)

Coastal engineering mainly deals with different hydrodynamic and sediment transport processes occurring in the coastal areas, including the nearshore, estuarine, marine, and shoreline areas. Problems arising in these areas could be either natural or human-induced. In the recent decades coastal engineering has helped man to develop numerical models in terms of wave generation and sediment transport patterns as well as assisting engineers to design coastal structures such as harbors and breakwaters. In addition, coastal engineering has provided various solutions for many coastal problems such as sediment transport, shore protection, and flooding.

Numerical models are one of the useful instruments of coastal engineering in terms of simulation and analysis beach topography change. Over the years, researchers have been developing these models to be applied in different coastal engineering projects, for example the estimation of topography change in nearshore. The results of these models are often satisfactory and in approximate agreement with data, although more validation is needed. Their application is often economically beneficial compared to laboratory experiments.

There are several numerical models for simulating topography change caused by different phenomena in coastal areas. Shoreline evolution models mainly deal with the changes in shoreline evolution, (*e.g.* Pelnard-Considere, 1956; Hanson & Kraus, 1989; Steetzel *et al.*, 2000), whereas cross-shore evolution models only calculate the sediment transport patterns in cross-shore direction (Larson & Kraus, 1989; Larson *et al*., 1989; Nairn & Southgate, 1993). Moreover, 3D morphological models account for the impact of vertical and horizontal movements of waves and currents, as well as including different types of phenomena important for the hydrodynamics, for example temperature gradients, wave forces, stratification, and flooding (Roelvink & Banning 1994; Lesser et al., 2004).

1.2 Objectives

The main objective of this study is to determine the sediment transport patterns and their implications for topographic change in the Ystad Bay, Skåne, Sweden at different time scales and for various types of wave conditions using advanced numerical models of waves, currents, and sediment transport.

1.3 Procedure

First of all, a review and preliminary analysis of the background data including geographic, morphological evolution and hydrodynamic conditions of Ystad Bay are described (Section 2). In section 3, the basic theories on the SWAN model and the EBED-modified model (Nam *et al.*, 2009) are presented and the two models are implemented for Ystad Bay to develop the wave field in the bay for different offshore wave conditions derived by Street (2011), either for extreme situations or for long-term representative conditions. Furthermore, the simulation results from the two models are also shown and a general analysis and analogy of the results from these two different models is performed in section 3. In section 4, the calculated waves from EBED-modified model will be used to derive a two-dimensional current model (Nam *et al.* 2009) and the simulation results are presented. In section 5, from the wave and current field, the near-shore sediment transport is computed (Nam *et al.* 2009). Finally in the last section, the sediment transport field will be employed to derive transport gradients and resulting topographic changes. These calculated changes will be qualitatively compared to observed changes.

2 Ystad Bay Study Area

2.1 Geographic and Geological Characteristics

Ystad Bay is located in the southern part of Sweden called Skåne (Figure 2). On the western part of Ystad Bay, the Ystad City is positioned and it is the largest coastal city on the Swedish Southern coast (figure 3). The Ystad coast includes different towns and it also has one of the main Swedish tourist beaches with substantial economical benefits for Sweden's tourist industry. In general, the coastal areas surrounding Sweden mainly consist of rocky shorelines (Bird, 1985; Bird & Schwartz 1985). In the southern part of Sweden, the county of Skåne where Ystad is located, and also part of the Hallands County (Lindh *et al.*, 1970; Rydell *et al.*, 2004), the coastal areas are largely covered by sand (Figure 4). In these areas the grain size varies from the very fine sand to boulder. Beach geological studies indicate that most of the beach material is the result of glacial deposits (Larson & Hanson, 2010) (Figure 4). This material is formed with poorly sorted soil and contains a high percentage of sand. However, there is also a fluvio-glacial deposit along the southern coast with a well sorted structure (Larson & Hanson, 2010).

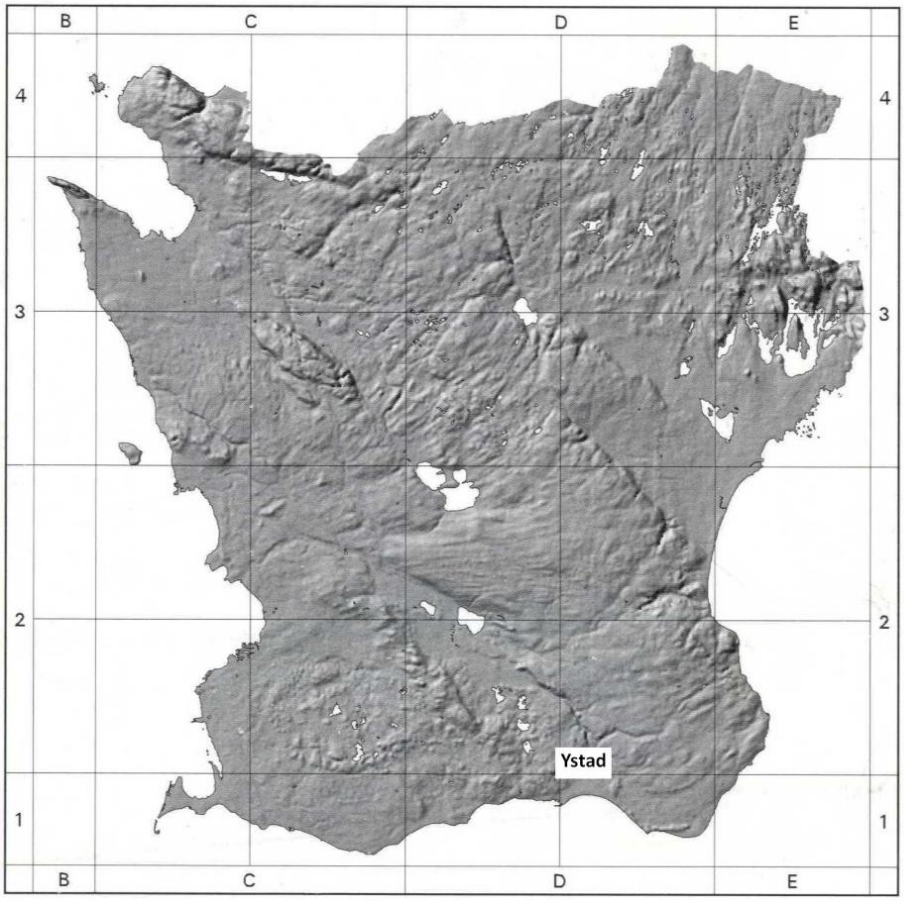

Figure 2. The map of Southern part of Sweden, Skåne, SGU series No. 55

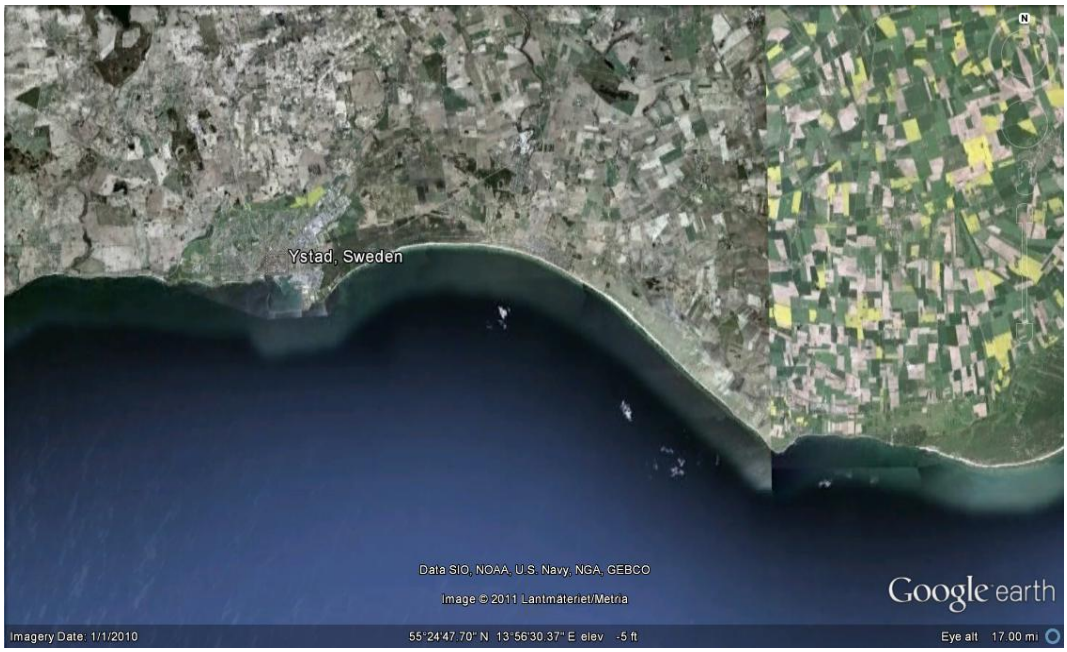

Figure 3. The Ystad Bay and Ystad City,

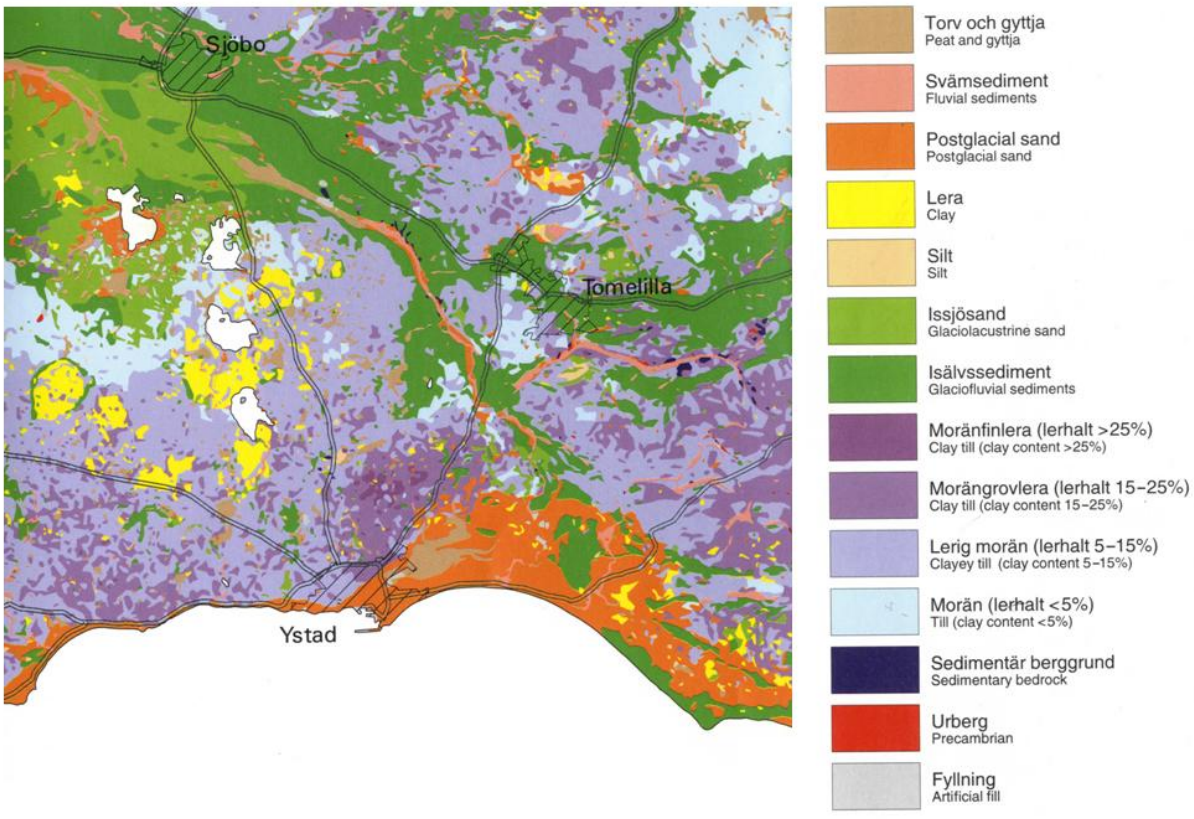

Figure 4. Quaternary deposits of Skåne, Scale 1:250 000, SGU series No. 55

2.2 The Hydrodynamic Conditions in Ystad Bay

2.2.1 Wind and Water Level

In order to investigate the sediment transport pattern and calculate the wave generation in the nearshore, the hydrodynamic conditions of Ystad Bay have to be studied. A recent investigations by Hanson & Larson, (2010) revealed that the main causes of water level variations in Ystad are the wind distribution at the water surface over the the Baltic Sea and the air pressure variation. These factors induce water level variations by moving the water mass in the Baltic Sea, which may be hydrodynamically characterized as an enclosed basin. The investigation of water level and wind direction demonstrated that high water levels are due to northerly winds in the direction of N to NE when the water is transported towards Skåne, the southern parts of the Baltic Sea, whereas winds generated from SW to W lead to low water levels in Skåne (Figure 5). For a more long-term analysis, the annual water level variation in Ystad has been determined from a time series of data from 1887 to 1986 (figure 6). By fitting a linear trend line to the measured data the annual increase rate of the mean water level for Ystad was calculated to be 0.55 mm/year (Hanson & Larson, 2010). Meier *et al.* (2004) investigated future annual average water levels based on different scenarios, which gave the following results: At the present wind speeds, the winter is expected to have the most changes in water level. Three parameters result in the changes: glacial rebound (-0.05mm/year in Ystad), the wind regime variation as well as the global sea level change depending on the applied model and scenario. Therefore, the simulation for a 100 year prediction indicates two scenarios. The first scenario for the best case (HB2) shows a reduction rate of 0.05 m, while the second scenario for the worst case (EA2) results in an increase by 0.85 m. However, the mean scenario results show an increase rate of 0.38 m for the water level by 2100 (Hanson & Larson, 2010). The analysis of gale and storm winds with regard to water level variation showed that the strong storms are not essentially the cause of higher water levels (because of the directional properties). Statistics showed that the water level variation is between -110 cm and +80 cm for the gale winds while for storms it varies between -40 cm and +40 cm.

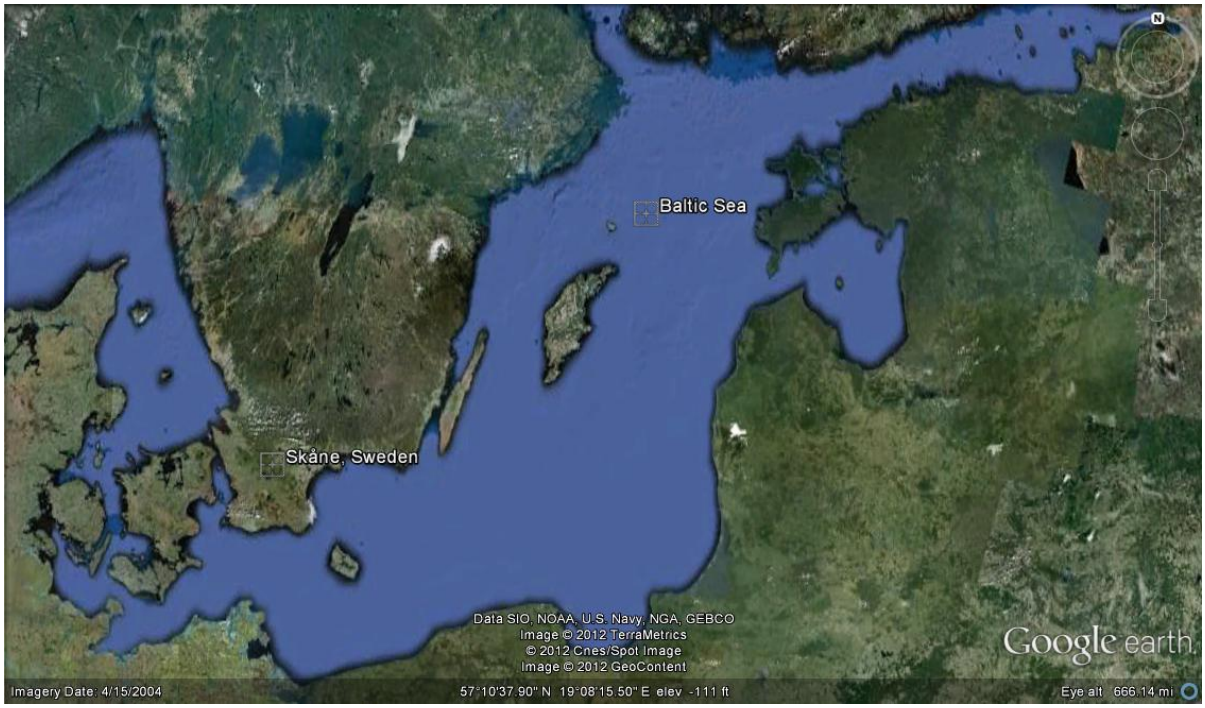

Figure 5. Baltic Sea region and Skåne

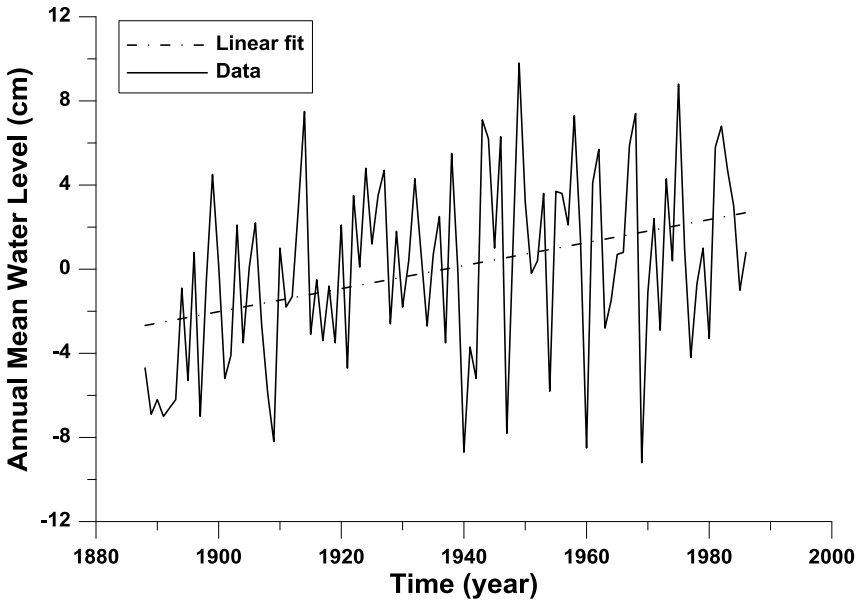

Figure 6. Annual mean water level in Ystad (1887-1986)

2.2.2 Wave Heights

The highest significant wave height in the Baltic Sea was recorded as 7.7 m (Street, 2011) at Åland on December 22nd 2004 (SMHI, 2010). However, the occurrence of high values of wave height is not common and is exception due to the hydrodynamic nature of Baltic Sea as an enclosed basin (Street, 2011) The wave conditions in the Baltic Sea where Ystad is located, is generally fetch-limited in the nearshore. The mean significant wave height for South Swedish coast was calculated as 0.4 m and the maximum of wave height was computed as 4.5 m based on a 16-year time series (Larson & Hanson, 1992). This investigation also showed that 95% of the waves consisted of significant wave heights below 2 m. Dahlerus & Egermeyer (2005) also came up with same results and their study indicated that waves with larger height travel towards the eastern side of Skåne, where the fetch length is longer, whereas the opposite is true for the western side with a milder wave climate and a shorter fetch length (Larson & Hanson, 2010) (see Figure 7).

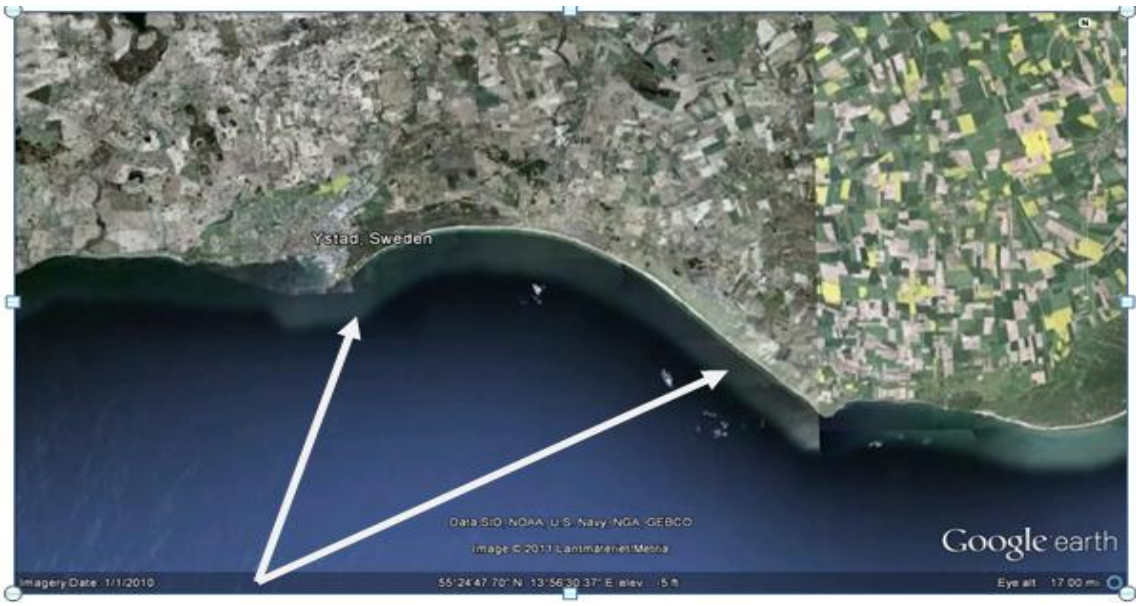

Figure 7. Westerly and Easterly waves with different fetch lengths

2.3 Sediment Transport Processes

A study was performed by Larson & Hanson (1992) based on the calculated transport gradients to determine the general pattern for sediment transport in the Ystad Bay and assess where erosion and accretion could take place inside the bay. This study indicates that significant erosion occurs in the western part of the bay and this is supported by observations (Larson & Hanson, 2010) . Shoreline data from the 1850's until present point out the fact that in the southern part of the bay there is no notable change and is totally stable, whereas in the western part of the bay there is constant erosion occurring (Larson & Hanson, 2010).

The investigation by Larson & Hanson (2010) was in agreement with the observed measurements and it showed that most of the erosion should take place in the western part of Ystad Bay, whereas the middle bay remains more and less stable, and eastern part of the bay remains stable with a slight accumulation without any significant changes in sediment transport. The calculation results also revealed that the sediment transport direction in the eastern part of the bay is towards the west, whereas the opposite is true in the western part of the bay (Larson & Hanson, 2010). This implies a zero transport in the centre of the bay at around 8 kilometers from the east of the bay close to the mouth of Kabusa River (Point A, Figure 8). This study also suggested that there is a point in which no shoreline changes occur and it is located about three kilometers toward east (Point B, Figure 8). Therefore, at a large scale erosion takes place at Y<3 km and accretion is expected to occur at Y>3 km (Figure 9).

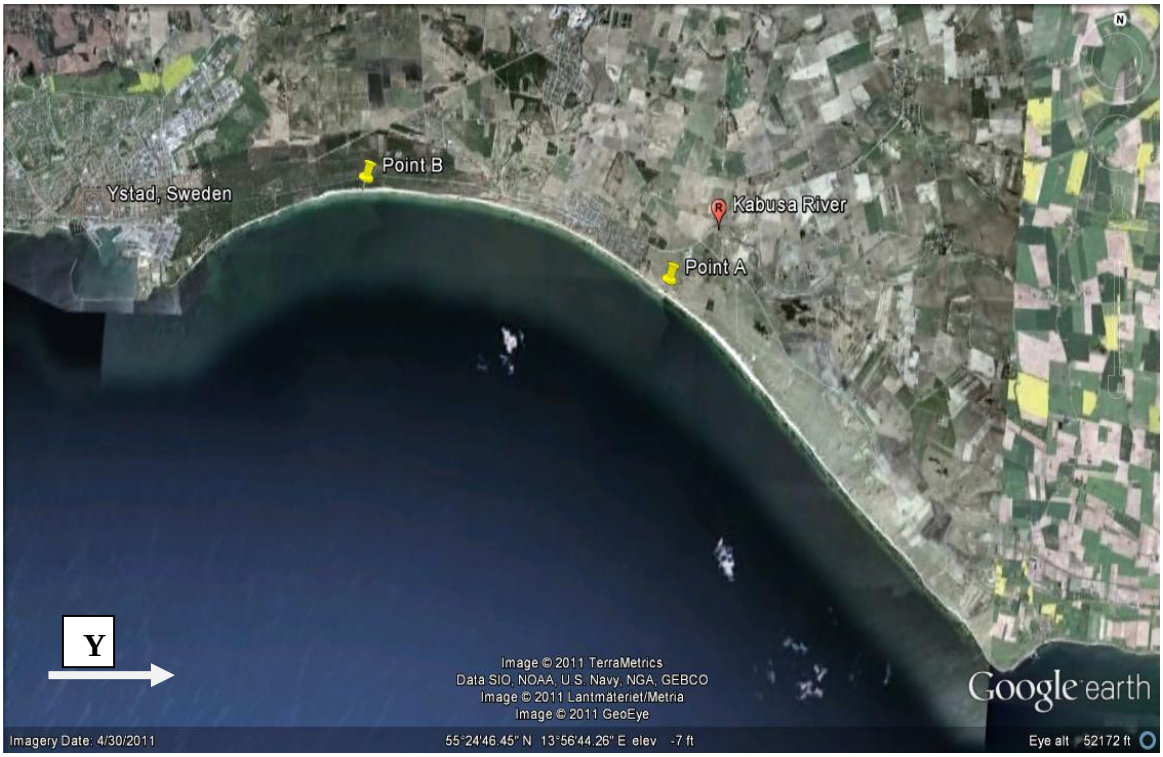

Figure 8. Point A with zero transport, point B with no shoreline changes

Figure 9. Erosion and Accumulation occurrence within the Ystad Bay

2.4 Beach change and Engineering Measures

The city of Ystad in Skåne has been exposed to extreme coastal erosion for over 150 years. The main causes of erosion in this area are the wind-generated waves from the Baltic Sea resulting in high runup and erosion of the sand dunes on the beach (Hanson & Larson, 2010). The material mobilized in this manner is then transport alongshore and deposited depending on the longshore transport gradients. Figure 10 shows the beach of Ystad after severe dune erosion due to the waves and high water levels. It has been investigated that a rising sea level will result in a 25% increase of the dune erosion by 2100 for the mean SLR scenario (+38 cm) and 75% for the extreme scenario (+85 cm) (Larson & Hanson, 2010). Therefore, it is predicted that shoreline would keep experiencing erosion in the western part and accumulation in the eastern bay.

Figure 10. Dune erosion in Ystad Bay due to waves and high water levels (Photo by Hans Hanson)

Ystad Bay is a clear example of a crescentic bay with regards to sand transport and erosion/depositional patterns (Larson & Hanson, 2010). As a measure to stop the erosion in the 1950's a large number of small groins were constructed in Ystad, but that measure was not successful. Therefore, in the 1960's, four larger groins were built for better stabilization (Figure 11). In addition, some seawalls were also built along some stretches of shoreline in Ystad Bay as an instant solution to prevent shoreline retreat (Figure 12).

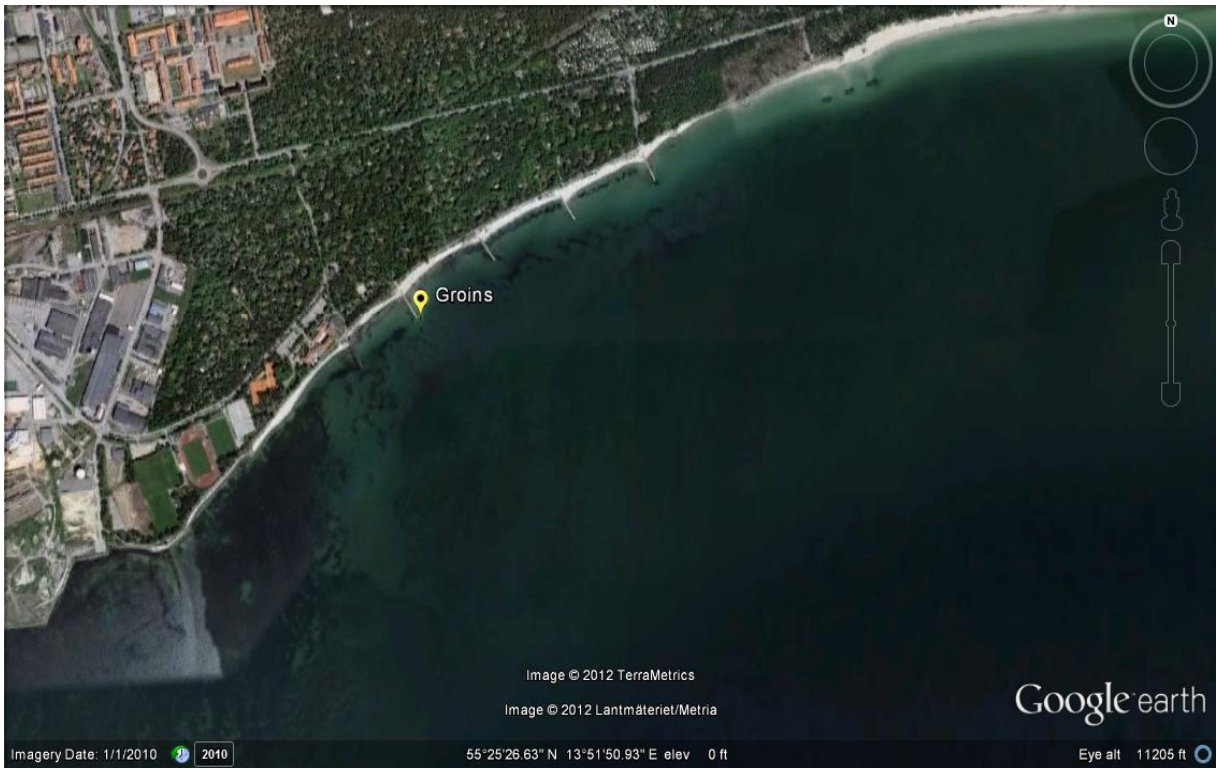

Figure 11. Groins as a solution to erosion in Ystad

Figure 12. Beach protection in Ystad, Seawalls (Photo by Hans Hanson year???)

3 Wave Modelling

3.1 The SWAN Wave Model

3.1.1 Background and Theory

The SWAN (Simulating Wave Nearshore) wave model is a free, open source, third-generation wave model that is used for research and engineering purposes worldwide (Booij *et al.*, 1999). SWAN has been coded and developed by Delft university of Technology in the Netherlands. The theories applied in the SWAN model are mainly described in the book "Waves in Oceanic and Coastal Waters" (Holthuijsen, 2010) based on different wave generation theories. Due to the SWAN's ability to calculate the wave-current interactions, the spectral action balance equation is employed as the basic equation in the model theory (Holthuijsen, 2010). The model is formulated both in Cartesian coordinate and additionally in spherical coordinate to cover small and large-scale calculations. SWAN has the compatibility to run from a full time-dependent two-dimensional scenario to the simplest one with one dimension and stationary mode. The SWAN also accounts for different hydrodynamic phenomena including bottom and current-induced shoaling, as well as calculating the refraction against coastal structures, but diffraction is very approximately calculated by SWAN (Holthuijsen, 2010) .

3.1.2 The Action Balance Equation

In SWAN the energy balance equation is substituted with the action balance equation. Also the relative radian frequency σ, has been selected instead of the absolute radian frequency ω, for further processes inside the model. Therefore, the conversion of the energy balance equation to the action balance equation in Cartesian –coordinate is presented as:

$$\frac{\partial N(\sigma,\theta;x,y,t)}{\partial t}+\frac{\partial c_{g,x}N(\sigma,\theta;x,y,t)}{\partial x}+\frac{\partial c_{g,y}N(\sigma,\theta;x,y,t)}{\partial y}+\frac{\partial c_{\theta}N(\sigma,\theta;x,y,t)}{\partial \theta}+\frac{\partial c_{\sigma}N(\sigma,\theta;x,y,t)}{\partial \sigma}=\frac{S(\sigma,\theta;x,y,t)}{\sigma} \quad (1)$$

In the absence of currents Eq. (2) is turned to:

$$\frac{\partial E(\sigma,\theta;x,y,t)}{\partial t}+\frac{\partial E(\sigma,\theta;x,y,t)}{\partial x}+\frac{\partial c_{g,y}E(\sigma,\theta;x,y,t)}{\partial y}+\frac{\partial c_{\theta}E(\sigma,\theta;x,y,t)}{\partial \theta}=S(\omega,\theta;x,y,t) \quad (2)$$

Where $N(\sigma,\theta)$ is defined as the action density spectrum, and $E(\sigma,\theta)$ is defined as the energy density spectrum. In Eq. (1) and Eq. (2), the left terms represent the changes of the energy (or action) density spectrum both in time (t) and location (x and y) (Holthuijsen, 2010).

Equation (2) is the main expression for wave generation and propagation in SWAN and it contains several source and sink terms as described in the following.

3.1.3 Source Terms

3.1.3.1 Generation By Wind

In the SWAN model the wind speed is the friction velocity u_* , which is the conversion of 10 meter speed velocity U_{10} , where:

$$u_* = C_D \times U_{10}^{\ 2} \tag{3}$$

In which C_D is the wind-drag coefficient:

$$\begin{cases} 1.287\times10^{-3} & for \quad U_{10} < 7.5 \text{ m/s} \\ (0.8+0.65U_{10})\times10^{-3} & for \quad U_{10} \geq 7.5 \text{ m/s} \end{cases} \tag{4}$$

The wind-generated waves in SWAN are determined by the theory of Miles together with initial wave growth (Holthuijsen, 2010).

$$S_{in}(\sigma,\theta) = \alpha + \beta . E(\sigma,\theta) \tag{5}$$

Where $S_{in}(\sigma,\theta)$ is the spectral density, θ is the space direction and α is the initial wave growth calculated from the experimental expression of Cavaleri & Malanotte-Rizzoli (1981)

$$\alpha = \begin{cases} \frac{1.5\times10^{-3}}{g^2.2\pi}\left[u_* \cos(\theta-\theta_{wind})\right]^4 .G & for \left|\theta-\theta_{wind}\right| \leq 90^\circ \\ 0 & for \left|\theta-\theta_{wind}\right| > 90^\circ \end{cases} \tag{6}$$

And G is:

$$G = \exp\left[-(\sigma/\sigma_{PM}^{\ *})^{-4}\right] \tag{7}$$

and

$$\sigma_{PM}^{\ *} = 2\pi\frac{0.13g}{28u_*} \tag{8}$$

Where θ_{wind} is the wind direction, θ is the acceleration due to gravity and $\sigma_{PM}^{\ *}$ is defined as the peak frequency of the Pierson & Moskowitz (1964) spectrum (Holthuijsen, 2010).

β is derived from Komen *et al.*, (1994) as:

$$\beta = \max\left\{0, \gamma.\sigma\frac{\rho_{air}}{\rho_{water}}\left(\frac{u_*}{c}\right)^2.\cos^2\left(\theta-\theta_{wind}\right)\right\} \quad (9)$$

Where c is the phase velocity, σ is the relative frequency, ρ_{air} is the density of air, and ρ_{water} is the water density.

γ owing to Janssen (1991) is calculated as:

$$\gamma = \frac{1.2}{k^2}\lambda.\ln^4\lambda \quad (10)$$

Where

$$\lambda = \frac{g.z_e}{c^2}\exp\left[kc/\left|u_*.\cos(\theta-\theta_{wind})\right|\right] \qquad for\ \lambda \le 1 \quad (11)$$

and

$$\beta = 0 \qquad for\ \lambda > 1 \quad (12)$$

k is the von Karman constant taken as 0.41, and z_e is defined as the effective surface roughness (Holthuijsen, 2010)

3.1.4 Sink Terms (dissipation)

Energy dissipation is a sink term in SWAN and it is determined by white-capping, $S_{wc}(\sigma,\theta)$, bottom friction $S_{bfr}(\sigma,\theta)$, and depth-induced breaking $S_{surf}(\sigma,\theta)$.

3.1.4.1 White-Capping

The dissipative impact of white-capping $S_{wc}(\sigma,\theta)$ on the coastal waves is not that substantial and is considered as sink term in the energy balance equation. White-capping presented in SWAN is from Hasselmann (1974) in which the white-capping is expressed as a pressure pulse acting on the sea-water surface (Holthuijsen, 2010).

3.1.4.2 Bottom Friction

Bottom friction $S_{bfr}(\sigma,\theta)$, is another sink term in the wave energy balance and it is more likely to occur in sandy coastal bottoms. In SWAN bottom friction is represented as:

$$S_{bfr}(\sigma,\theta) = -\frac{C_{bfr}}{g}\left[\frac{\sigma}{\sin(kd)}\right]^2 E(\sigma,\theta)u_{rms,bottom} \qquad (13)$$

Where C_{bfr}, is the bottom friction coefficient, d is the water depth and $u_{rms,bottom}$ stands for "the root-mean-square orbital bottom velocity" (Holthuijsen, 2010). For the JONSWAP spectrum model, applied in this study, C_{bfr} is defined as:

$$C_{bfr,JONSWAP} = \begin{cases} 0.038/u_{rms,bottom} & for \quad \text{swell} \\ 0.067/u_{rms,bottom} & for \quad \text{wind sea} \end{cases} \qquad (14)$$

3.1.4.3 Depth -induced breaking

In SWAN model the total dissipation by depth-induced wave breaking (surf breaking) could be simulated with the dissipation of a bore concerning the breaking waves in a random case in shallow water (Battjes & Janssen, 1978). On this occasion the mean zero-crossing frequency $\overline{f_0}$, is substituted with $\overline{f} = m_1/m_0$ where m_0 and m_1 are the zeroth and the first moments of the variance density spectrum $E(f)$, respectively. The maximum potential wave height is calculated as $H_{max} = \gamma D$ in which D is the total water depth and γ is defined as the breaker parameter (Holthuijsen, 2010).

3.2 SWAN Model Implementation for Ystad Bay

SWAN version 40.81 for windows has been used for the wave generation and propagation within the Ystad Bay. This version is freely available at the SWAN homepage[1]. In order to implement the model, some input values have been modified in the SWAN input file for the Ystad Bay case. The SWAN input file is a data file with .swn extension that includes some initial terms as well as some variable parameters such as: project name, input values for water density, water level, wave spectrum, wave parameters, bathymetry. For Ystad Bay these values have been modified as described below.

3.2.1 Model setup and input

The density of water has been set equal to $\rho_{water} = 1008 kg/m^3$. For the wave spectrum, JONSWAP spectrum has been used for a stationary run. The requested output parameters including significant wave height and the wave directions will be created by SWAN as output request. The bathymetry file for Ystad is a 240×360 resolution data file. The direction of 'X' axis is defined positive from deep water (offshore) towards shallow water (shoreline). There are 240 grid points in X direction with the total length of 2050m and the mesh size of 50m, and the 'Y'axis has been defined positive in the Eastern direction alongshore and consists of 360 grid points with the total length of 36000m and the mesh size of 100m (Figure 13).

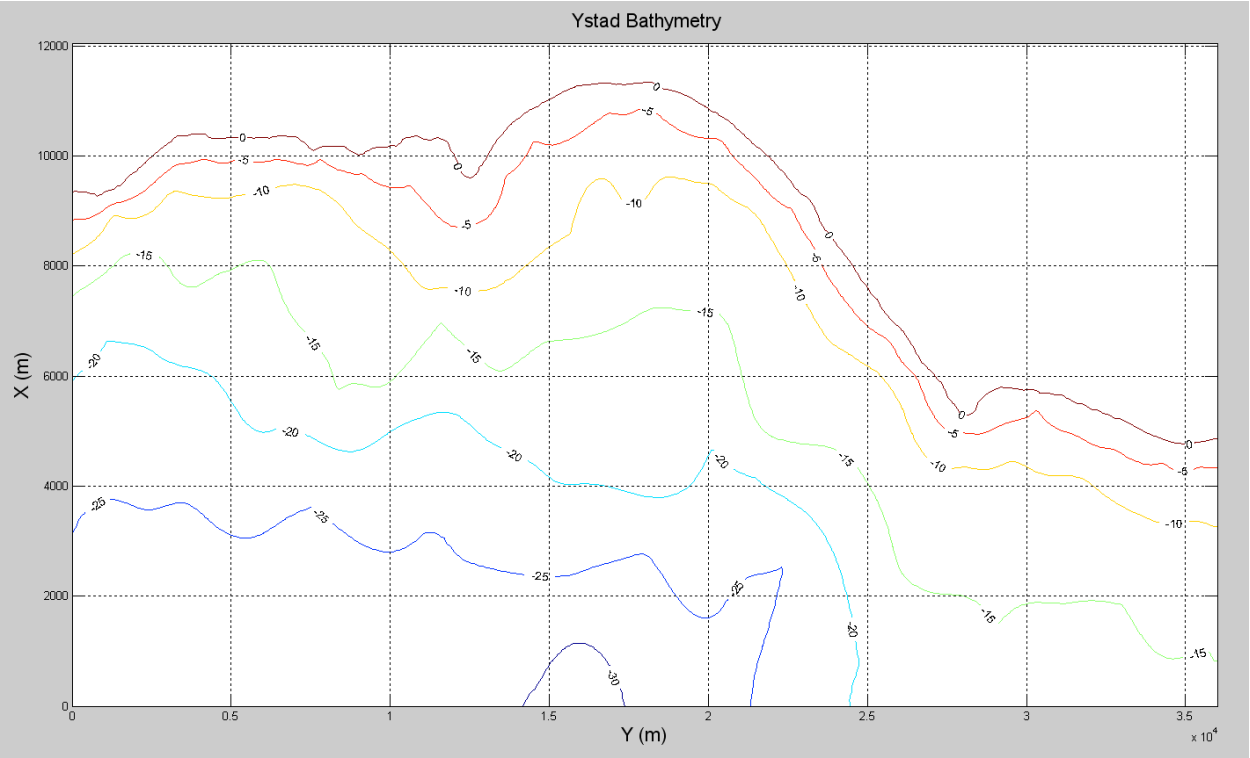

Figure 13. Ystad bottom change (bathymetry)

[1] SWAN homepage (http://swanmodel.sourceforge.net/download/info.htm)

Figure 14 shows a three-dimensional image of the bottom elevation based on the input bathymetry file.

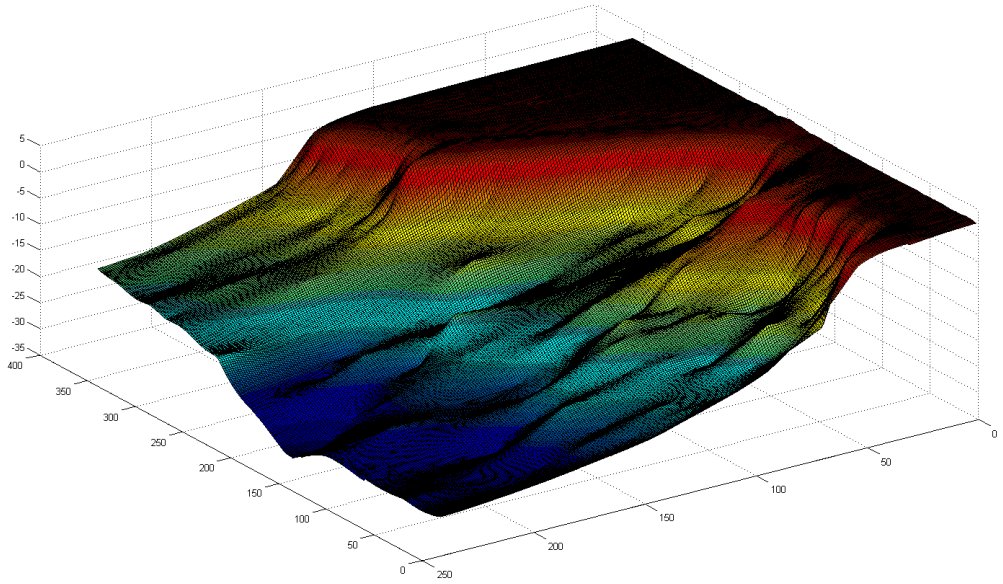

Figure 14. Three-dimensional shape of bottom bathymetry in Ystad Bay

Shoaling effect will take place at abrupt changes of the bathymetry (a bump or a sand bar) and can be simulated in SWAN. With SWAN one calculates the propagation of wave energy. When going from offshore to nearshore (deep to shallow), wave energy dissipation will occur due to white capping, bottom friction and wave breaking. This leads to a decrease of wave energy, thus decrease of wave height. When there is a net component of wind blowing in the nearshore direction, the process wind growth will lead to an increase of wave energy (thus wave height). And due to waves propagating towards the shallow waters shoaling will occur (increasing wave height (not wave energy)). Although depending on the conditions, usually the depth-induced breaking of the waves is the most dominant process and therefore the waves (slightly) decrease when propagating towards the coast. Most of the dissipation will occur when approaching the depth contours 0~4m and the wave height decreases to zero.

The boundaries for the computational grid in SWAN model are defined either as land or water. The land boundary will absorb all the wave energy and does not cause any problem in terms of wave generation, whereas the water boundary simulation may be problematic in some cases. Along the lateral water boundaries there is often lack of information for the wave conditions for the lateral water boundaries, therefore, SWAN assumes that there is no wave entering the computational grids and other waves can leave the computation area freely. The spectral densities are assumed to be zero along the lateral boundaries (Holthuijsen, 2010). This assumption may cause errors in the calculation of the wave propagation and therefore the

results near the water boundaries are often unrealistic. In order to solve this problem in the application of SWAN model, the water boundaries should be selected far enough away from the area of interest. In the Ystad case the wave condition is only known at deep water in the south whereas there is no information about wave conditions for the west boundary, therefore, a large enough bathymetry for Ystad Bay (Figure 13) has been selected to cover the entire area of calculation and prevent errors in the area of interest.

3.2.2 Simulation Cases

The wave conditions in the Ystad Bay have been determined by a previous study by Street (2011). The WAM model was run for the entire Baltic Sea to hindcast the wave climate in the Baltic region, and the results from the Ystad station, including significant wave height H_s, significant wave period T_s, and the mean wave direction $\bar{\theta}$, have been utilized in the simulations here. According to Street (2011), there are 17535 waves in the simulation period with different periods, directions, and significant height at Ystad station, whereas only 12807 waves travel towards Ystad Bay (Table 1 and Table 2). Wave directions in SWAN are defined positive counterclockwise from the Y axis.

In order to save computational time, all waves travelling towards Ystad are classified according to their directions into eighteen scenarios with ten-degree interval (Figure 15). For each scenario there is a different number of waves. The percentage of total waves for every single scenario is indicated in table 2. Table 1 and table 2 illustrate that the highest percentage of waves travel at directions between 30^0 - 40^0 from the Y axis, whereas the lowest percentage of waves travel at directions between 150^0 – 160^0.

Table 1. Wave conditions for every scenario for Ystad Bay

Scenario	*Total waves*	*Degree-Interval*	*Percentage*	*T_s (Average) (Second)*	*ϴ (Average) (degree)*	*H_s (average) (m)*
1	371	170-18	2.91	5.14	174.91	0.93
2	366	160-170	2.89	4.76	165.77	0.88
3	336	150-160	2.62	4.47	155.75	0.86
4	377	140-150	2.94	4.57	145.71	0.91
5	437	130-140	3.41	4.39	135.53	0.89
6	523	120-130	4.10	4.46	125.64	0.99
7	643	110-120	5.02	4.30	115.39	0.92
8	889	100-110	6.94	4.35	105.3	0.99
9	845	90-100	6.60	4.44	95.38	0.99
10	495	80-90	3.87	4.52	84.994	0.98
11	534	70-80	4.17	4.53	74.287	0.98
12	724	60-70	5.65	4.75	64.34	1.08
13	1006	50-60	7.86	4.88	54.29	1.11
14	1350	40-50	10.54	5.16	43.87	1.18
15	1548	30-40	12.09	5.43	34.71	1.23
16	1031	20-30	8.05	5.28	24.68	1.19
17	825	10-20	6.44	5.12	15	1.19
18	500	0-10	3.90	4.62	5.42	1.09

Table 2. Pie chart over wave percentage for each scenario

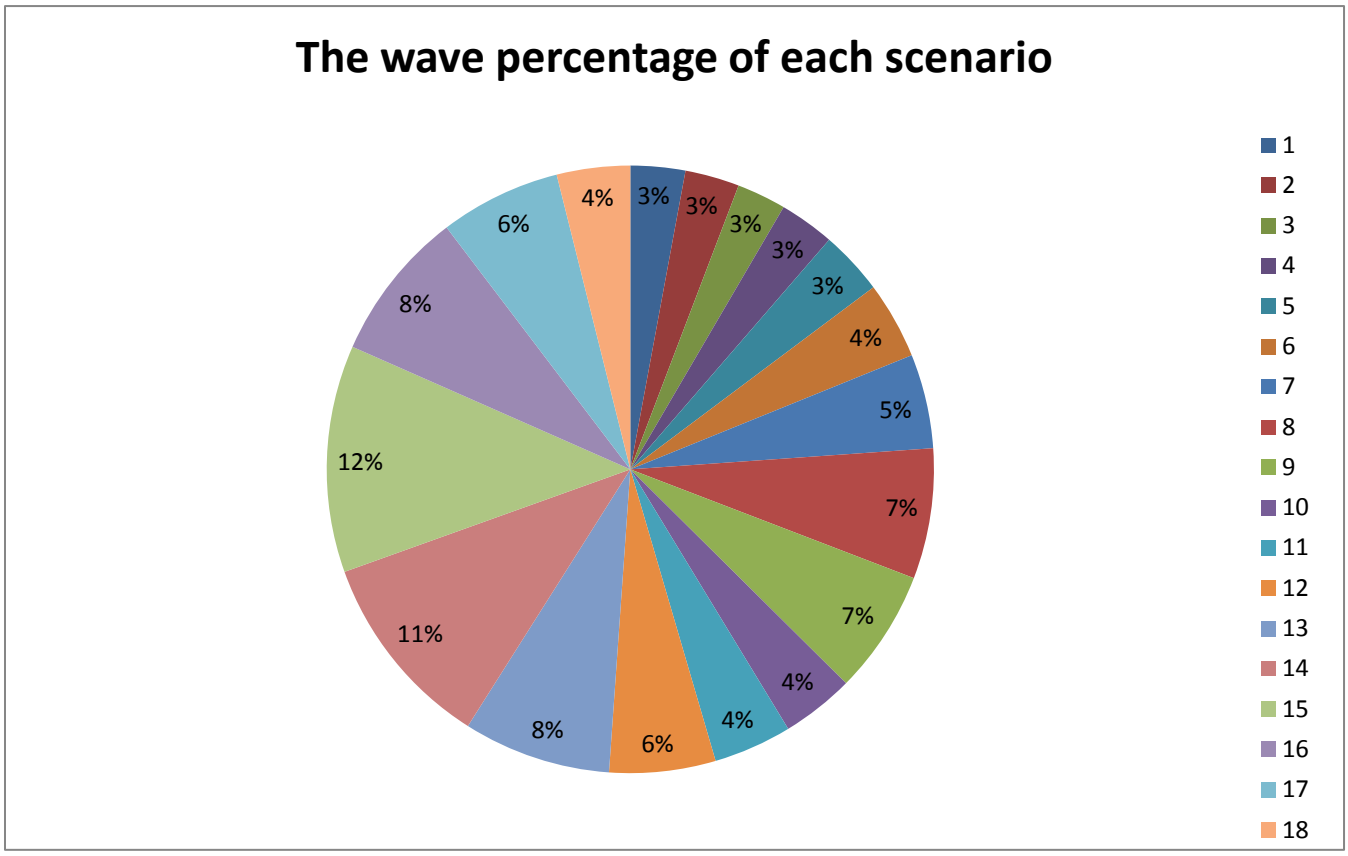

Figure 15. Wave directions offshore Ystad

After the wave classification, the mean value of the wave periods (Ts), the average of significant height (H_s) as well as the wave direction (θ), have been calculated for each scenario with different number of waves (see Table 1).

With regard to the longshore sediment transport, which is assumed to dominate coastal change in Ystad Bay over longer periods of time, the wave height is often taken to be proportional to wave height raised to the power of 2.5. Therefore, in order to obtain more representative results, for the modification of significant wave height (H_s) in SWAN model, the wave height H_{snew} was introduced and calculated as:

$$H_{snew} = \frac{1}{n}\sum_{i=1}^{n}(H_{si}{}^{2.5})^{\frac{1}{2.5}} \qquad (15)$$

Where the new wave height H_{snew}, used as input in SWAN, n is the total number of waves in each scenario and H_{si} is the significant wave height for every single wave (Table 3).

Table 3. The calculated values on Hsnew for every scenario

Scenario	*ϴ (Average) (degree)*	*Compass Directions*	*The average of H_s (m)*	*H_{snew} (m)*
1	174.91	W	0.93	1.06
2	165.77	W	0.88	1.01
3	155.75	NW	0.86	1.00
4	145.71	NW	0.91	1.07
5	135.53	NW	0.89	1.07
6	125.64	NW	0.99	1.19
7	115.39	NW	0.92	1.08
8	105.3	N	0.99	1.16
9	95.38	N	0.99	1.15
10	84.994	N	0.98	1.28
11	74.287	NE	0.98	1.14
12	64.34	NE	1.08	1.26
13	54.29	NE	1.11	1.27
14	43.87	NE	1.18	1.36
15	34.71	NE	1.23	1.42
16	24.68	NE	1.19	1.36
17	15	NE	1.19	1.38
18	5.42	E	1.09	1.24

3.2.3 Simulation Results

For the simulation results, two scenarios with the lowest and the highest significant wave heights, for two different wave directions, have been selected to illustrate the wave transformation at different directions, i.e., from the western and eastern direction (Table 1). Table 1 indicates that a significant number of waves travel towards NE whereas only a slight percentage of waves travel in the opposite direction. Therefore, the hydrodynamics and the morphology of the Ystad Bay are markedly affected by NE waves. In this study two scenarios are selected to present the wave conditions at two different directions. For the first run, scenario number (3) is selected as a good representative condition for westerly waves. Consequently, scenario number (15) with the highest number of waves and the highest value of significant height is selected to present a general wave condition for the NE direction, where most of the waves from the Baltic Sea travel in the present case. These two scenarios have been run in the SWAN model and the results are illustrated in the following (Figures 16 and 17). The rest of figures for the other scenarios may be found in the Appendix.

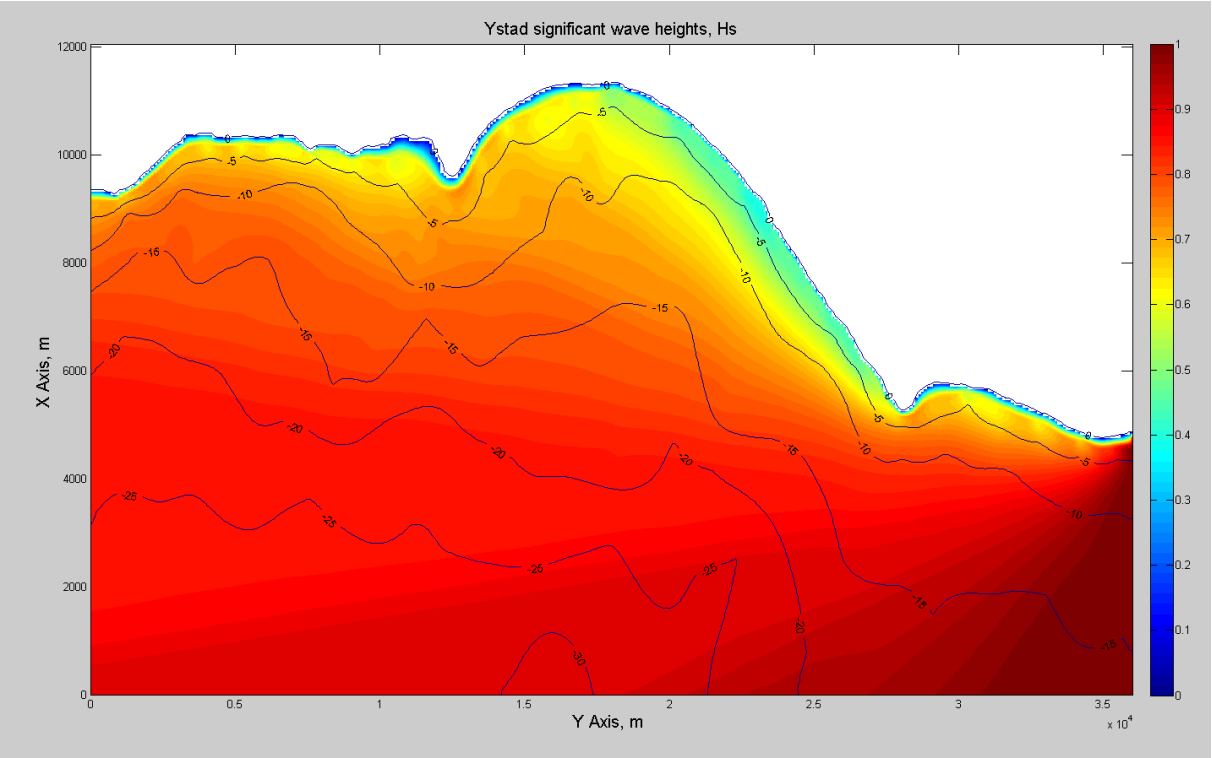

Figure 16a. Significant wave height for Ystad Bay, Scenario 3 with the initial H_s=1m at offshore

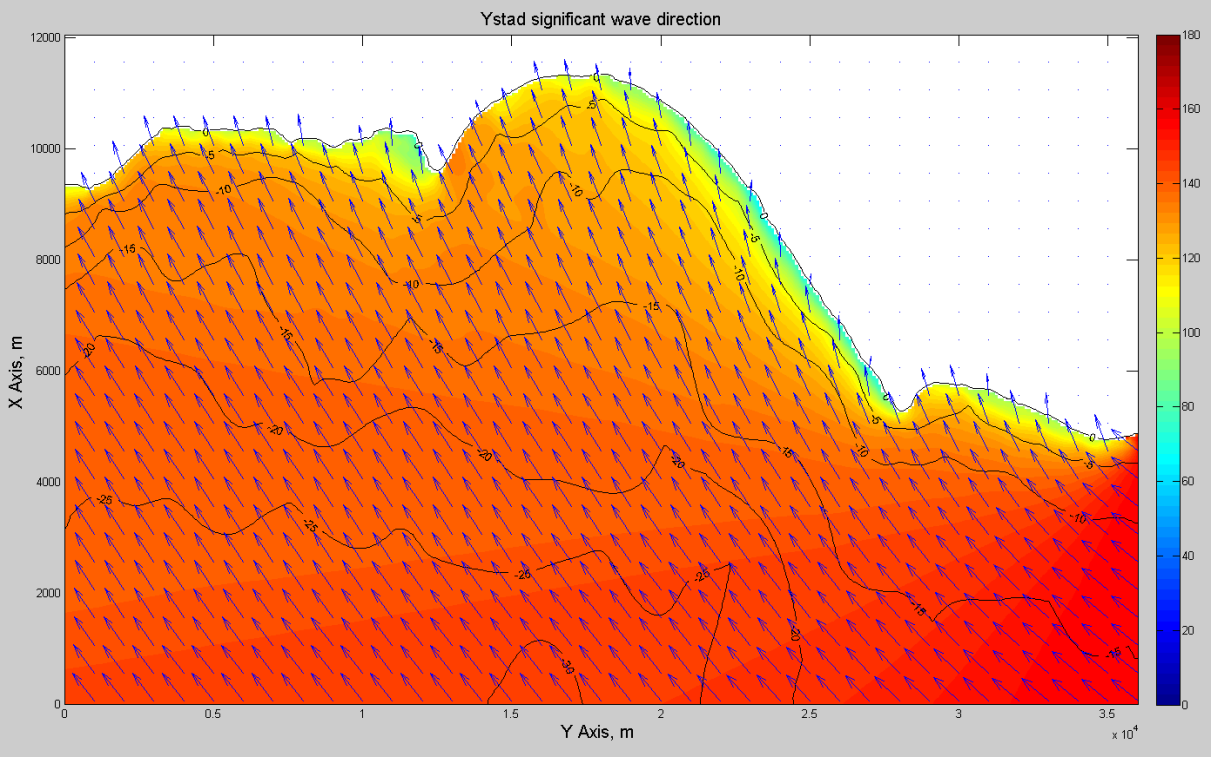

Figure 16b. Wave directions for Ystad Bay, Scenario 3 with the initial θ=155.75 ^{0} at offshore

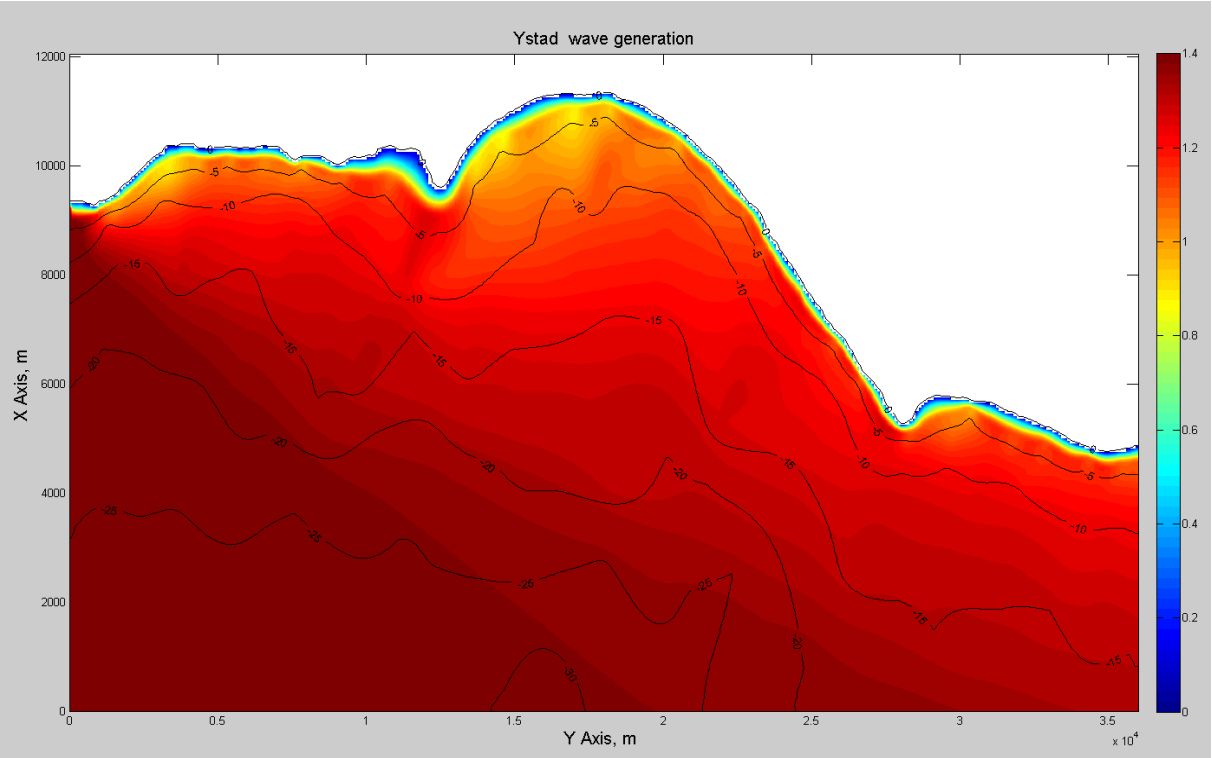

Figure 17a. Significant wave height for Ystad Bay, Scenario 15 with the initial H_s=1.42m at offshore

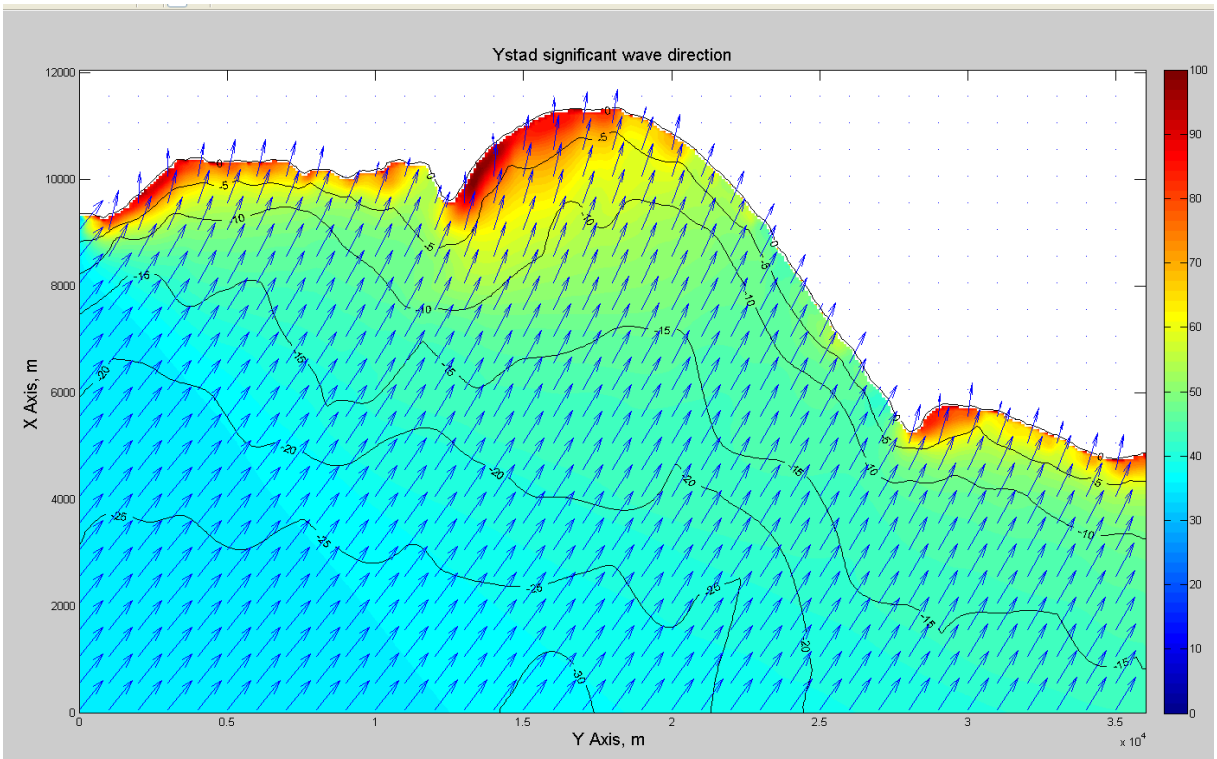

Figure 17b. Wave directions for Ystad Bay, Scenario 15 with the initial direction θ=34.71 ^{0} at offshore

Figures 16a and 17a show the wave generation and wave heights at different locations with different water depths from deep water towards shallow water in the entire Ystad Bay. In figures 16b and 17b the wave directions and the wave refractions are illustrated with vector plots. These figures clearly show how waves are refracted toward the shallow water, the wave direction changes when it reaches the shallow water as it starts turning perpendicular towards the coastline. For a better illustration of the simulation results the wave height variation versus the water depth is plotted for a straight line in the middle of the bay (Figure 18).

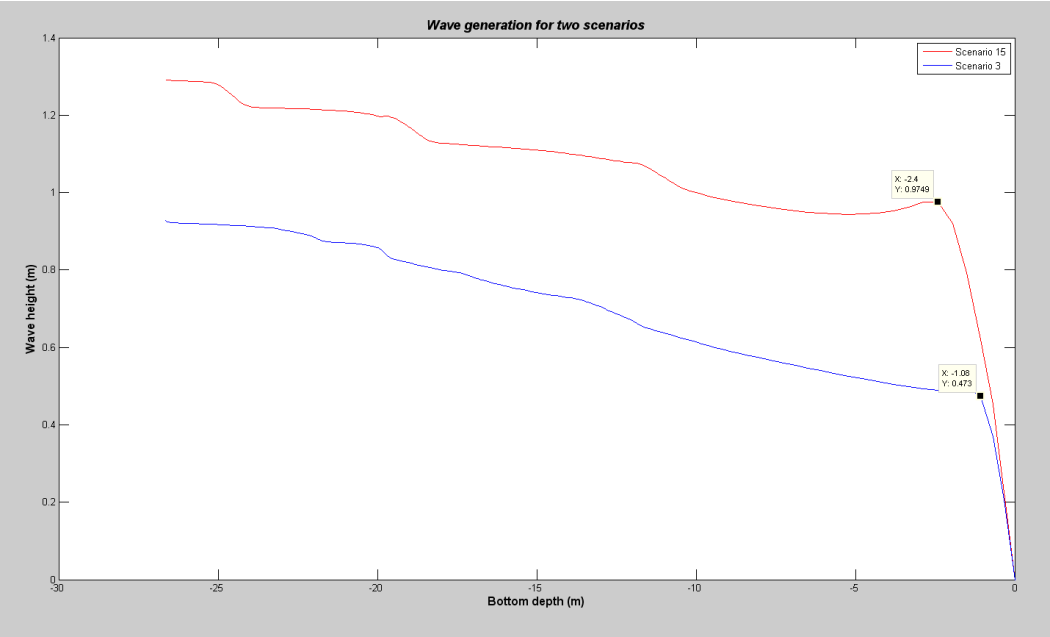

Figure 18. The wave height variation for scenarios 3 and 15 for different depths

The simulation results from SWAN indicate that in scenario 3 with H_s=1 m there is a continuous decrease in the in the wave height until the waves reach a depth of about 2 m where the waves start interacting with the bottom and a sudden increase in Hs is observed due to the shoaling (Figure 18). Then, as wave breaking occurs at the depth of 1m, the significant height starts to decrease and at it approaches zero at the shoreline. The significant wave height varies from about 0.6 m to 0.5 m between the depth of 10 m and 2 m at which shoaling occurred for this simulation (Figure 18).

The simulation results in figure 18 also indicate that for scenario 15 with Hs=1.42 m the wave heights start decreasing till the waves reach a water depth of 4.5 m, where the shoaling will increase the wave height slightly and then wave breaking occurs at the depth of 2.4 m and the wave height starts to decrease.

Figure19 illustrates the changes in the wave heights with the distance from the shoreline along the same straight line in the middle of the bay for scenarios 3 and 15.

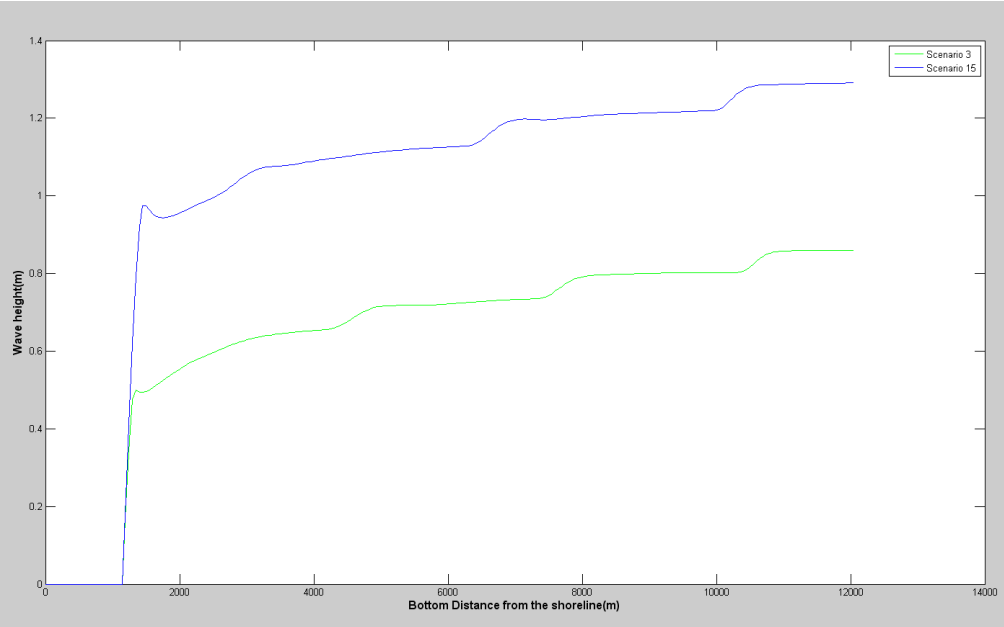

Figure 19. The wave height variation versus the distance from the shoreline for scenarios 3 and 15

It is derived from figure 19 that shoaling takes place at the distance of about 1000-1500 m from the shoreline in both scenarios while breaking occurs closer to the shoreline for scenario 3 with a smaller wave height at offshore.

3.3 The EBED-Modified Wave Model

3.3.1 Background and Theory

The EBED is a wave model for the calculation of waves in the nearshore, including detailed description of wave diffraction. The model was developed by Mase (2001) and is based on the conservation of wave energy flux. Recently, Nam *et al.* (2010) modified EBED to better quantify energy dissipation due to wave breaking (EBED modified). The EBED modified was employed in this study, and the model was made available by the developers: Pham Thanh Nam[1], Magnus Larson[2] and Hans Hanson[3].

3.3.2 Energy Balance Equation

The random wave transformation model was originally derived by Mase (2001). The energy balance equation with diffraction and energy dissipation terms (EBED) is the basis for this model (Equation 16).

$$\frac{\partial(v_x S)}{\partial x}+\frac{\partial(v_y S)}{\partial y}+\frac{\partial(v_\theta S)}{\partial \theta}=\underbrace{\frac{\kappa}{2\omega}\left\{\left(CC_g\cos^2\theta S_y\right)_y-\frac{1}{2}CC_g\cos^2\theta S_{yy}\right\}}_{\text{I}}-\underbrace{\varepsilon_b S}_{\text{II}} \qquad (16)$$

where S is the angular-frequency spectrum density, (x ,y) are the coordinates, where x points in the longshore direction and y in the cross-shore direction, θ is the angle measured counterclockwise from x axis; v_x ,v_y , and v_θ are propagation velocities in resepective coordinate direction, ω is the angular frequency, C , C_g are the phase speed and group speed respectively, κ is defined as an independent variable number applied to change the diffraction impact, and ε_b is a dissipation coefficient. The propagation velocities are:

$$\left\{v_x, v_y, v_\theta\right\}=\left\{C_g\cos\theta,\ C_g\sin\theta,\ \frac{C_g}{C}\left(\sin\theta\frac{\partial C}{\partial x}-\cos\theta\frac{\partial C}{\partial y}\right)\right\} \qquad (17)$$

The first term (I) on the right side of Eq. (16), describes the diffraction effects (Mase, 2001) and the second term (II) accounts for dissipation due to wave breaking. Moreover, because of the overestimation of the energy dissipation term in the surf zone a special study was performed by Nam *et al*, (2010) to modify and develop the (EBED) model (Nam, 2010). The new modified equation is used in the model (EBED-modified) that has been used in this study and is written:

$$\frac{\partial(v_x S)}{\partial x}+\frac{\partial(v_y S)}{\partial y}+\frac{\partial(v_\theta S)}{\partial \theta}=\frac{\kappa}{2\omega}\left\{\left(CC_g\cos^2\theta S_y\right)_y-\frac{1}{2}CC_g\cos^2\theta S_{yy}\right\}-\frac{K}{h}C_g S\left\{1-\left(\frac{\Gamma h}{H_s}\right)^2\right\} \qquad (18)$$

[1] Water Resources Engineering, Lund University, Box 118, Lund, Sweden (Thanh_Nam.Pham@tvrl.lth.se)

[2] Ditto (Magnus.Larson@tvrl.lth.se)

[3] Ditto (Hans.Hanson@tvrl.lth.se)

In which h is the still-water depth, κ and Γ are the non-dimensional experimental coefficients modified by Goda (2006) and calculated as:

$$\begin{cases} \Gamma = 0.45,\ K = \dfrac{3}{8}(0.3 - 19.2\,m) & : m < 0 \\ \Gamma = 0.45 + 1.5\,m,\ K = \dfrac{3}{8}(0.3 - 0.5\,m) & : 0 \le m \le 0.6 \end{cases} \tag{19}$$

where m is the bottom slope (Nam, 2010).

Furthermore, the radiation stresses could be calculated from the wave transformation and might be written as:

$$S_{xx} = \frac{E}{2}\left[2n\left(1+\cos^2\bar{\theta}\right)-1\right] \tag{20}$$

$$S_{yy} = \frac{E}{2}\left[2n\left(1+\sin^2\bar{\theta}\right)-1\right] \tag{21}$$

$$S_{xy} = S_{yx}\frac{E}{2}n\sin 2\bar{\theta} \tag{22}$$

Where S_{xx} is the radiation stress calculated as time-averaged transport of x -momentum in x - direction, S_{xy} is the radiation stress of the transported x momentum in y direction, S_{yx} is the radiation stress of the transported y - momentum in x -direction while S_{yy} is time-averaged transport of y -momentum in y -direction. E is the wave energy calculated per unit area given as:

$$E = \rho_w g.H_{rms}^2 / 8 \tag{23}$$

And n is known as the wave index derived as:

$$n = C_g / C \tag{24}$$

Where C_g is the group velocity and C stands for the phase speed.

3.4 EBED (modified) Model implementation for Ystad Bay

3.4.1 Model Setup and Input

The implementation of the EBED-modified model is similar to the implementation of SWAN, in which there is a data file with the input parameters. The same hydrodynamic condition, as well as the same bathymetry setup as in SWAN was used in the EBED-modified model in order to calculate the wave generation and propagation in Ystad Bay, see section (3.2.2) and tables (1,2,3).

3.4.2 Simulation Results

The same scenarios (Scenario 3 and 15) applied earlier in SWAN have also been simulated in EBED-modified model and the results are illustrated in figures 20 and 21.

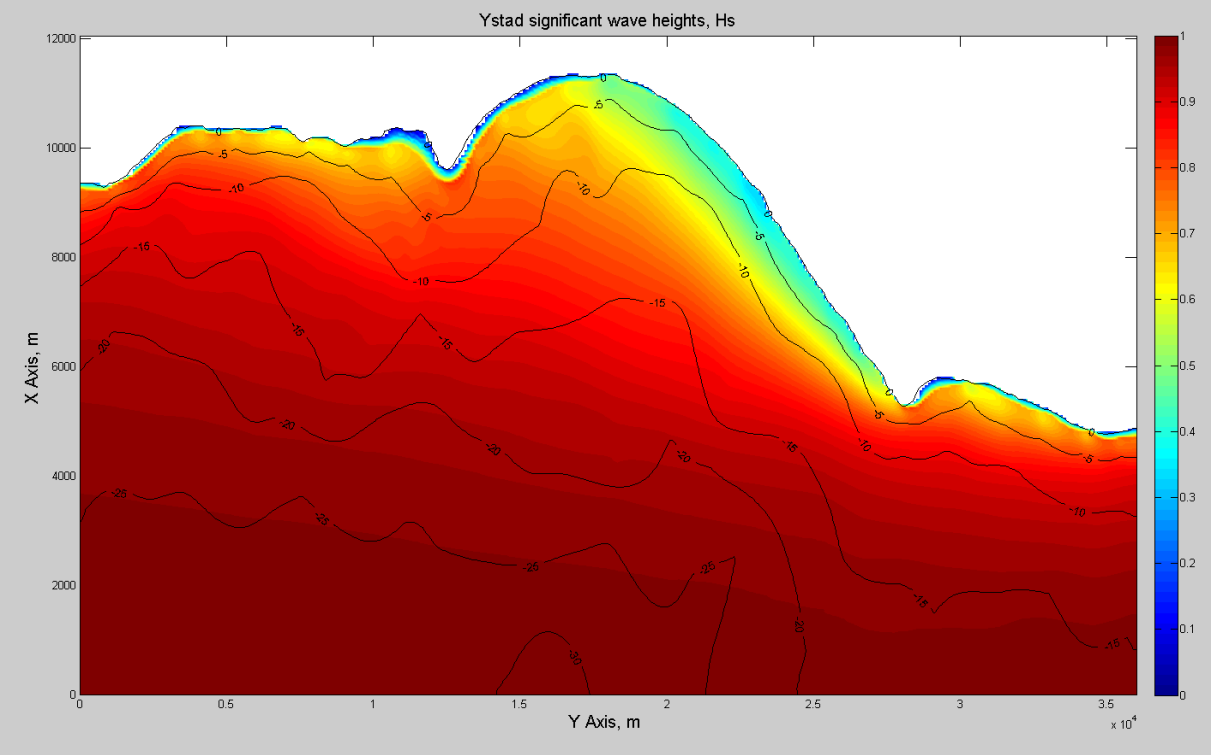

Figure 20a. Significant wave height for Ystad Bay, Scenario 3 with the initial *Hs*=1m at offshore

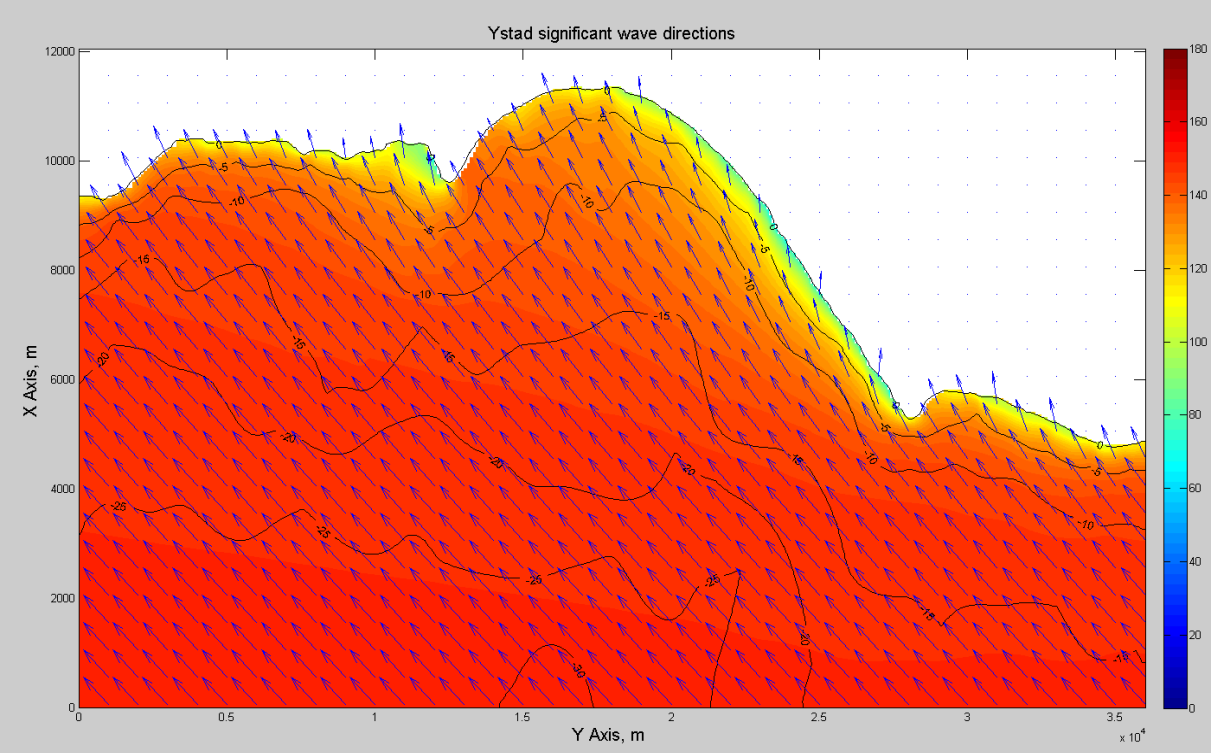

Figure 20b. Wave directions for Ystad Bay, Scenario 3 with the initial θ=155.75 ^{0} at offshore

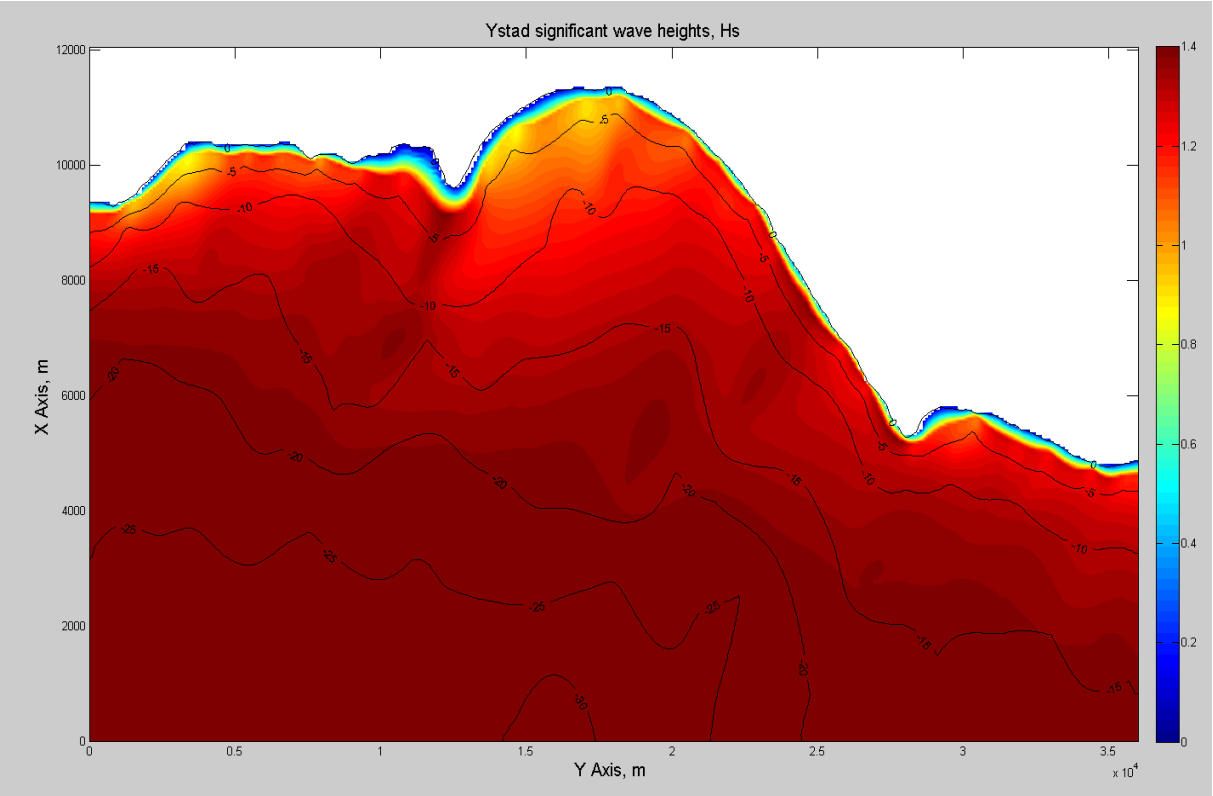

Figure 21a. Significant wave height for Ystad Bay, Scenario 15 with the initial H_s=1.42m at offshore

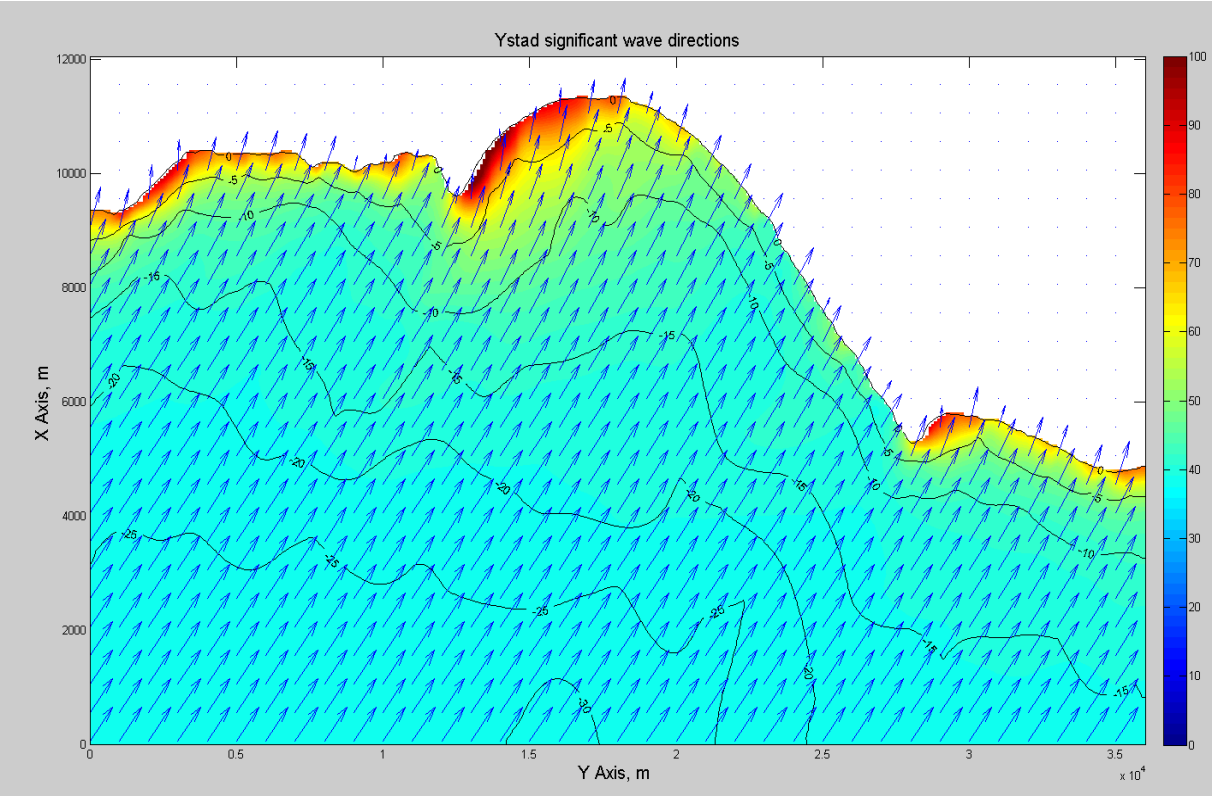

Figure 21b. Wave directions for Ystad Bay, Scenario 15 with the initial θ=34.71 ^{0} at offshore

3.5 Comparison between SWAN and EBED (modified) Results

In order to compare the results from SWAN with EBED-modified model, the wave generations for the two scenarios have been illustrated as contour-plots (Figures 22-25).

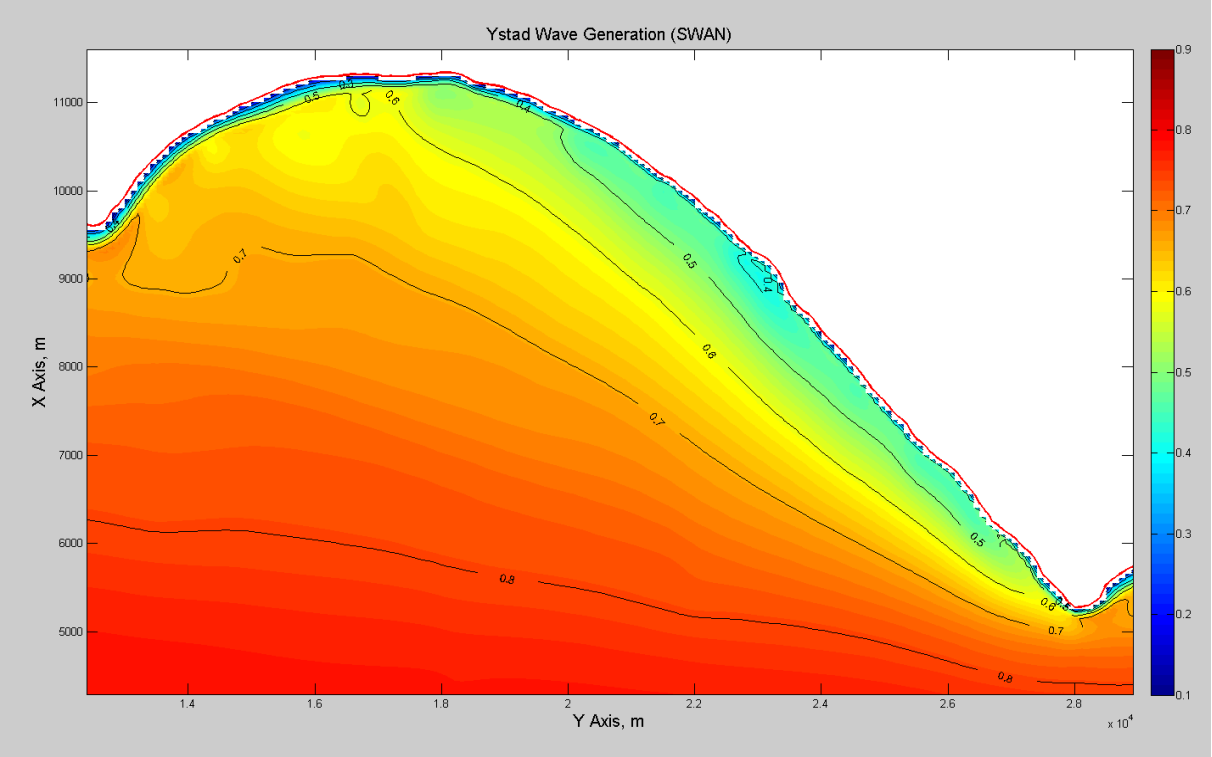

Figure 22. Contour plots for wave generation, Scenario 3, SWAN

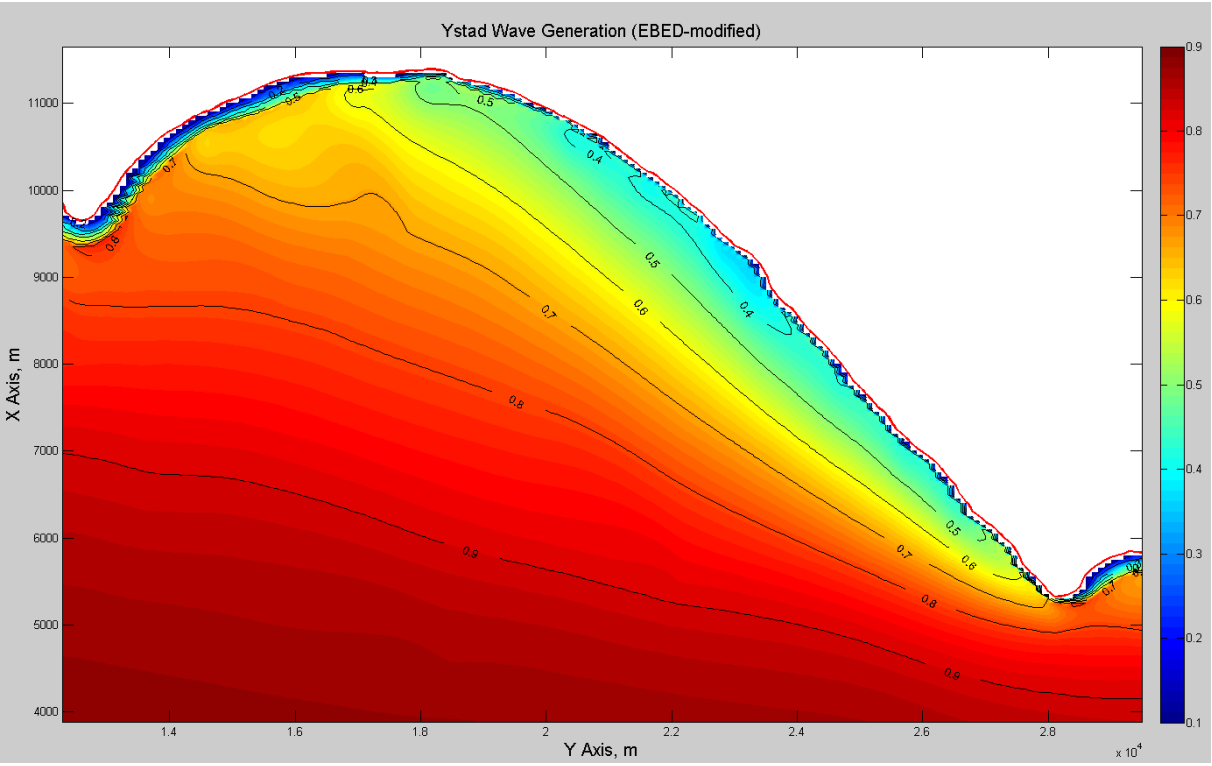

Figure 23. Contour plots for wave generation, Scenario 3, EBED-modified

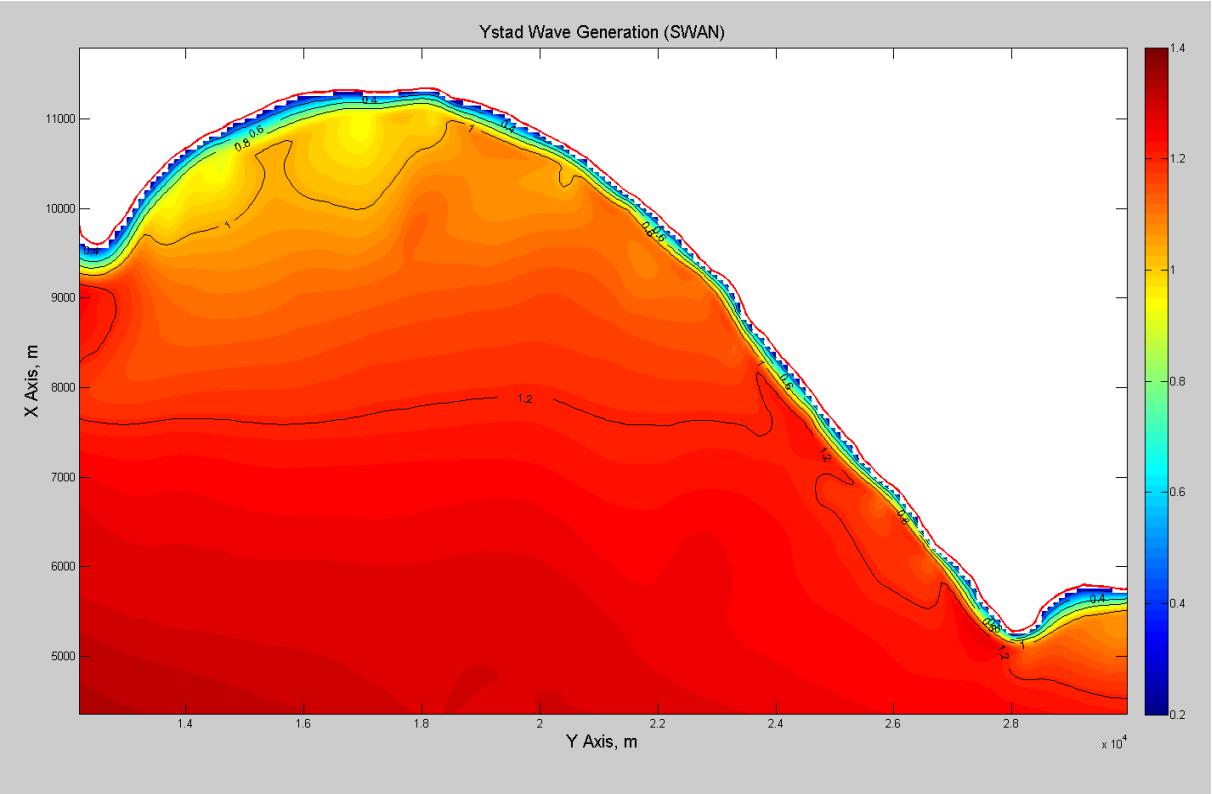

Figure 24. Contour plots for wave generation, Scenario 15, SWAN

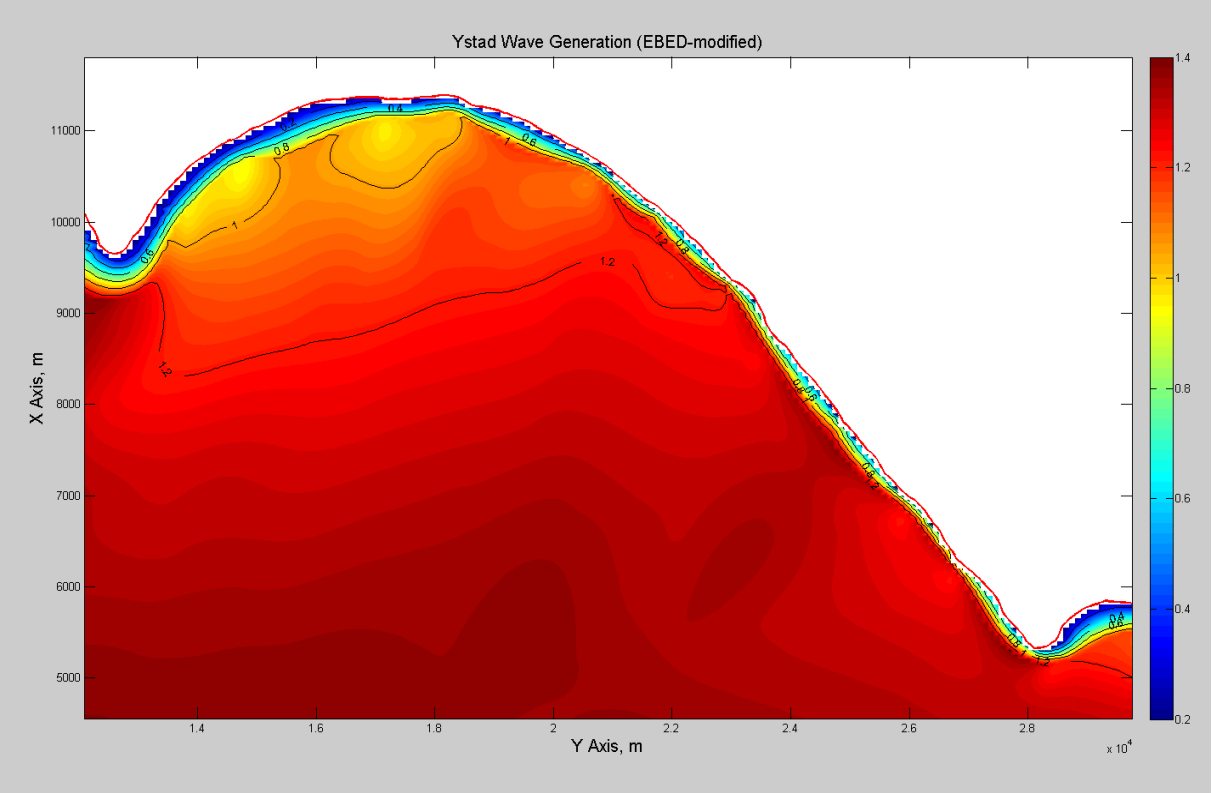

Figure 25. Contour plots for wave generation, Scenario 15, EBED-modified

As shown in Figures 22-25, the results from SWAN and the EBED-modified model are agreeing fairly well. The wave generation in both models is closely matching in the nearshore. This similarity is mainly because of the common theory behind these models in which the Energy Balance Equation in coastal waters is employed to describe wave transformation in both models. There are merely some slight differences in wave height calculations at some points particularly near the boundaries. The reason for this small change is that the Energy Balance Equation in SWAN includes different terms than the EBED-modified model. Another reason could be the different conditions used at the lateral boundaries, as explained in the model theory section. Although EBED-modified is expected to better simulate diffraction, this effect is not pronounced in the present setup.

4 Nearshore Current Model

Longuet-Higgins & Stewart (1964) introduced a new concept known as radiation stress into the wave modeling theory. Since then there have been numerous models based on radiation stress theory in order to simulate nearshore currents generated by waves (Nam, 2010). Initially, most of these models were semi-analytic with errors in current generation at the break point since quite simplified description of the wave breaking was necessary (Bowen (1969), Longuet-Higgins (1970), and Thornton (1970)). After the introduction of the eddy viscosity parameter, the momentum equation for current generation was improved and the errors were reduced. Nam (2010) developed a two-dimensional, vertically integrated nearshore current model, using the wave output from the EBED-modified model. Also, a roller model was included based on the studies by Dally & Brown (1995) and Larson & Kraus (2005). In this study the Nam model is used for the calculating of wave-generated currents. Since the Nam model employs output from EBED-modified, SWAN was not used to calculate the nearshore current.

4.1 Background and Theory

The governing equations applied for the nearshore current calculation are (Militello *et al.*, 2004; Nam *et al.*, 2009; Nam & Larson, 2010):

$$\frac{\partial(h+\eta)}{\partial t}+\frac{\partial q_x}{\partial x}+\frac{\partial q_y}{\partial y}=0 \tag{25}$$

$$\frac{\partial q_x}{\partial t}+\frac{\partial u q_x}{\partial x}+\frac{\partial v q_x}{\partial y}+g(h+\eta)\frac{\partial \eta}{\partial x}=\frac{\partial}{\partial x}D_x\frac{\partial q_x}{\partial x}+\frac{\partial}{\partial y}D_y\frac{\partial q_x}{\partial y}+fq_y-\tau_{bx}+\tau_{Sx} \tag{26}$$

$$\frac{\partial q_y}{\partial t}+\frac{\partial u q_y}{\partial x}+\frac{\partial v q_y}{\partial y}+g(h+\eta)\frac{\partial \eta}{\partial y}=\frac{\partial}{\partial x}D_x\frac{\partial q_y}{\partial x}+\frac{\partial}{\partial y}D_y\frac{\partial q_y}{\partial y}-fq_x-\tau_{by}+\tau_{Sy} \tag{27}$$

where η is the water elevation, t is the time, q_x , q_y are the flow per unit width (m^2/s) at x and y axes. v is the average of velocity in depth for x and y directions, f is the Coriolis factor, D_x and D_y are the eddy viscosity coefficients, τ_{bx} and τ_{by} are the bottom stresses and τ_{Sx} and τ_{Sy} are the wave stresses at x and y directions respectively (Nam, et al., 2009), (Nam & Larson, 2010) and (Larson, et al., 2010).

In the above equations, the velocity through the water column is constant for both x and y directions, implying, for example, that the vertical structure of importance for the material exchange in the cross-shore direction is not described.

4.2 Model Setup and Input

In order for a better illustration, the simulation results for the current patterns in Ystad Bay the entire bay has been divided into four separate areas of interest (Figure 26).

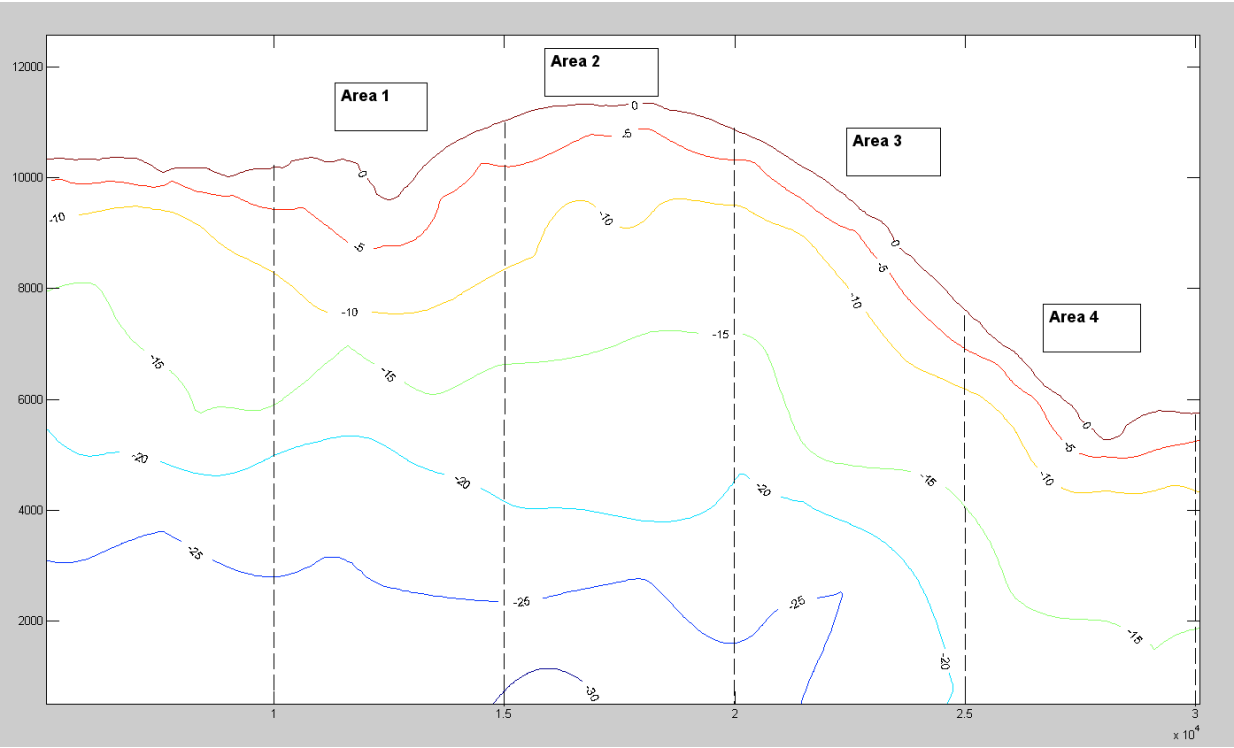

Figure 26. Ystad Bay divided into four areas for illustrating current patterns

4.3 Simulation Results

The results for wave-induced current directions have been illustrated for the two scenarios with different wave directions and generated current patterns (Figures 27-34).

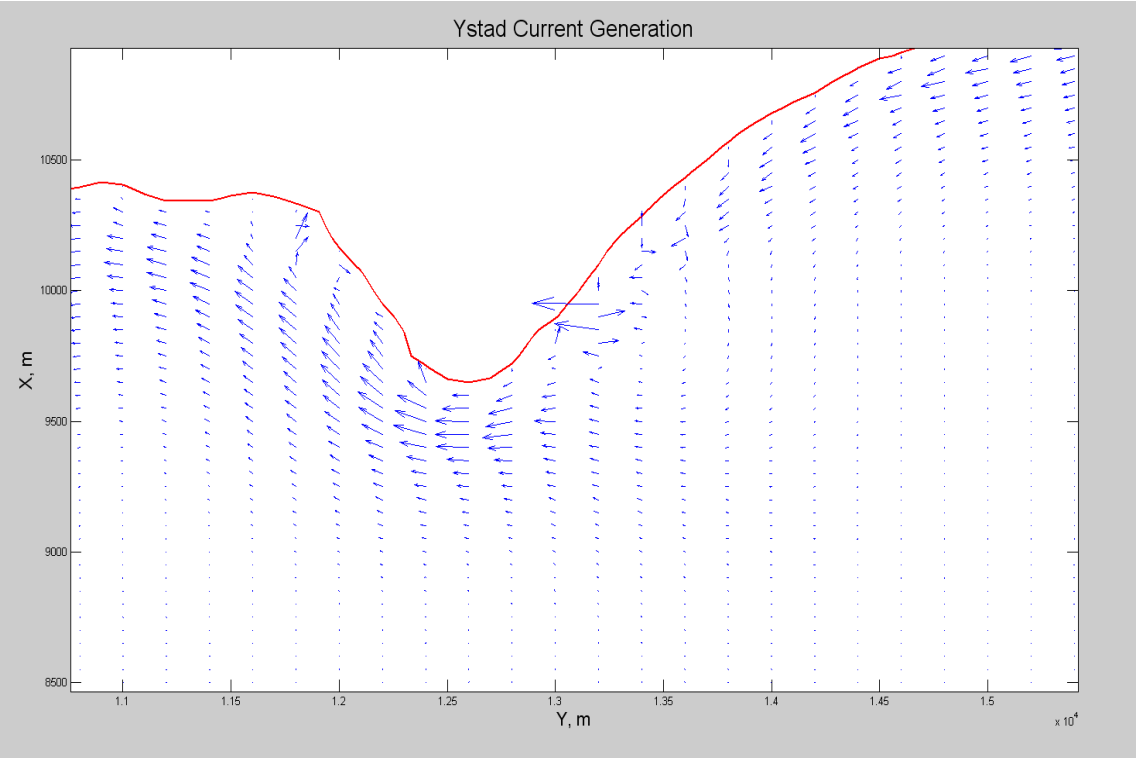

Figure 27. Ystad Bay current generation for Area 1, Scenario 3

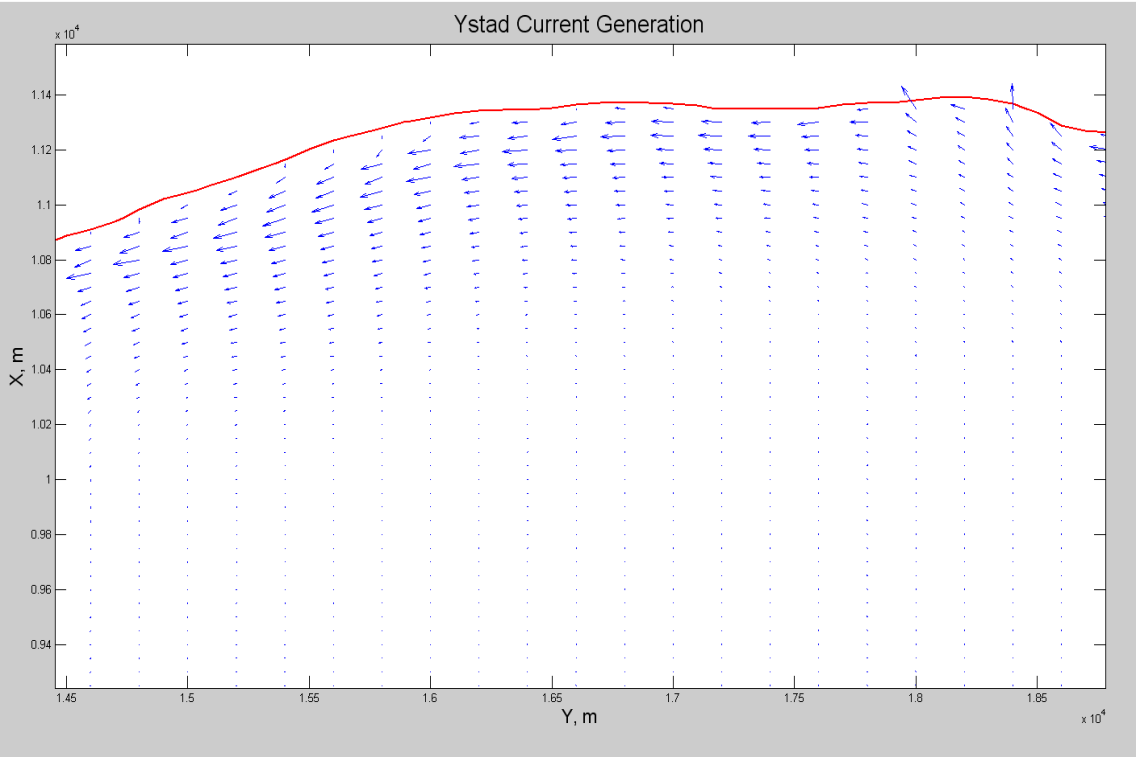

Figure 28. Ystad Bay current generation for Area 2, Scenario 3

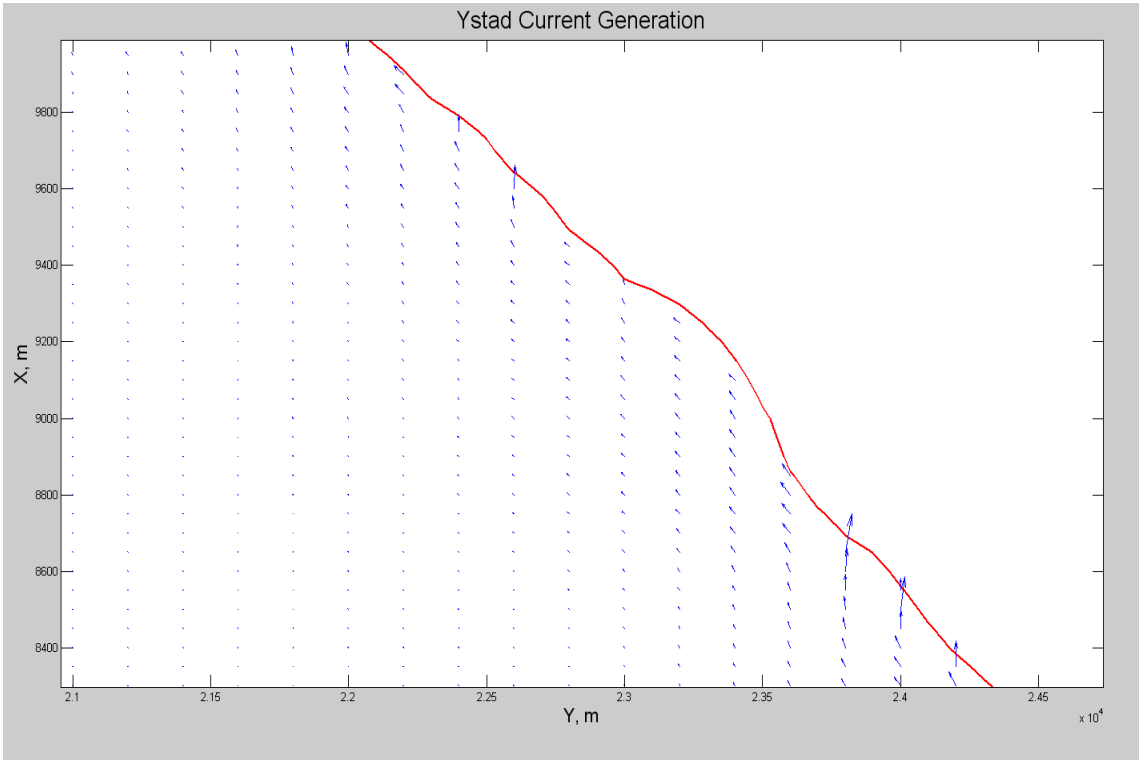

Figure 29. Ystad Bay current generation for Area 3, Scenario 3

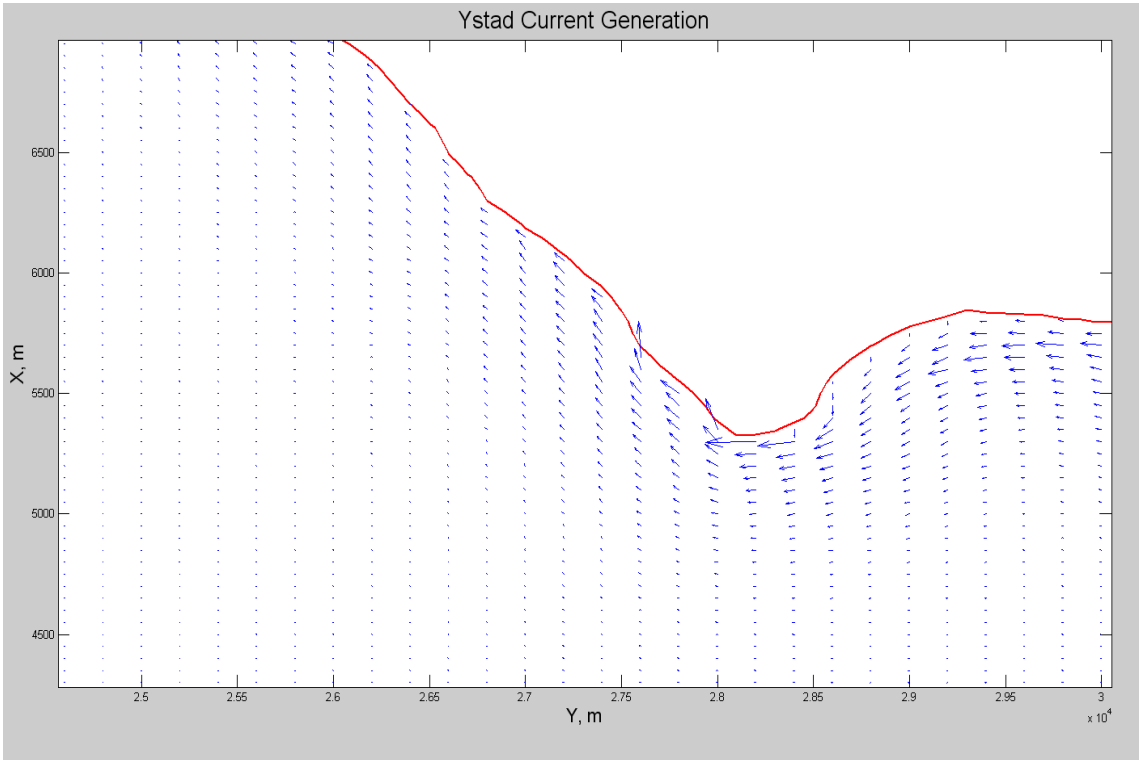

Figure 30. Ystad Bay current generation for Area 4, Scenario 3

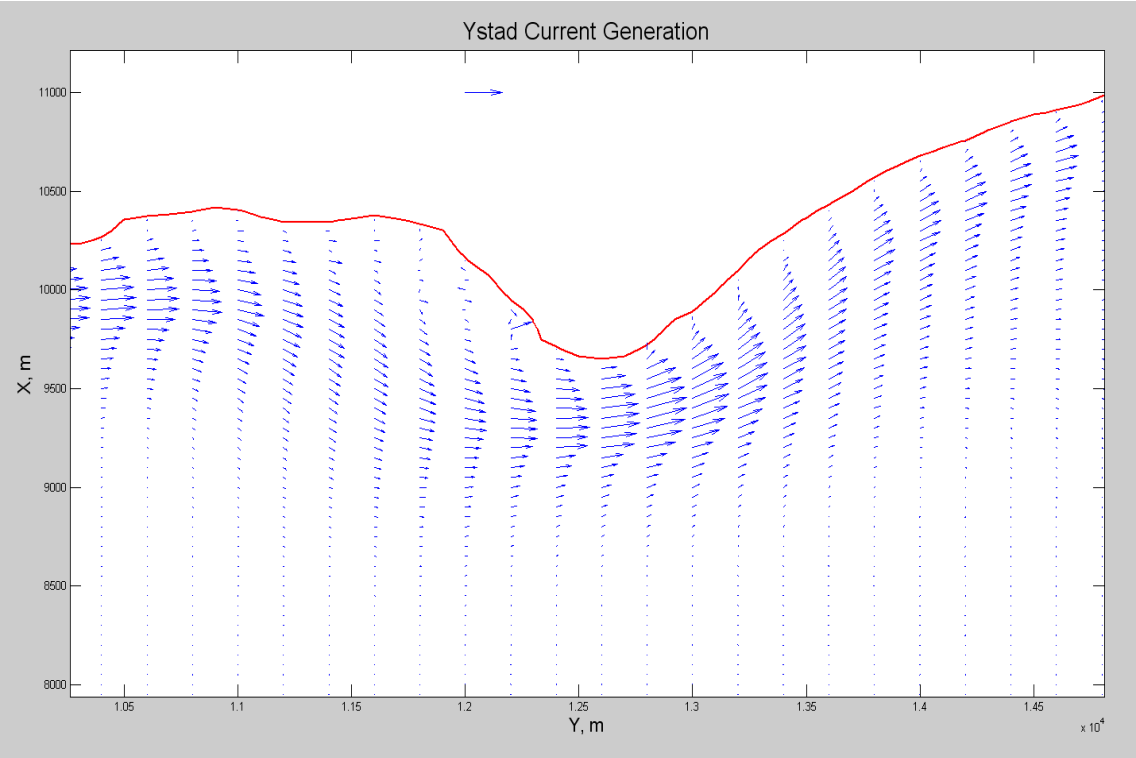

Figure 31. Ystad Bay current generation for Area 1, Scenario 15

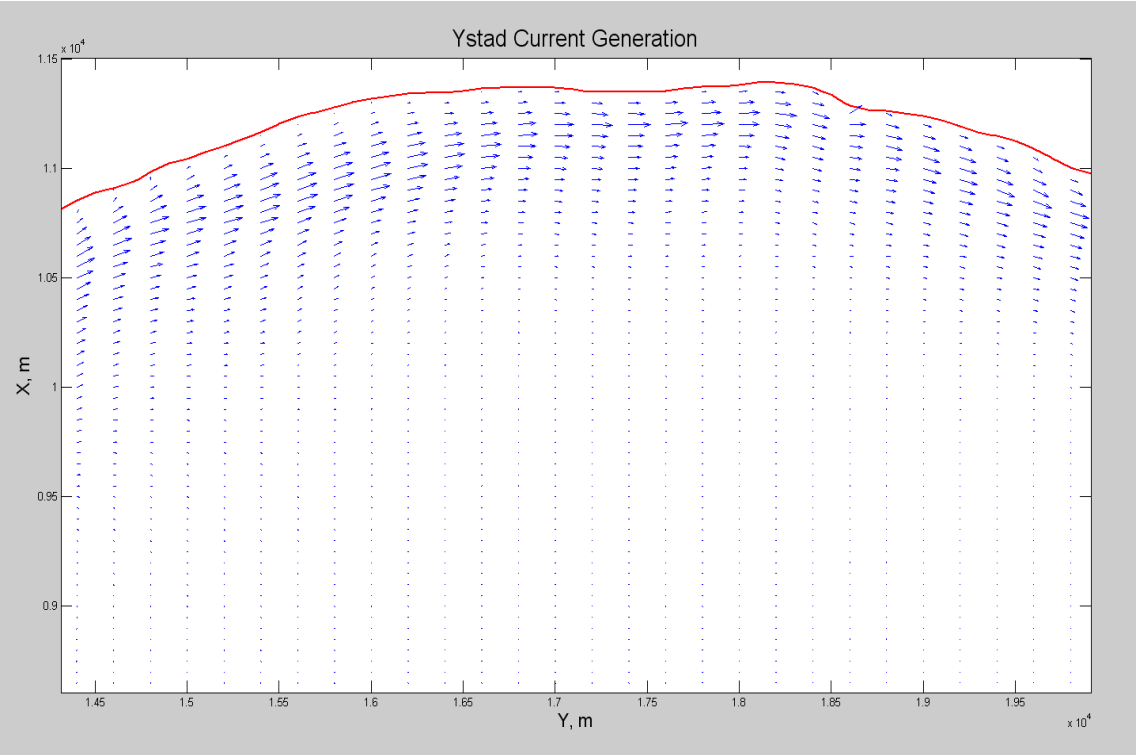

Figure 32. Ystad Bay current generation for Area 2, Scenario 15

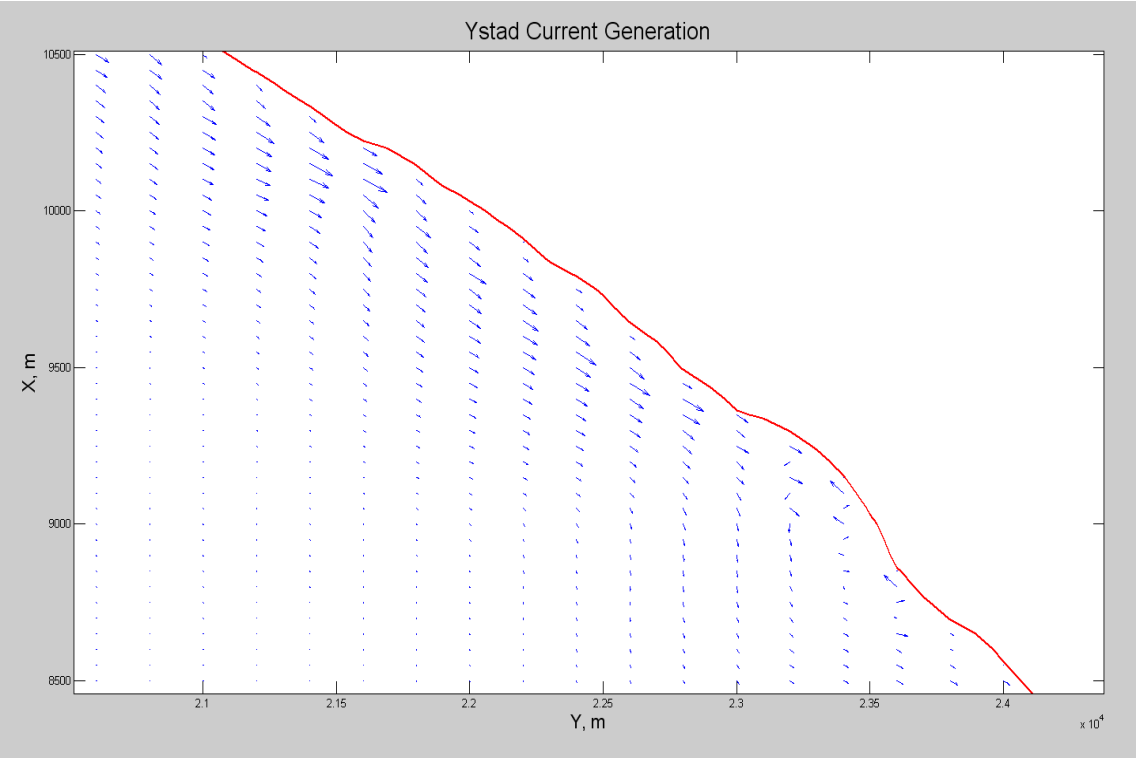

Figure 33. Ystad Bay current generation for Area 3, Scenario 15

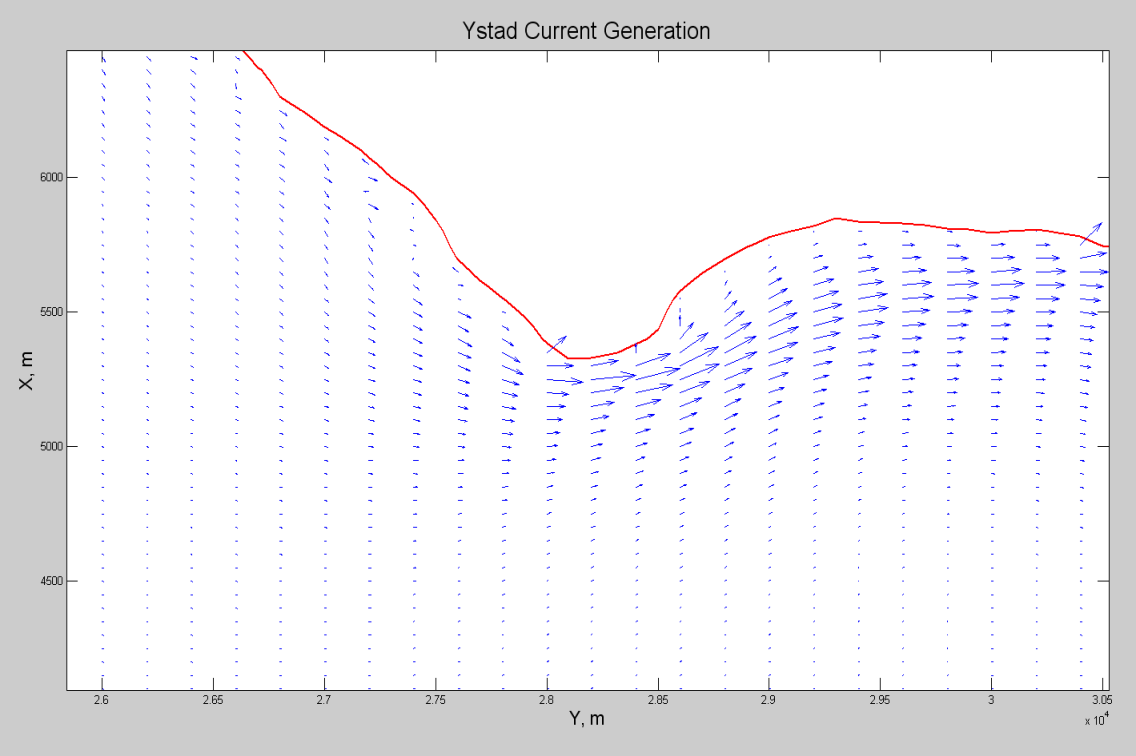

Figure 34. Ystad Bay current generation for Area 4, Scenario 15

Figures 27-34 show the simulation results from the nearshore current model for Ystad Bay with regard to the two different scenarios (3 and 15). The nearshore current model developed by Nam (2010) mainly describes the long-shore current generation, since it is vertically integrated and the cross-shore circulation through the water column is not described. The wave-induced currents for Scenario 3 are mostly in the wave direction, that is, from east to west parallel to the shoreline. Conversely, for scenario 15 with the direction of NE, the current direction is from west to east. In figures 27 and 33, there are a few vectors with the opposite directions compared to the main current direction. The reason for this is the presence of recirculation zones where the coastline changes orientation abruptly. However, these zones do not influence the main current directions some distance away from the shoreline. In section 5 are the simulation results from the current generation used in the model for simulating the sediment transport.

5 Sediment Transport Model

The complex hydrodynamics of the nearshore makes it difficult to carry out sediment transport modeling. Many investigations and studies on sediment transport have been performed through years resulting in a variety of models. For example, Bayram *et al*. (2001) and Camenen & Larroude (2003) examined and further developed different expressions for the sediment transport. In the recent years Camenen & Larson (2005, 2007, 2008) have proposed validated expressions for the sediment transport applicable both for the longshore and cross-shore directions. Nam (2010) employed these expressions and numerically developed a model for sediment transport which is used in this study.

5.1 Swash Transport

Larson and Wamsley (2007) developed a set of formulas for calculating the sediment transport rate in the swash zone, both in the cross-shore and longshore direction. These formulas have been numerically applied in the sediment transport model. The formulas can be summarized as:

$$q_{bc,net} = K_c \frac{\tan\phi_m}{\tan^2\phi_m - (dh/dx)^2} \frac{u_0^3}{g}\left(\frac{dh}{dx} - \tan\beta_e\right)\frac{t_0}{T} \tag{28}$$

$$q_{bl,net} = K_l \frac{\tan\phi_m}{\tan^2\phi_m - (dh/dx)^2} \frac{u_0^2 v_0}{g} \frac{t_0}{T} \tag{29}$$

Where $q_{bc,net}$, $q_{bl,net}$ represent the net rates of sediment transport in cross-shore and longshore direction, respectively, K_c and K_l are the empirical coefficients, ϕ_m is the friction angle of a moving grain (30^0), β_e is the foreshore equilibrium slope, u_0 and v_0 are characteristic velocities in cross-shore and longshore direction, respectively, t_0 is the duration a certain location is covered by water during a swash cycle, and T is defined as the swash duration (typically set equal to the incident wave period; (Nam, et al., 2009))

5.2 Nearshore and Offshore Transport

5.2.1 Bed Load

A unified transport model for bed load and suspended load under the presence of waves and currents was developed by Camenen & Larson (2005, 2007, and 2008). This formulation accounts for both sinusoidal and asymmetric waves (Nam, 2010). In order to achieve a simplified form of this general expression, it is assumed that the waves are sinusoidal and the effects of waves on moving material is negligible, meaning that only currents cause the material transport (Nam, 2010). Therefore, the simplified equation can be written as:

$$\frac{q_{bc}}{\sqrt{(s-1)gd_{50}^3}} = a_c\sqrt{\theta_c}\,\theta_{cw,m}\exp\left(-b_c\frac{\theta_{cr}}{\theta_{cw}}\right) \tag{30}$$

where q_{bc} is the calculated transport rate in the current direction, s is the proportion of water density to sediment density (ρ_s/ρ_w), d_{50} is the median grain size, a_c and b_c are the experimental coefficients, θ_{cr} is the critical Shields parameter for initiation of motion, $\theta_{cw,m}$ and θ_{cw} indicate the average and the maximum value of Shields parameters with regard to wave-current interaction, respectively (Nam, 2010). The critical Shields parameter is obtained from the expression introduced by Soulsby & Whitehouse (1997):

$$\theta_{cr} = \frac{0.24}{d_*} + 0.055\left[1-\exp\left(-0.02d_*\right)\right] \tag{31}$$

where d_{50} is dimensionless grain size defined as,

$$d_* = \sqrt[3]{g(s-1)/\nu^2}\,d_{50} \tag{32}$$

with ν =the kinematic viscosity of water.

The Shields parameters $\theta_{cw,m}$ and θ_{cw} can be written as:

$$\theta_{cw,m} = \left(\theta_c^2 + \theta_{w,m}^2 + 2\theta_{w,m}\theta_c\cos\varphi\right)^{1/2} \tag{33}$$

$$\theta_{cw} = \left(\theta_c^2 + \theta_w^2 + 2\theta_w\theta_c\cos\varphi\right)^{1/2} \tag{34}$$

where θ_c and θ_w are the Shields parameters owing to current and wave, respectively, $\theta_{w,m}$ is the mean Shields wave parameter, assumed to be $\theta_{w,m} = \theta_w/2$ for a sinusoidal wave, and φ is the angle between the wave and current directions.

The parameters θ_c and θ_w could be expressed as:

$$\theta_c = \frac{\tau_c}{\rho_w (s-1) d_{50}} \tag{35}$$

$$\theta_w = \frac{\tau_w}{\rho_w (s-1) d_{50}} \tag{36}$$

in which τ_c and τ_w stand for shear stresses induced by current and wave, respectively (Nam, 2010).

5.2.2 Suspended Load

The calculation of suspended load can either be determined by the Lund-CIRP formula or by the Advection-diffusion (AD) equation (Nam, 2010).

Camenen & Larson (2007 and 2008) assumed an exponential shape for the suspended concentration profile, together with a uniform, constant velocity for the current, ultimately deriving the following equation:

$$q_s = U_c c_R \frac{\varepsilon}{w_s}\left[1 - \exp\left(-\frac{w_s d}{\varepsilon}\right)\right] \tag{37}$$

In which c_R is the reference concentration at bottom, w_s is the sediment fall speed and ε is the sediment diffusivity (Nam, 2010).

The c_R could be written as:

$$c_R = A_{cR}\theta_{cw,m} \exp\left(-4.5\frac{\theta_{cr}}{\theta_{cw}}\right) \tag{38}$$

with

$$A_{cR} = 3.5\times10^{-3}\exp(-0.3 d_*) \tag{39}$$

The sediment fall velocity w_s is based on Soulsby (1997) formulated as:

$$w_s = \frac{\nu}{d_{50}}\left[\left(10.36^2 + 1.049 d_*^3\right)^{1/2} - 10.36\right] \tag{40}$$

The sediment diffusivity term ε , is due to the energy dissipation (Battjes, 1975; Camenen & Larson 2008) and expressed as:

$$\varepsilon = \left(\frac{k_b^3 D_b + k_c^3 D_c + k_w^3 D_w}{\rho} \right)^{1/3} d \tag{41}$$

where k_b , k_c and k_w are the empirical coefficients, D_b is the energy dissipation owing to wave breaking while D_c and D_w are, respectively, the energy dissipation induced by bottom friction owing to current and wave (Nam, 2010)

On the other hand, the AD equation can also be employed in suspended load calculations. The two-dimensional form of the AD equation can be written as (Nam, 2010);

$$\frac{\partial(\overline{C}d)}{\partial t} + \frac{\partial(\overline{C}q_x)}{\partial x} + \frac{\partial(\overline{C}q_y)}{\partial y} = \frac{\partial}{\partial x}\left(K_x \frac{\partial \overline{C}q_x}{\partial x} \right) + \frac{\partial}{\partial y}\left(K_y \frac{\partial \overline{C}q_y}{\partial y} \right) + P - D \tag{42}$$

Where $\overline{C}$ is the depth-averaged sediment concentration (Nam, 2010), K_x and K_y are the coefficients of sediment diffusion in and direction respectively, P is the sediment pick-up rate, and D stands for the sediment deposit rate (Nam, 2010). However, in this model only the Lund-CIRP formula has been used for the calculation of suspended loads.

5.3 Simulation Results

The two scenarios (3, 15) have also been applied in the model to illustrate sediment transport pattern in the bay for both western and eastern directions. For a better illustration the simulation results for the sediment patterns in Ystad Bay. The entire bay has been divided into three separate areas of interest (Figure 35). The results are shown in figures 36 -41.

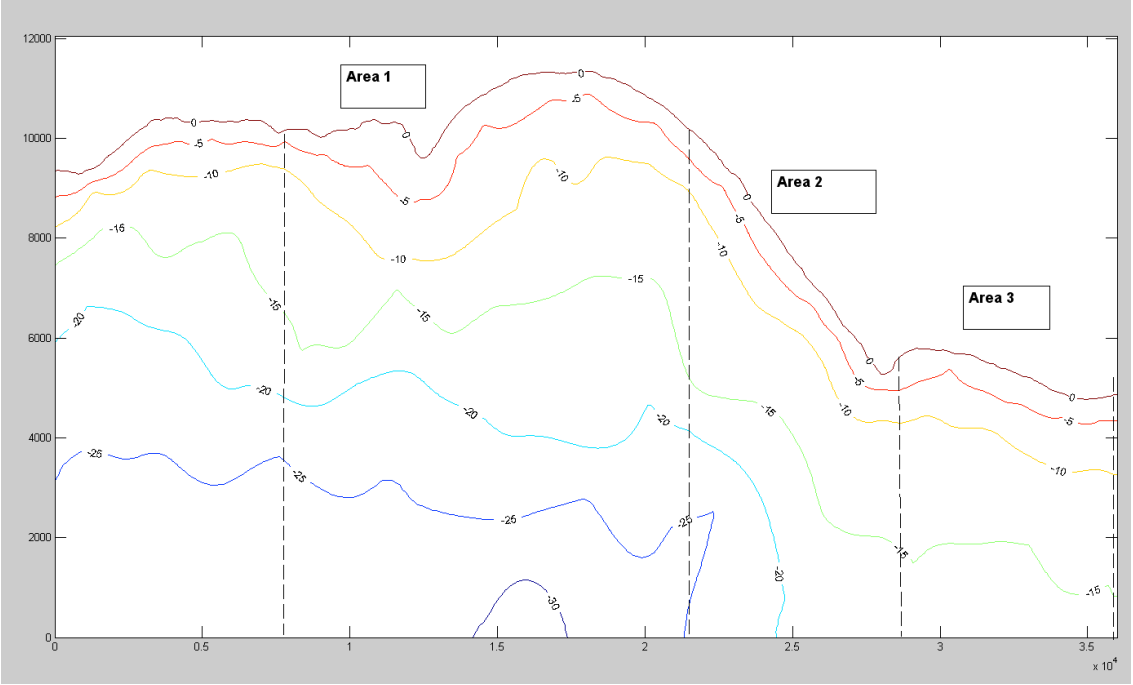

Figure 35. Ystad Bay divided into three areas for illustrating sediment patterns

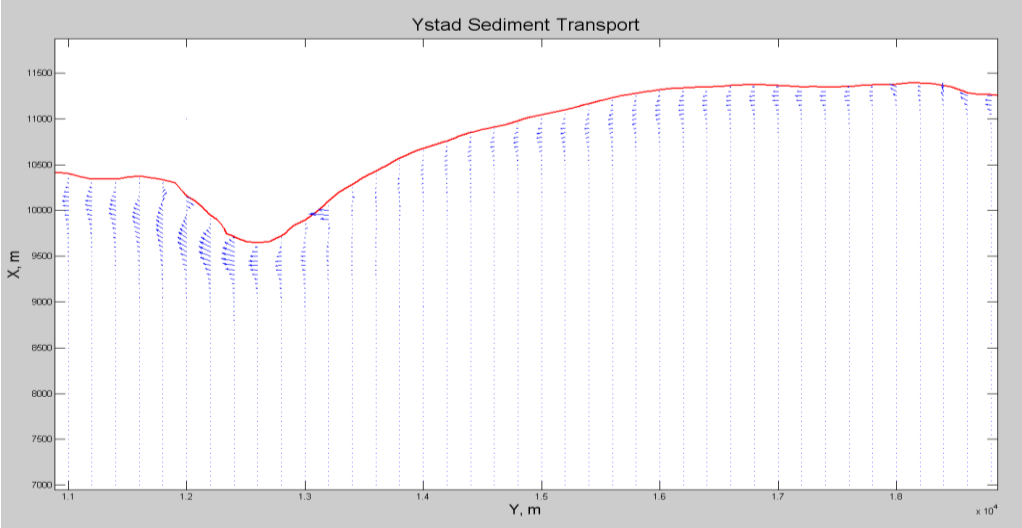

Figure 36. Ystad Bay sediment transport for Area 1, Scenario 3

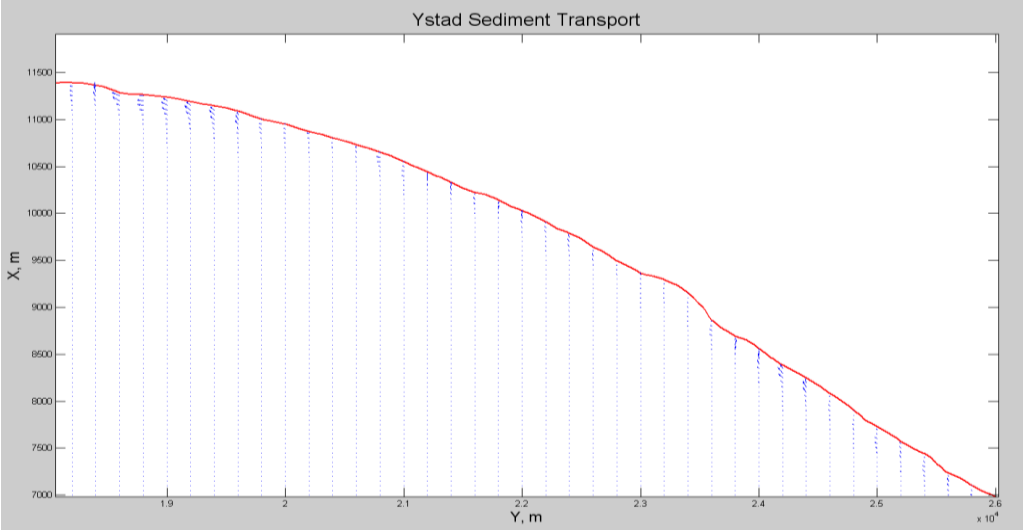

Figure 37. Ystad Bay sediment transport for Area 2, Scenario 3

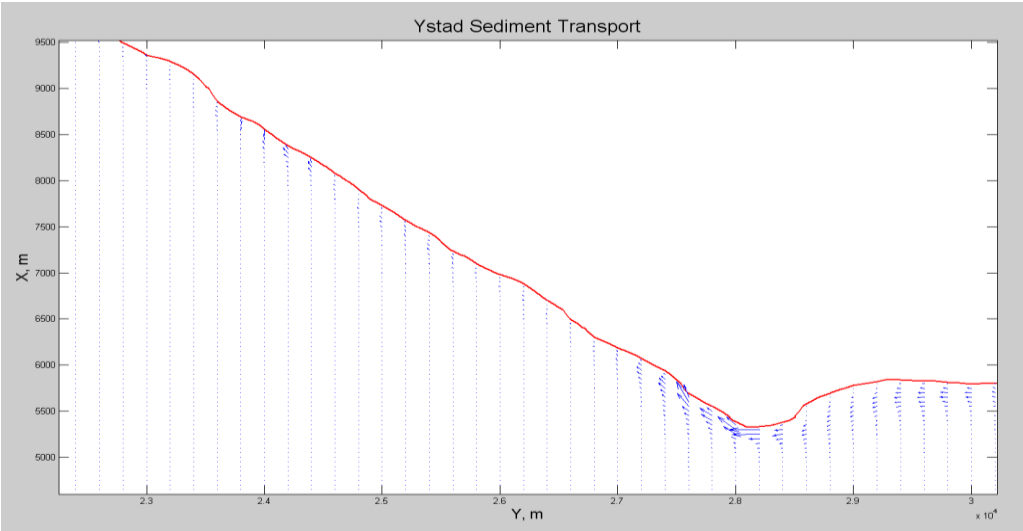

Figure 38. Ystad Bay sediment transport for Area3, Scenario 3

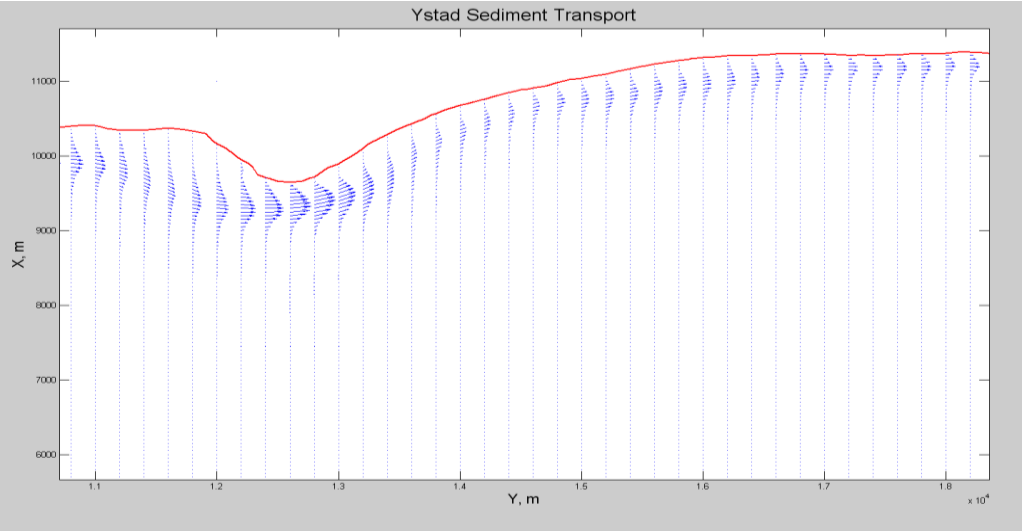

Figure 39. Ystad Bay sediment transport for Area 1, Scenario 15

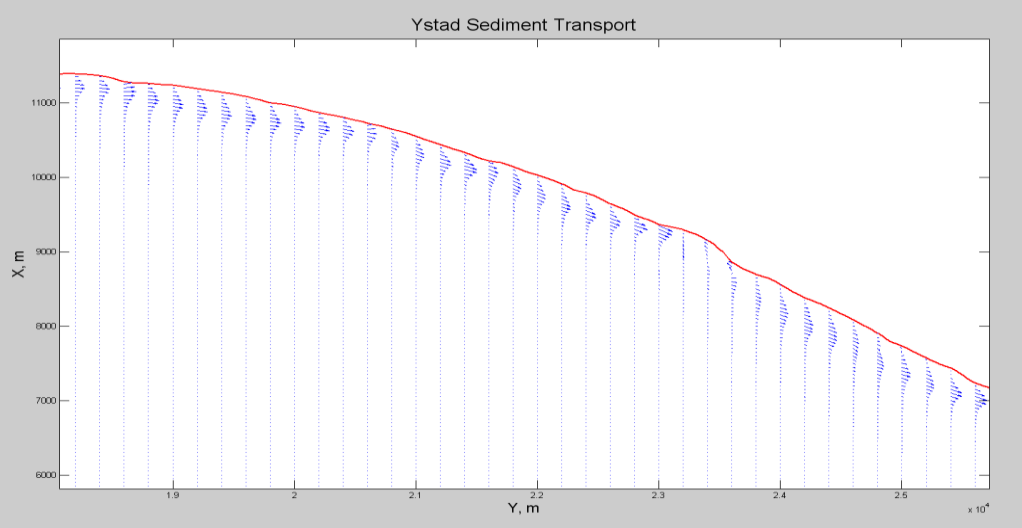

Figure 40. Ystad Bay sediment transport for Area 2, Scenario 15

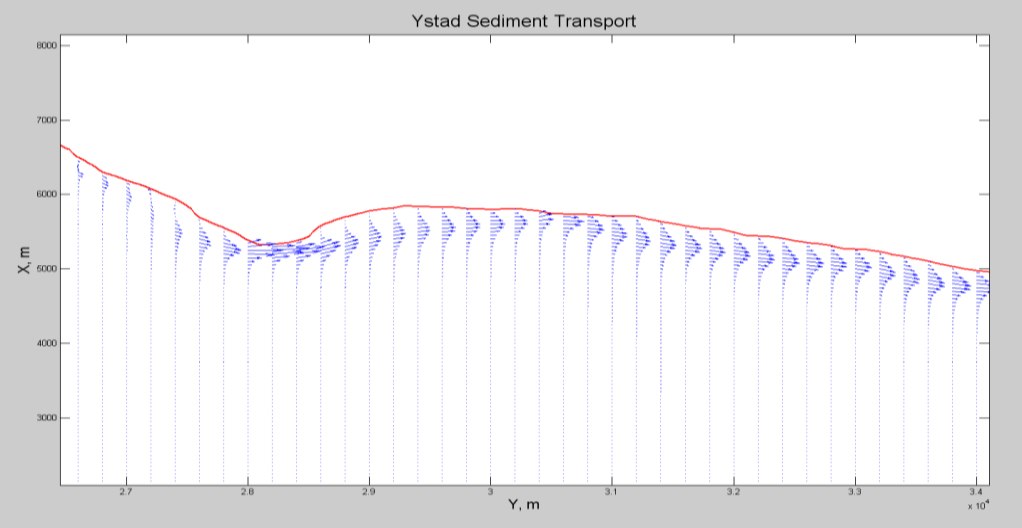

Figure 41. Ystad Bay sediment transport for Area 3, Scenario 15

Figures 36-41 mainly display the longshore sediment transport in the Ystad Bay for the two different directions. The results indicated that there is no considerable sediment transport in deepwater due to the absence of current in deepwater as currents start to be generated in the nearshore, which together with the waves induce sediment transport. The direction of the sediment transport in both scenarios is the same direction as for the currents generated Figures 29-34.

A comparison between the two figures shows that the rate of sediment transport in scenario 15 is higher than in scenario 3. It is also deduced from the figures that the dominant sediment transport direction is from west to east in Ystad Bay, which is in agreement with the observation.

6 Morphological Evolution Model

The morphological evolution model calculates the bottom change due to the waves and currents, indicating areas of erosion and accretion. As previously discussed, the sediment transport model employed primarily focuses on the longshore sediment transport, whereas the cross-shore transport is not described. In order to calculate the erosion and accumulation due to the present scenarios of wave condition in Ystad Bay, the continuity equation is applied to calculate the bottom change in each single cell in the model. The continuity equation is written as:

$$\frac{dh}{dt} = \frac{\Delta q_x}{\Delta x} + \frac{\Delta q_y}{\Delta y} \tag{43}$$

and,

$$\Delta q_x = q_{x_{i+1}} - q_{x_i} \tag{44}$$

$$\Delta q_y = q_{y_{i+1}} - q_{y_i} \tag{45}$$

Where q_{x_i} is the sediment transport rate in cell i, at x direction ($m^3/m.s$), q_{y_i} is the sediment transport rate in cell i, at y ($m^3/m.s$), $\Delta x = 50m$ is the grid size in x direction, $\Delta y = 100m$ is the grid size in y direction, dh is the change in bottom elevation, and dt is the time step (s). If dh >0 erosion occurs and if dh <0 then sediments would be accumulated.

An annual calculation based on the continuity equation has been performed to investigate the bottom change in the Ystad Bay (Figures 42 and 43).

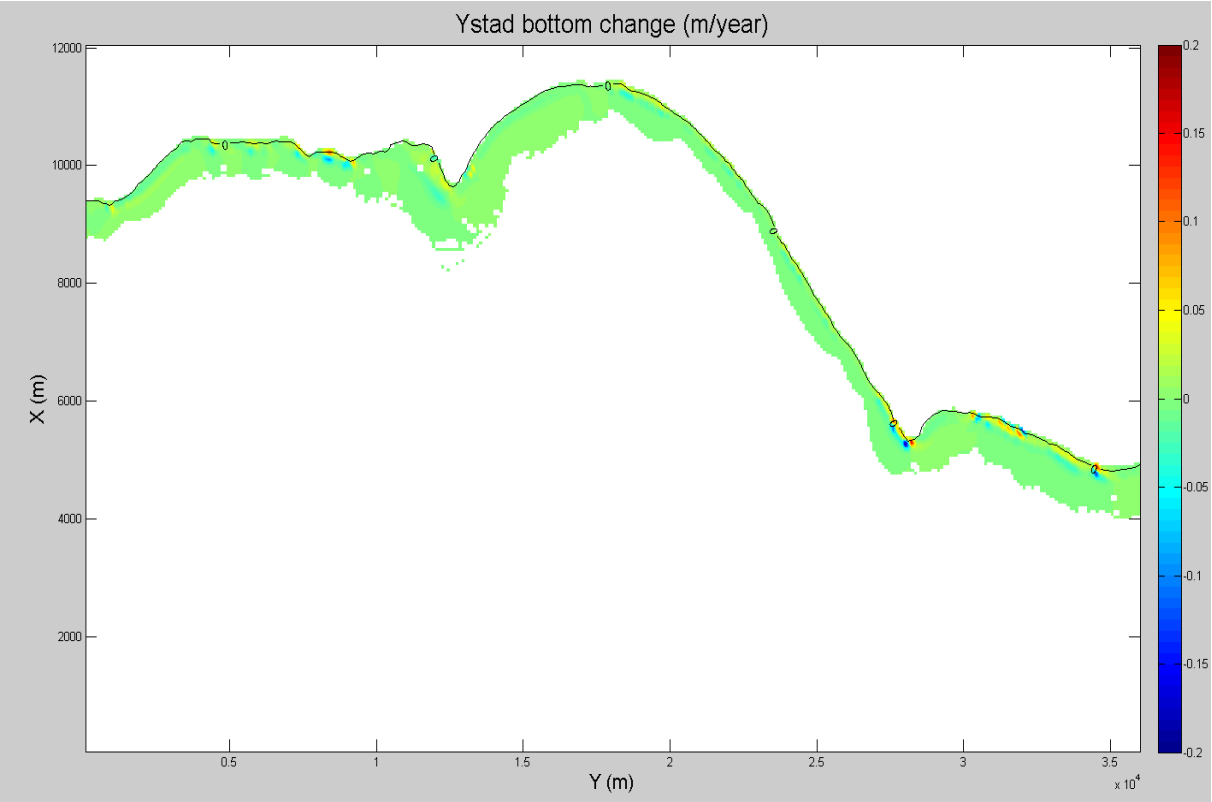

Figure 42. Bottom change in Ystad (m/year), Scenario 3 with NW waves

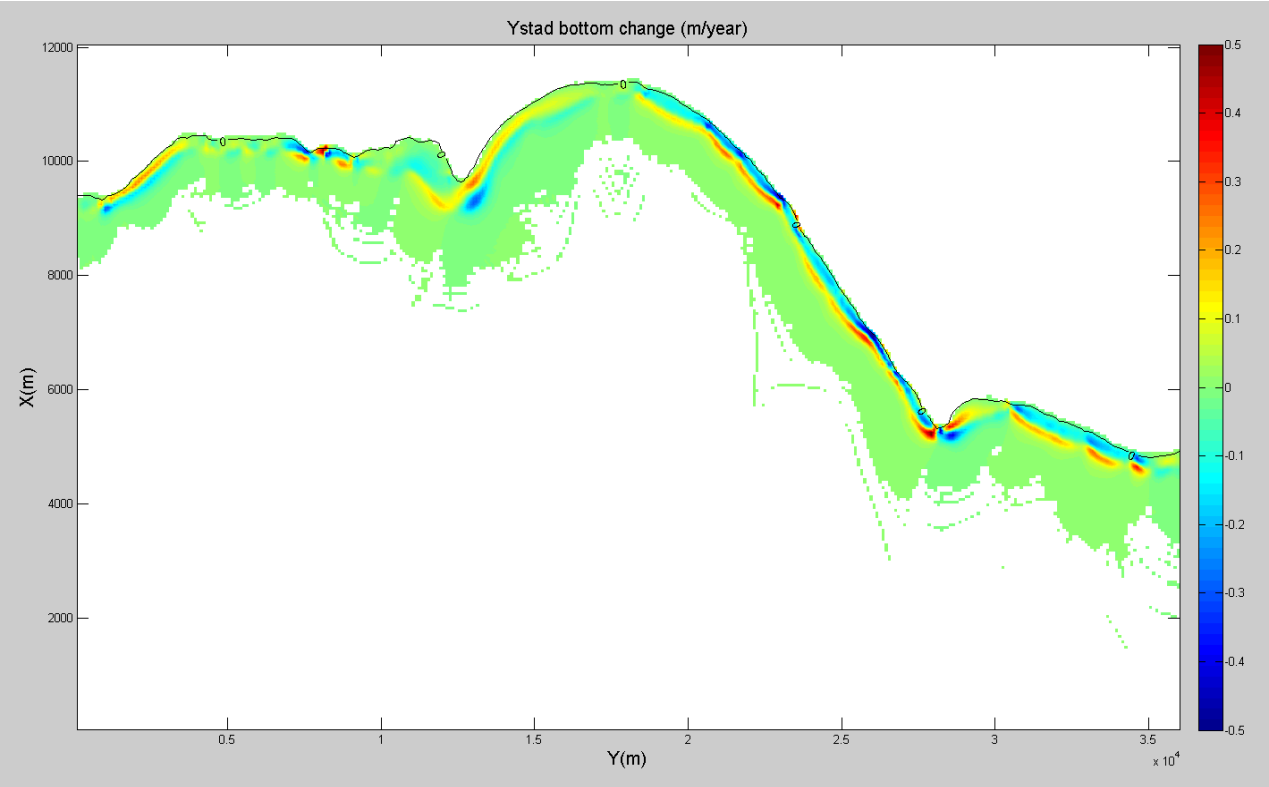

Figure 43. Bottom change in Ystad (m/year), Scenario 15 with NE waves

Figure 43 indicates the bottom change (m/per year) in the Ystad Bay due to the NE waves on an annual basis. The bottom change varies from -0.2 m to + 0.2 m, where the maximum values only occur in the corner of the southern part of Ystad where the coastline is oriented. This could be because of the recirculation, where currents have a local deviation from the longshore direction. Figure 43 indicates that for most regions in the bay, especially in deep water, there is no significant bottom change and the values are close to zero. In the nearshore zone, where the waves are broken and currents are generated, the bottom change is slightly higher. In the middle of the bay at Y=17.5 km, close to the shoreline the bottom changes are mainly negative showing accretion in the western Ystad Bay. The bottom change in this area varies from 0 to 5 cm whereas for other parts it shows very slight erosion and the values are smaller than 2 cm. the mean value of the bottom change for the total bay is calculated as 0.004 cm. Therefore, based on the simulation results, it is concluded that western waves have a small effect on the sediment transport pattern in Ystad, as has been confirmed by the observations.

Conversely, for scenario 15 where most of the waves travel at the NE direction, the results are totally different. As indicated in figure 44 the bottom change is considerably higher than for the previous wave condition based on the same annual analysis. The results from figure 38 mainly indicate that at Y=0 to Y=15km the bottom change in the nearshore is negative with an average value around 15 cm erosion in the western Ystad Bay, which agrees with observations. At Y=15 km to Y=22 km the bottom change is very small and the values are close to zero showing no significant bottom change. This is also in agreement with observations. In the eastern part of the bay at Y>22 km the bottom change starts to decrease with a mean rate of 20 cm for the extreme condition resulting in accumulation for the eastern part of the bay. This is well matched with the visual observations.

In figures 43 and 44 there is sometimes a mixed behavior in the cross-shore direction, with both erosion and accretion along a profile line. In general, one may expect a similar response along the profile, although it may vary depending on the hydrodynamic conditions. Deviations from the former type of behavior may have several reasons, including improper default values in the sediment transport models (some values are based on laboratory experiments and not field data), neglect of the vertical structure in the water column (important for cross-shore sediment transport), and complex geometry in the bay. However, the total results are fairly well in agreement with the present situation in Ystad Bay.

After summing up all the scenarios, the total bottom change in Ystad Bay based on all the wave directions is shown in figure 44.

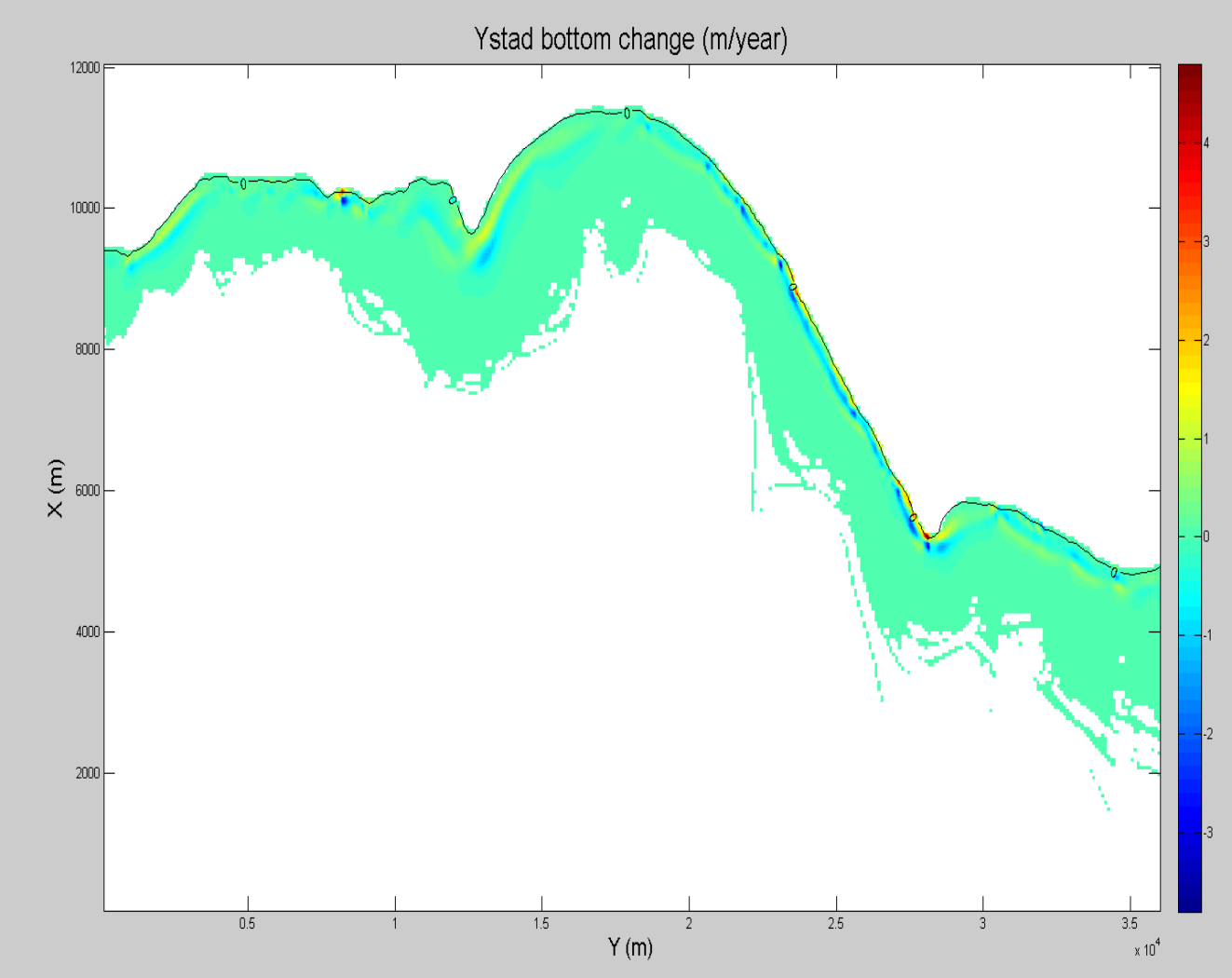

Figure 44. Bottom change in Ystad (m/year), including all wave scenarios

Figure 44 displays the net result of all the waves and the total bottom change in Ystad Bay based on all the wave scenarios. The results show that similar to scenario 15, erosion mainly takes place in the western part of Ystad bay, with slightly high values at the location of coastline orientation. There is not a notable bottom change in the middle of the bay and it is also indicated that accretion mainly starts from the middle part of Ystad bay at Y=20 km.

7 Conclusions

The major conclusions derived from this study are summarized in the following:

- The application of the numerical models for the simulation of waves, currents and sediment transport is generally an appropriate method for the investigation of the present and future hydrodynamic conditions of the bay.
- The wave generation results from SWAN and EBED–modified model are fairly similar and valid for the entire basin.
- Choosing an extended bathymetry for the basin in SWAN application can solve the errors in the wave calculations caused by the lateral boundaries.
- The results from the sediment transport calculations and bottom topography change assessment are in good agreement with observations.
- The orientation of the shoreline with respect to the grid can cause errors in the numerical models in terms of current generation and sediment transport. Therefore, some improvements of the model is needed in this respect. (not discussed before)
- Based on the wind-generated waves from the Baltic Sea, the south Swedish coast, and particularly Ystad Bay, will keep experiencing eastern-directed transport with erosion in the western part of the bay and accumulation in the eastern part.
- Due to the high speed of erosion in the western part of Ystad, more coastal protection is needed.

References

Battjes, J. A. & Janssen, J. P. F. M., 1978. Energy loss and set-up due to breaking of random waves, Proc. 16 th Conf. Coastal Engineering (Hamburg), New York, ASCE , pp. 569–587

Bird, E.C., 1985. "Coastline Changes. A Global Review," John Wiley and Sons, Chichester.

Bird, E.C. & Schwartz, M.L., 1985. "The World's Coastline," Van Nostrand Reinhold Company, New York.

Booij.N. & L.H. Holthuijsen., 1999. A third- generation wave model for Coastal regions, Part I, Model description and validation ,j. geophys. Res., Volume, 104, pp. 7649-7666

Bowen, A.J., 1969. The generation of longshore currents on a plane beach, Journal of Marine Research, Volume, 27, pp. 206-215

Camenen, B. & larroude, P., 2003. Comparison of sediment transport formula for the coastal environment. Coastal Engineering, Volume 48, pp. 111-132.

Camenen, B. & Larson, M., 2005. A general formula for non-cohesive bed load sediment transport in Estuarine, Coastal and Shelf Science, Volume, 63, pp. 249-260.

Camenen, B. & Larson, M., 2007. A unified sediment transport formulation for coastal inlet application. Technical report ERDC/CHL CR-07-1, US Army Engineer Research and Development Center, Vicksburg, MS.

Camenen, B. & Larson, M., 2008. A general formula for noncohesive suspended sediment transport. Journal of Coastal Research, Volume 24, pp. 615-627.

Dally, W. R. & Brown, C. A., 1995. A modeling investigation of the breaking wave roller with application to cross-shore currents. Journal of Geophysical Research, Volume100, pp. 24873-24883.

Deltawerken, 2004. [Online]
Available at: http://www.deltawerken.com/Lock-and-bridge/425.html
[Accessed 2010].

Hanson, H. & Kraus, N. C., 1989. GENESIS: Generalized model for simulating shoreline change, Report 1: Technical Reference. Technical Report CERC-89-19, U.S. Army Engineer Waterways Experiment Station, Coastal Engineering Research Center, Vicksburg, MS.

Hanson, H. & Larson, M., 2010. Implication of extreme waves and water levels in the southern Baltic Sea. Journal of Hydraulic Research, Volume 46, pp. 292-302.

Hanson, H. & Larson, M., 2010. Implication of extreme waves and water levels in the southern Baltic Sea. Journal of Hydraulic Research, Volume 46, pp. 292-302.

Hoan, l. X. et al., 2010. Modeling shoreline evolution at Hai Hau Beach, vietnam. Journal of coastal research, Volume 26, pp. 31-43.

Holthuijsen, L. H., 2010. The SWAN wave model. In: Waves in Oceanic and Coastal Waters. Delft: Cambridge University Press, pp. 286-309.

Larson, M., Camenen, B. & Nam, P. T., 2010. A unified sediment transport model for inlet application. Journal of coastal research.

Larson, M. & Hanson, H., 2010. Coastal Erosion and Protection in Sweden

Larson, M. & Hanson, H., 2011. Extreme Waves and Water Levels in the Southern Baltic Sea: Implication for Flooding and Dune Erosion at Present and Future Conditions, Lund: Lund University.

Nam, P. T., 2010. Numerical Model of Beach Topograghy Evolution due to Waves and Currents, Special Emphasis on Coastal Structures. Lund: Lund university.

Nam, P. T. & Larson, M., 2010. Model of nearshore waves and wave-induced currents around detached breakwater. Journal of Waterway, Port, Coastal and Ocean Enigineeing, Volume 136 , pp. 156-176.

Nam, P. T., Larson, M., Hanson, H. & Hoan, L. X., 2009. A numerical model of nearshore waves, currents, and sediment transport. Journal of Coastal Engineering, Volume 56, pp. 1084-1096.

Nam, P. T., Larson, M., Hanson, H. & Hoan, L. X.,. 2010. A numerical model of beach morphological evolution due to waves and currents in the vicinity of coastal structures. Journal of Coastal Engineering(under review).

Street, S. I., 2011. A wave atlas over the south-eastern coast of Sweden, M.Sc thesis report, TVVR 11/5007. Lund: Lund University.

Thornton, E.B., 1970. Variation of longshore current across the surf zone. Proceeding 12th International Conference on coastal Engineering, ASCE, Washington D.C., pp. 291-308

Appendix A

Wave Generation Results from SWAN

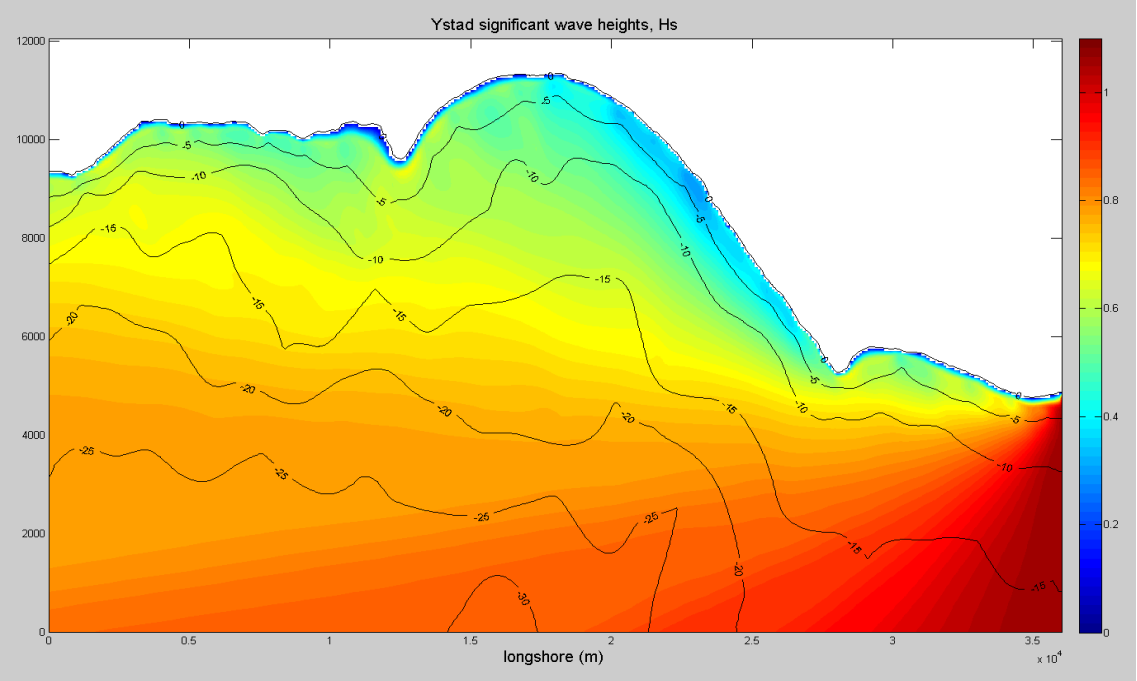

Figure A1. Scenario 1 with the initial Hs=1.06m at offshore

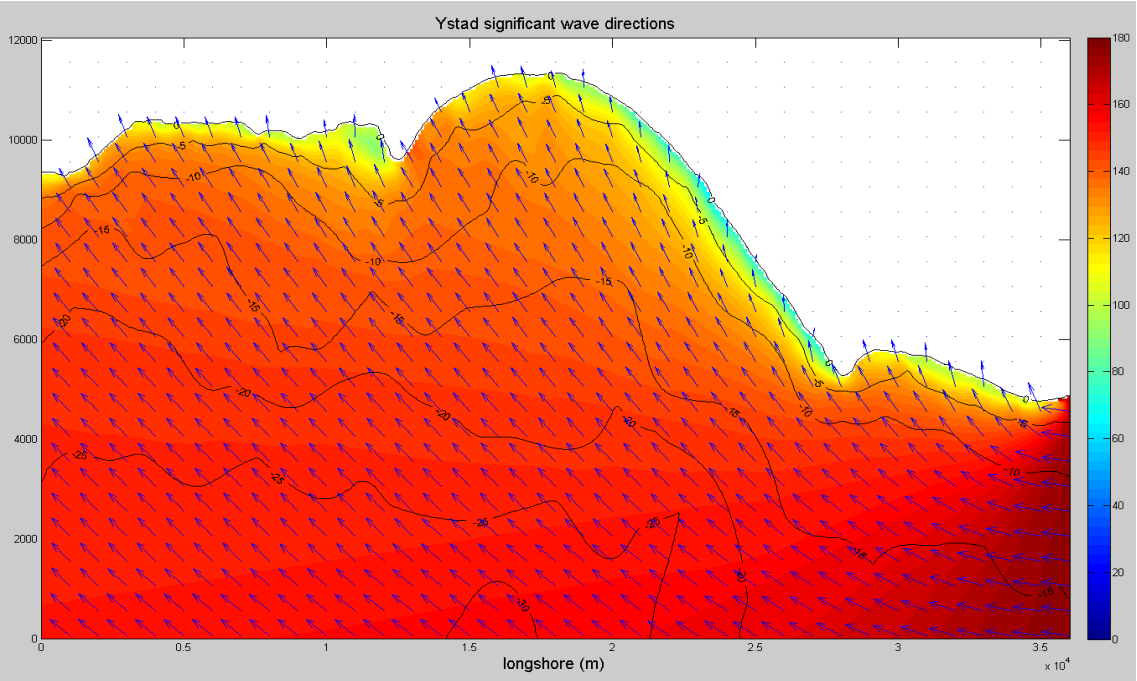

Figure A2. Wave Directions for Ystad Bay, Scenario 1 with the initial direction($\theta=175^{0}$) at offshore

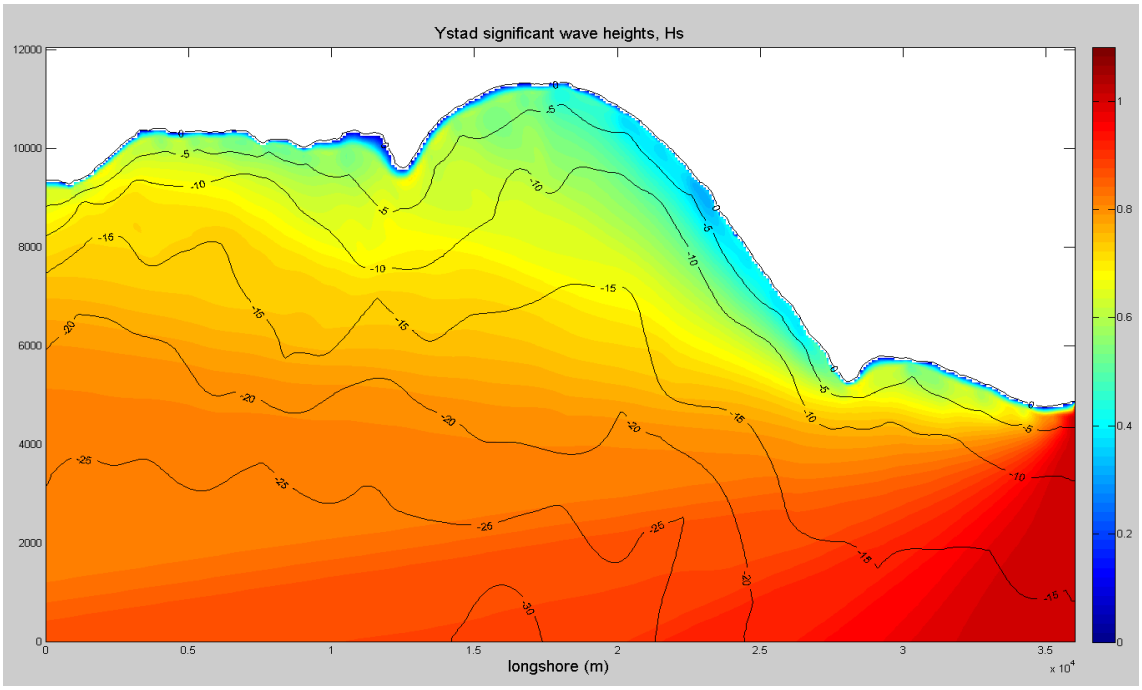

Figure A3. Scenario 2 with the initial Hs=1.01m at offshore

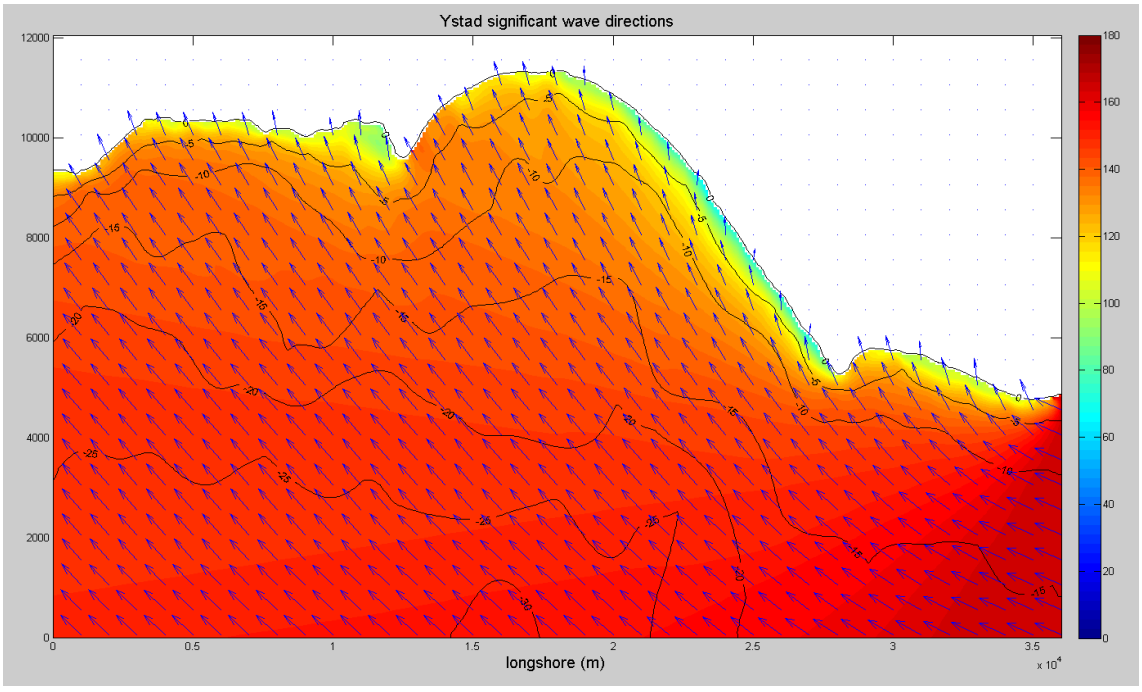

Figure A4. Wave Directions for Ystad Bay, Scenario 2 with the initial direction(θ=166 ^{0}) at offshore

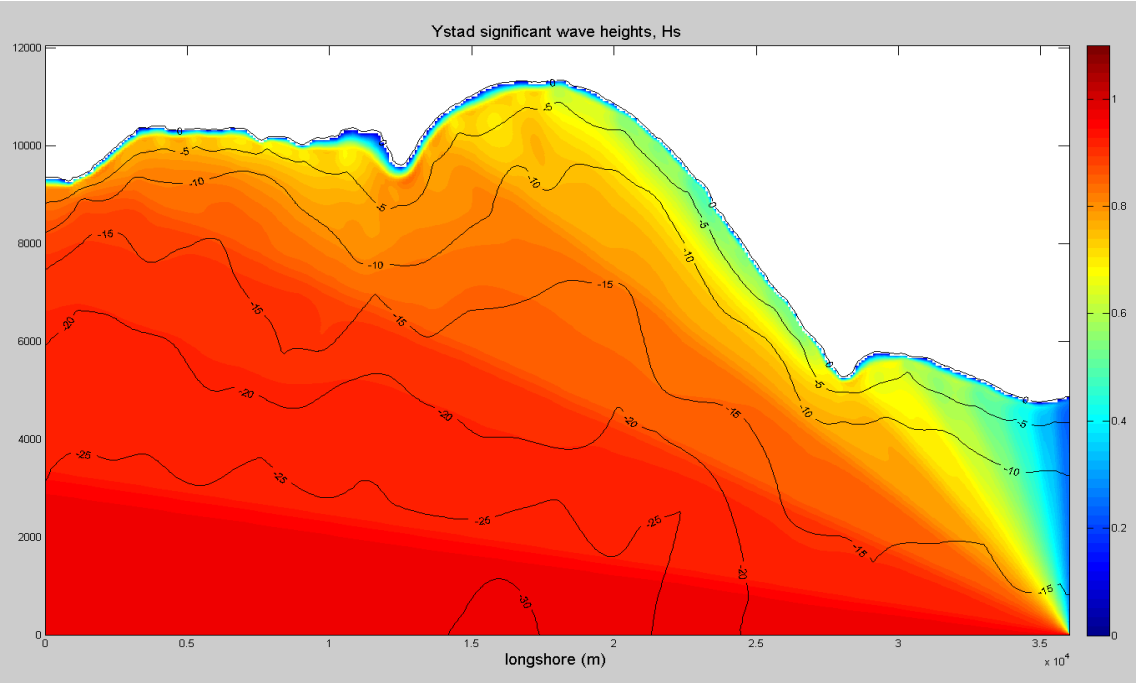

Figure A5. Scenario 4 with the initial Hs=1.07m at offshore

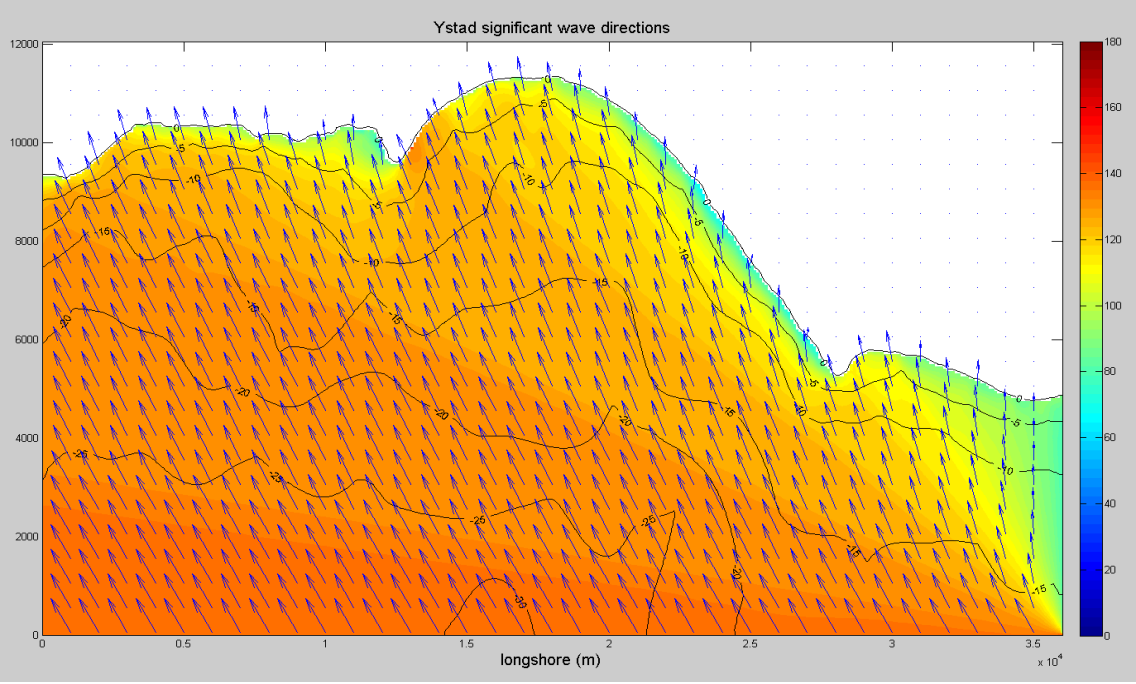

Figure A6. Wave Directions for Ystad Bay, Scenario 4 with the initial direction(θ=145 ^{0}) at offshore

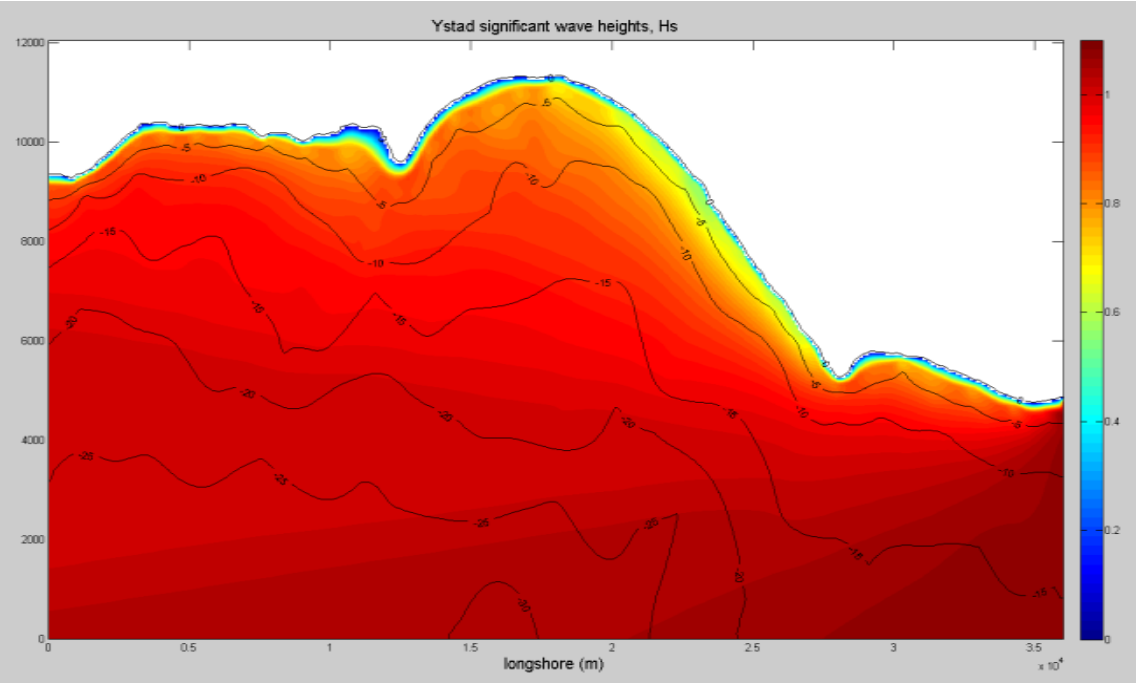

Figure A7. Scenario 5 with the initial Hs=1.07m at offshore

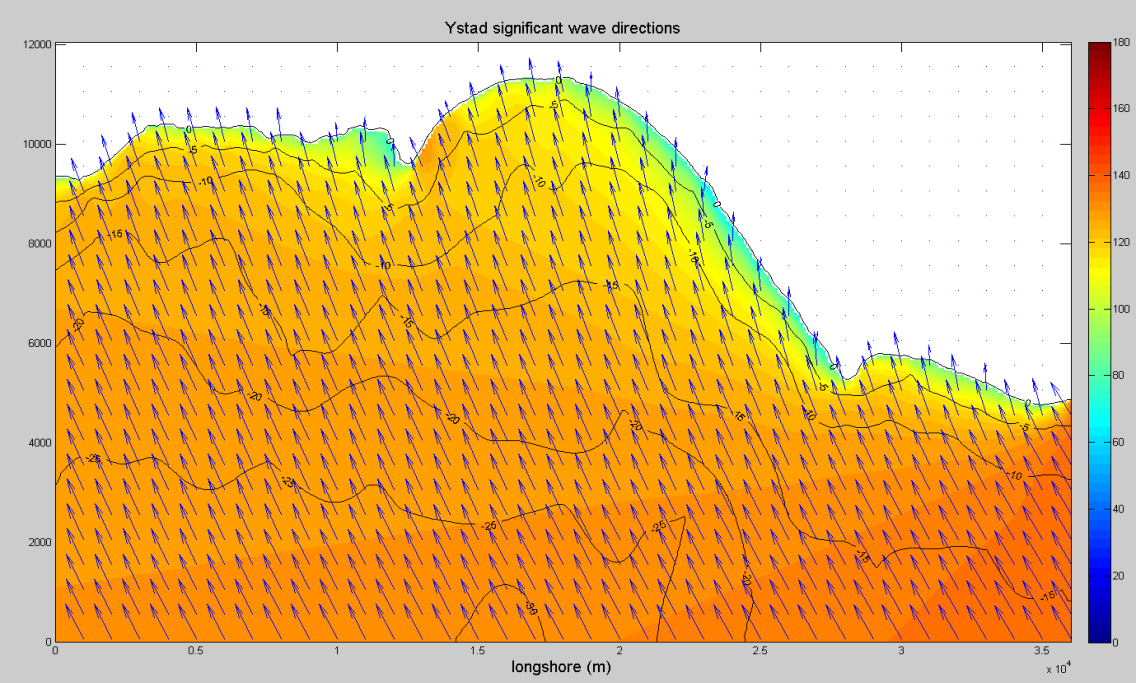

Figure A8. Wave Directions for Ystad Bay, Scenario 5 with the initial direction($\theta=136^{0}$) at offshore

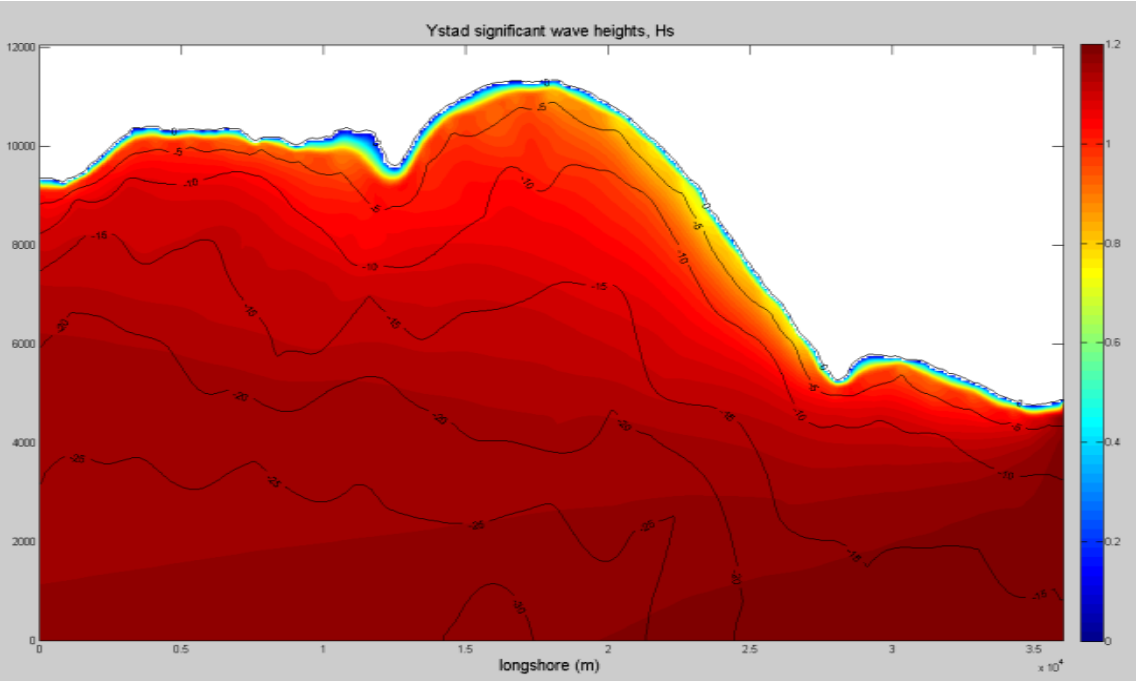

Figure A9. Scenario 6 with the initial Hs=1.19m at offshore

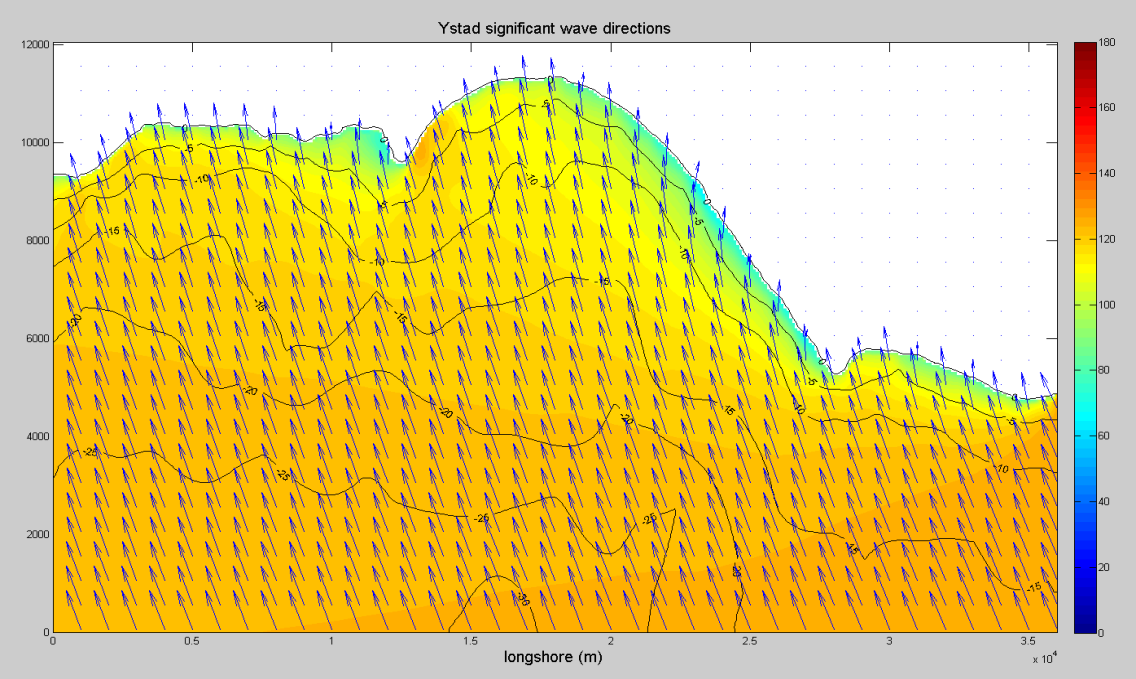

Figure A10. Wave Directions for Ystad Bay, Scenario 6 with the initial direction(θ=126 ^{0}) at offshore

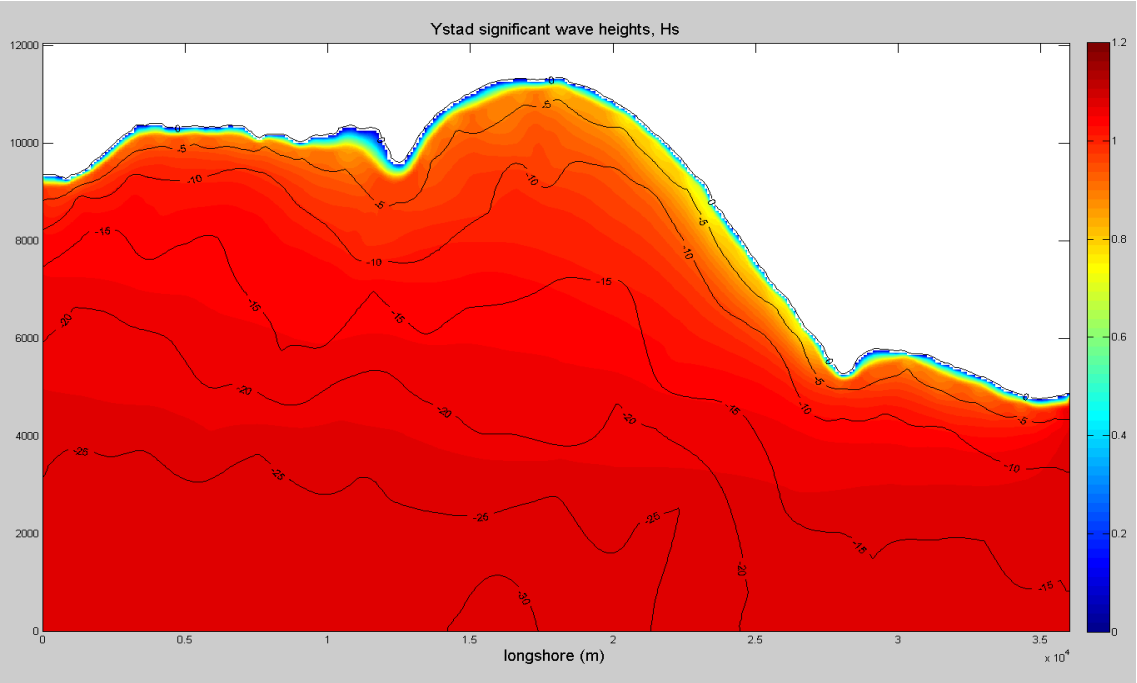

Figure A11. Scenario 7 with the initial Hs=1.08m at offshore

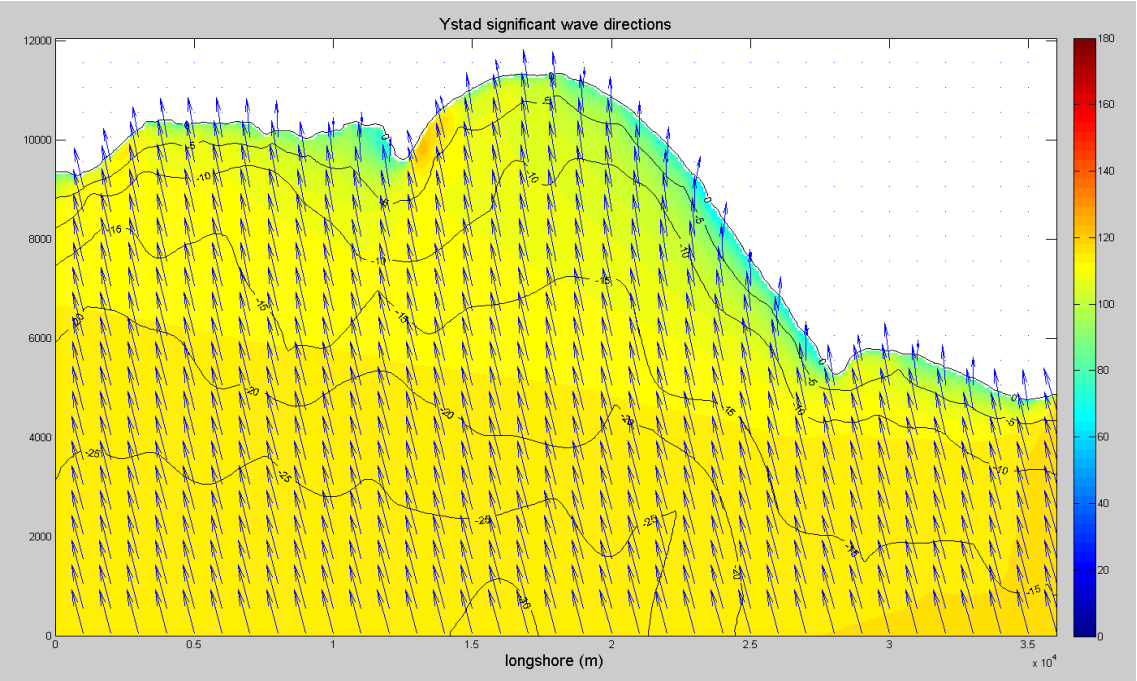

Figure A12. Wave Directions for Ystad Bay, Scenario 7 with the initial direction(θ=115 ^{0}) at offshore

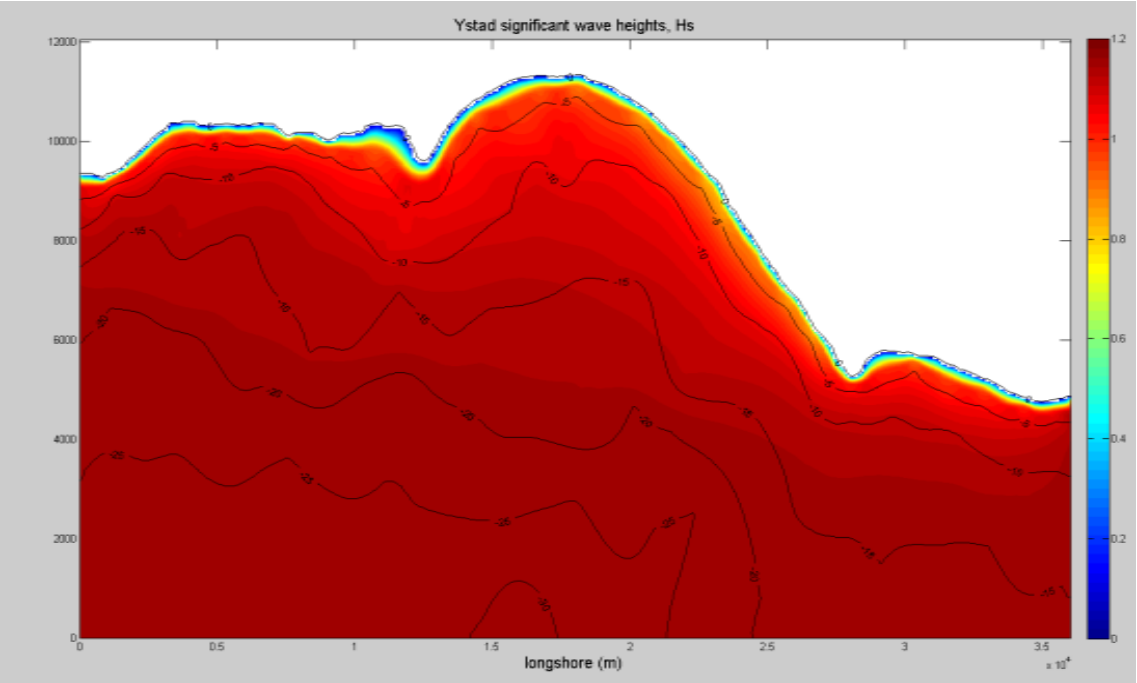

Figure A13. Scenario 8 with the initial Hs=1.16m at offshore

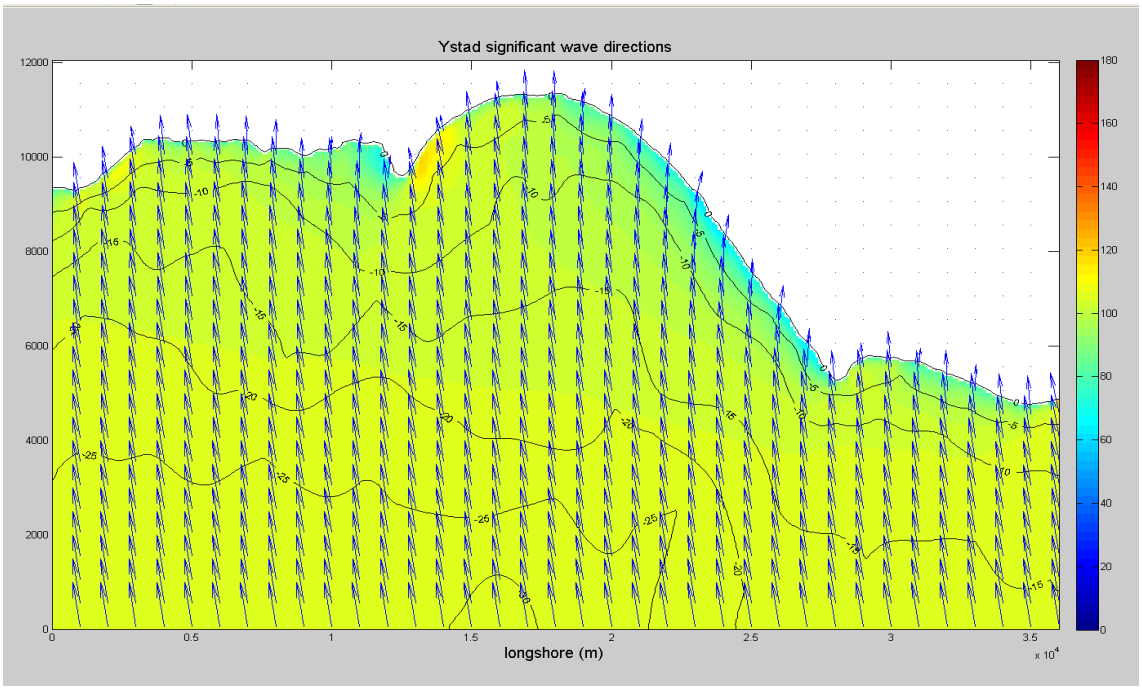

Figure A14. Wave Directions for Ystad Bay, Scenario 8 with the initial direction($\theta=105^{0}$) at offshore

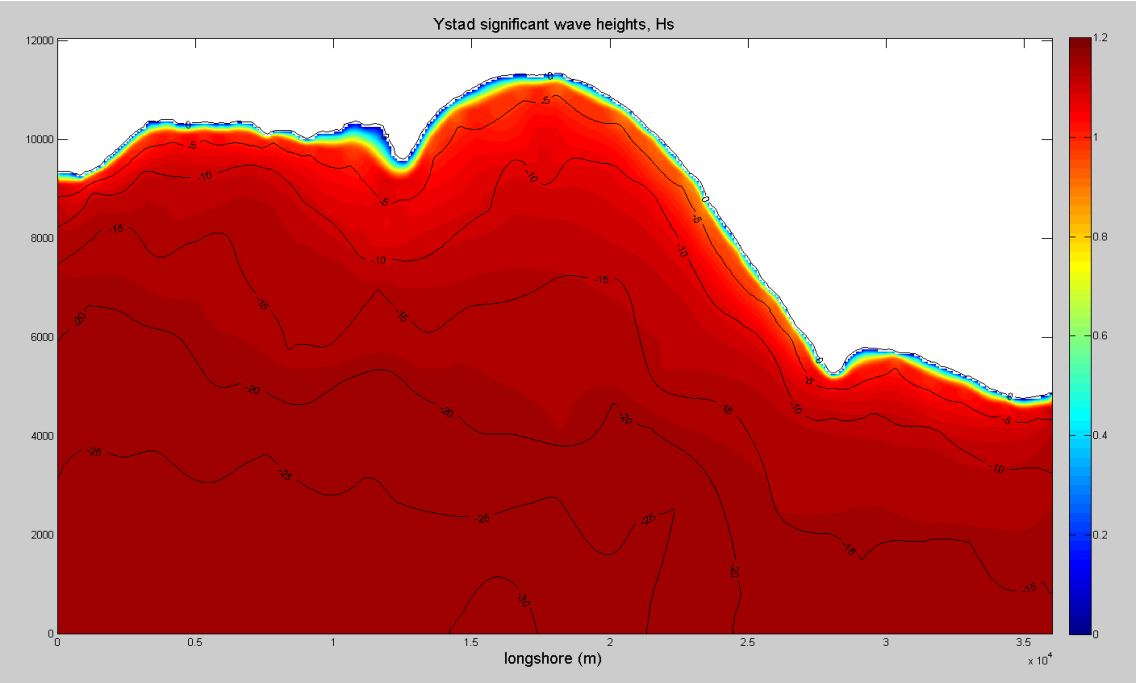

Figure A15. Scenario 9 with the initial Hs=1.15m at offshore

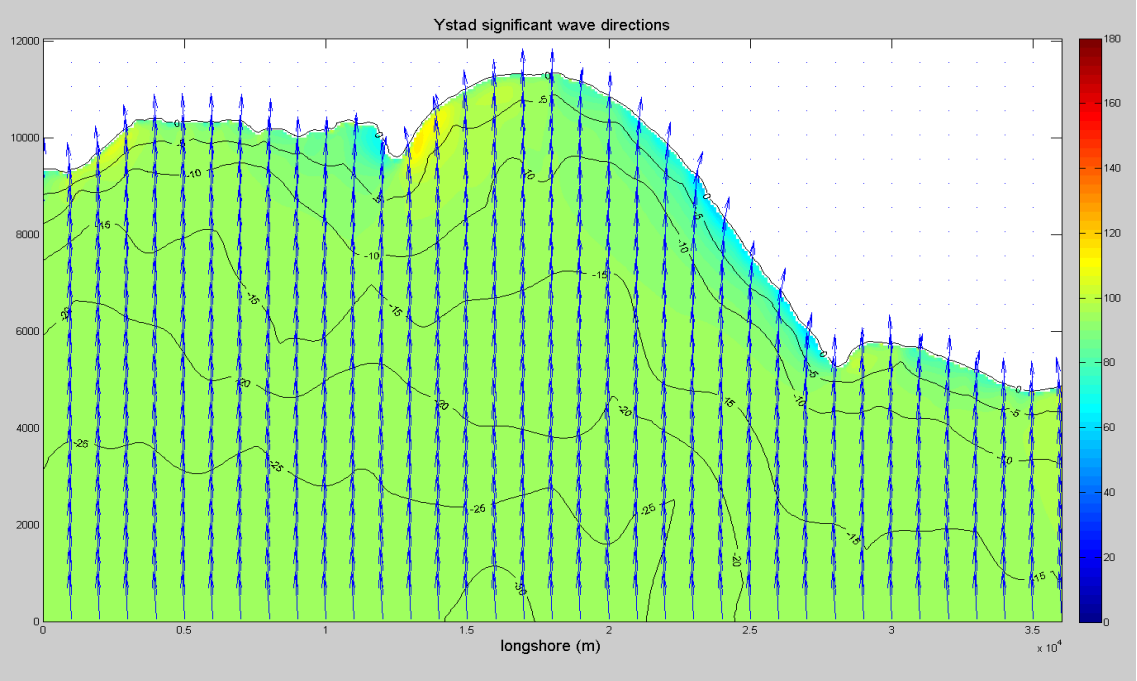

Figure A16. Wave Directions for Ystad Bay, Scenario 9 with the initial direction (θ=95 ^{0}) at offshore

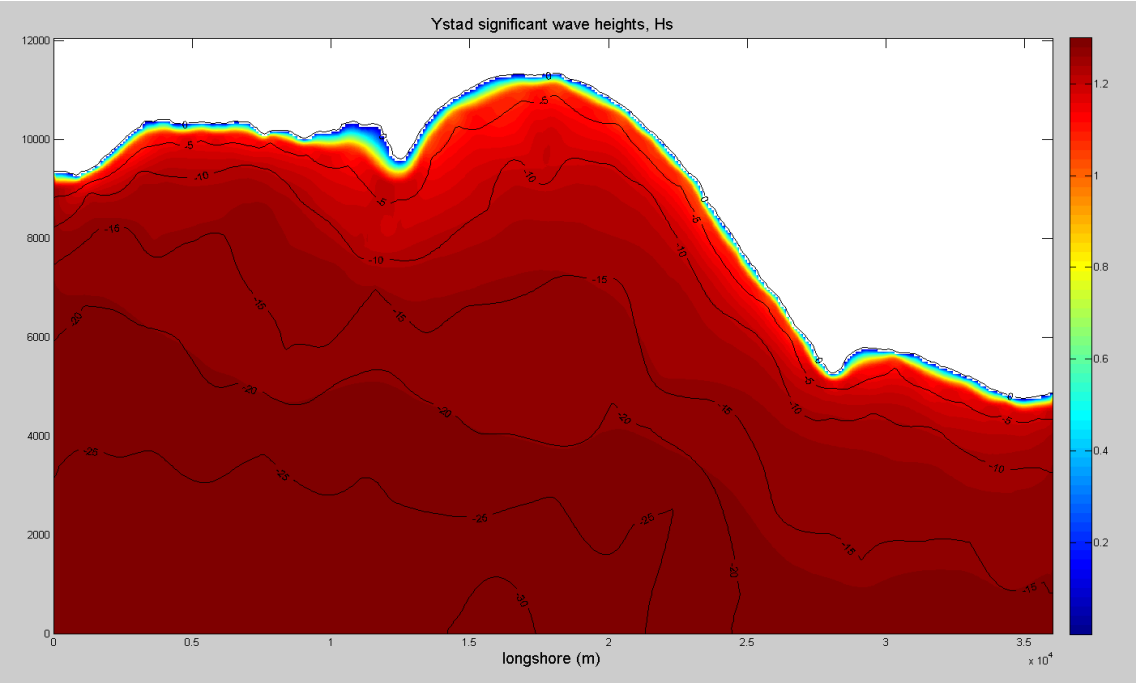

Figure A17. Scenario 10 with the initial Hs=1.28m at offshore

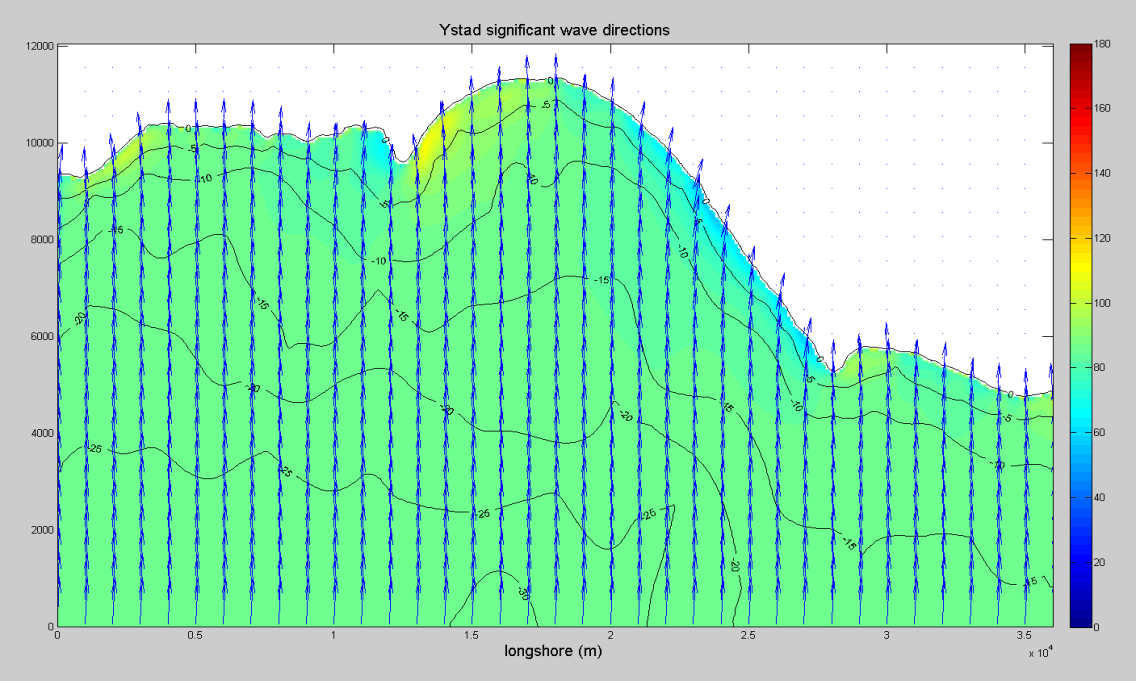

Figure A17. Scenario 10 with the initial Hs=1.28m at offshore

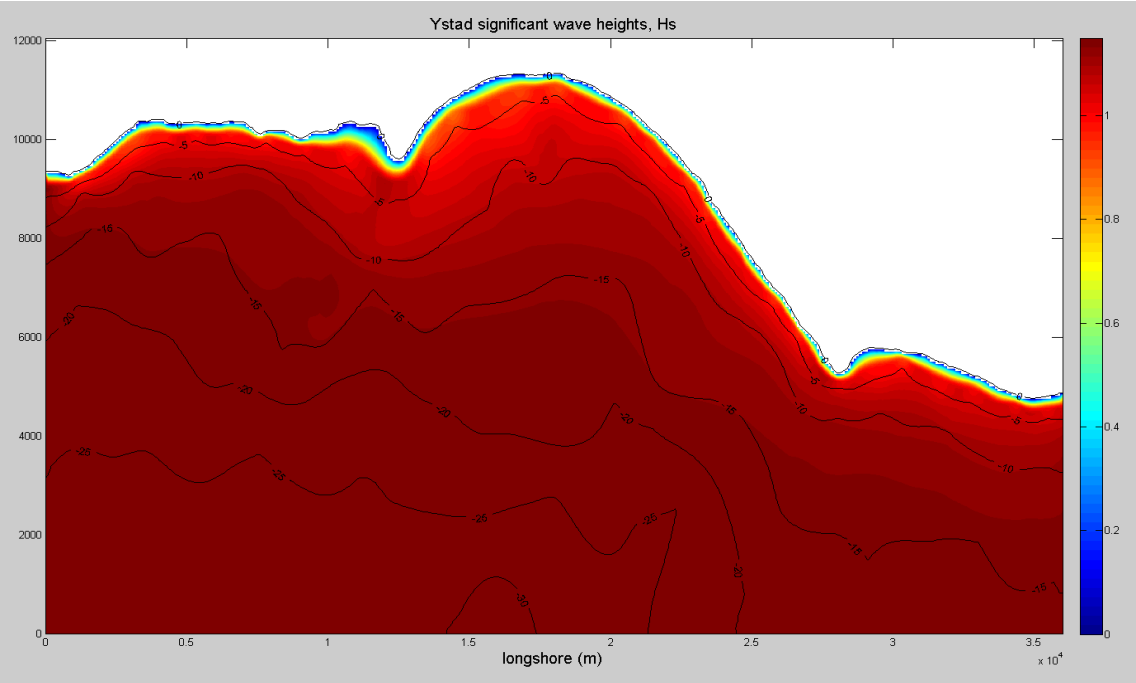

Figure A19. Scenario 11 with the initial Hs=1.14m at offshore

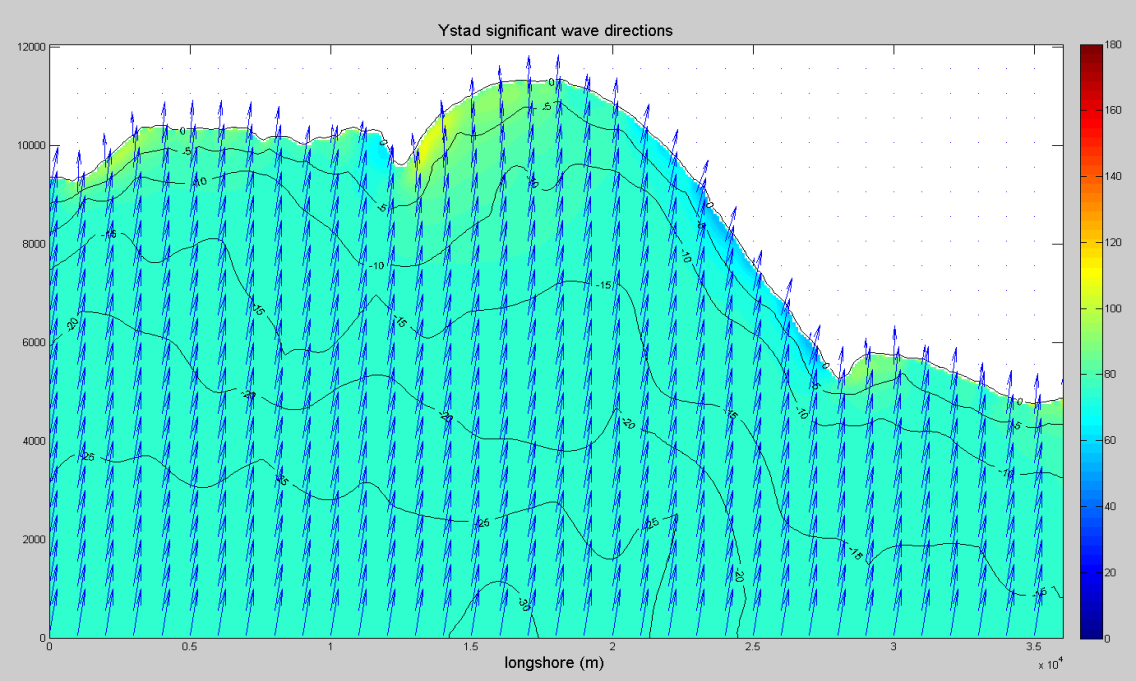

Figure A20. Wave Directions for Ystad Bay, Scenario 11 with the initial direction(θ=74 ^{0}) at offshore

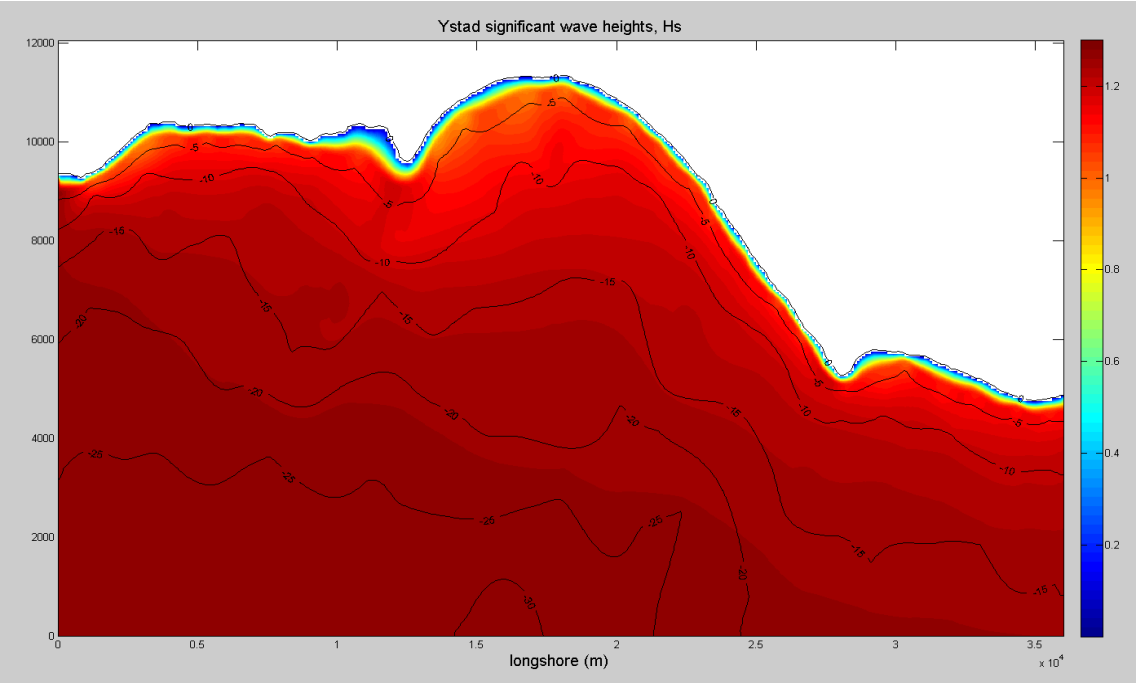

Figure A21. Scenario 12 with the initial Hs=1.26m at offshore

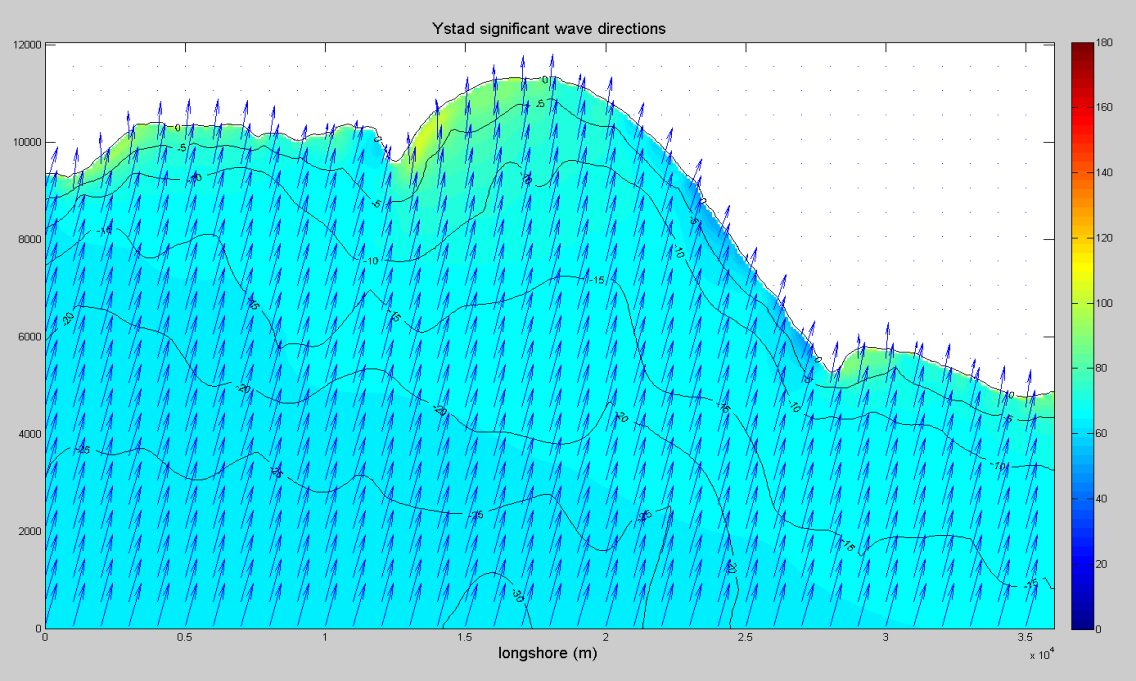

Figure A22. Wave Directions for Ystad Bay, Scenario 12 with the initial direction(θ=64 ^{0}) at offshore

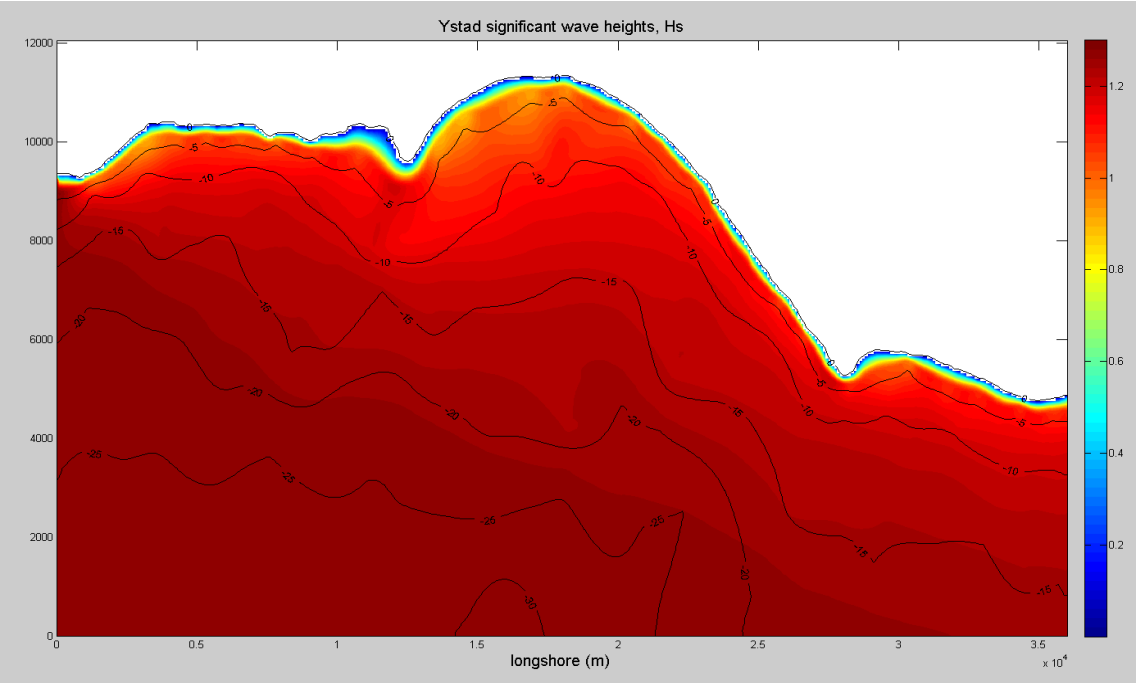

Figure A23. Scenario 13 with the initial Hs=1.27m at offshore

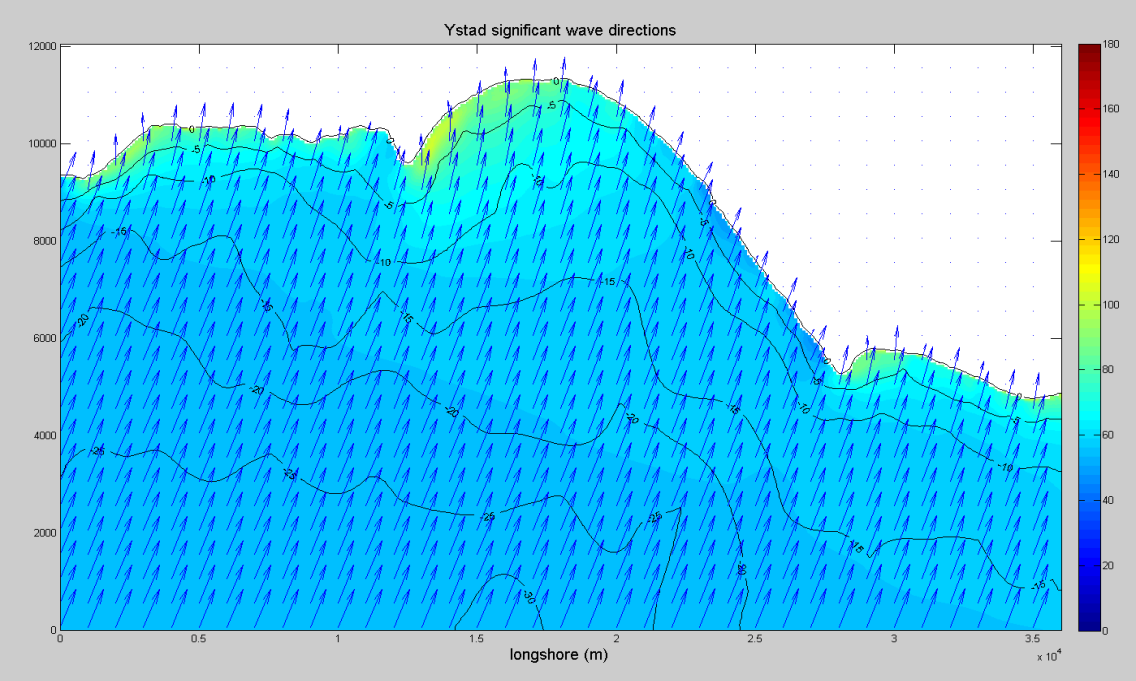

Figure A24. Wave Directions for Ystad Bay, Scenario 13 with the initial direction(θ=54 ^{0}) at offshore

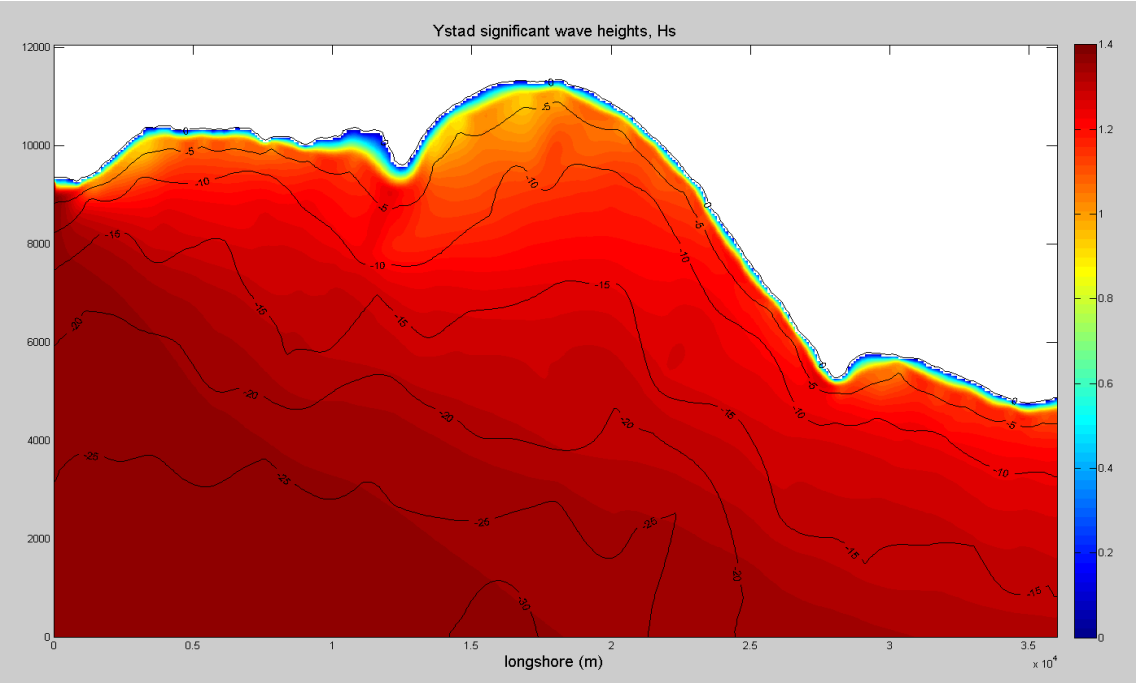

Figure A25. Scenario 14 with the initial Hs=1.36m at offshore

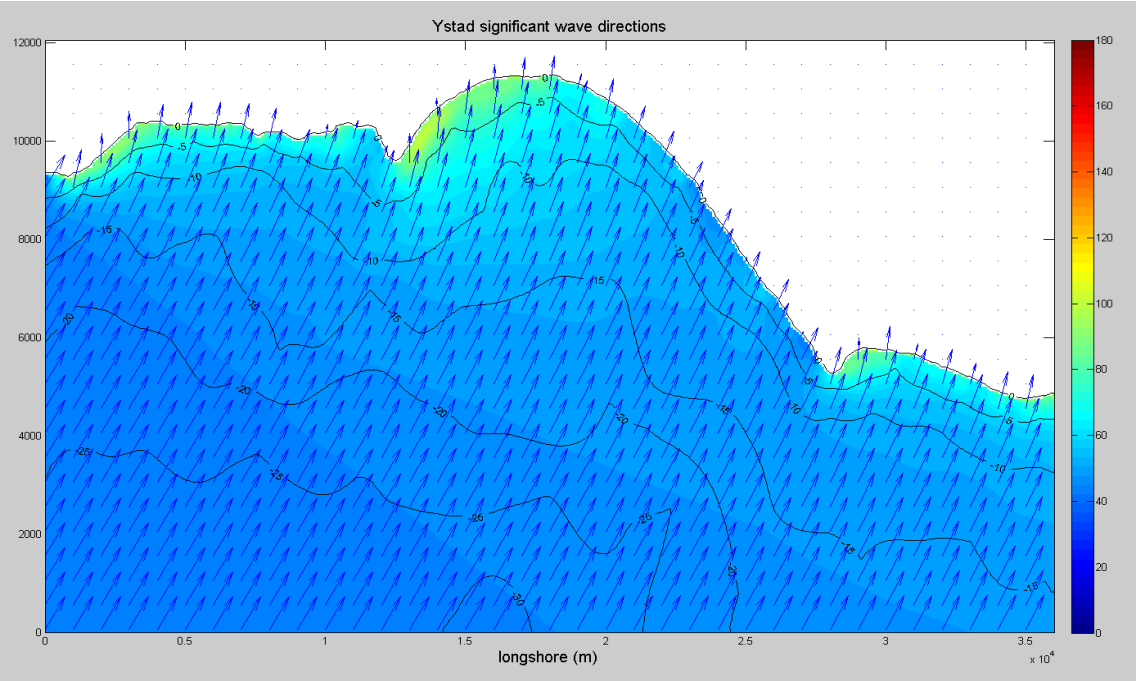

Figure A26. Wave Directions for Ystad Bay, Scenario 14 with the initial direction (θ=44 ^{0}) at offshore

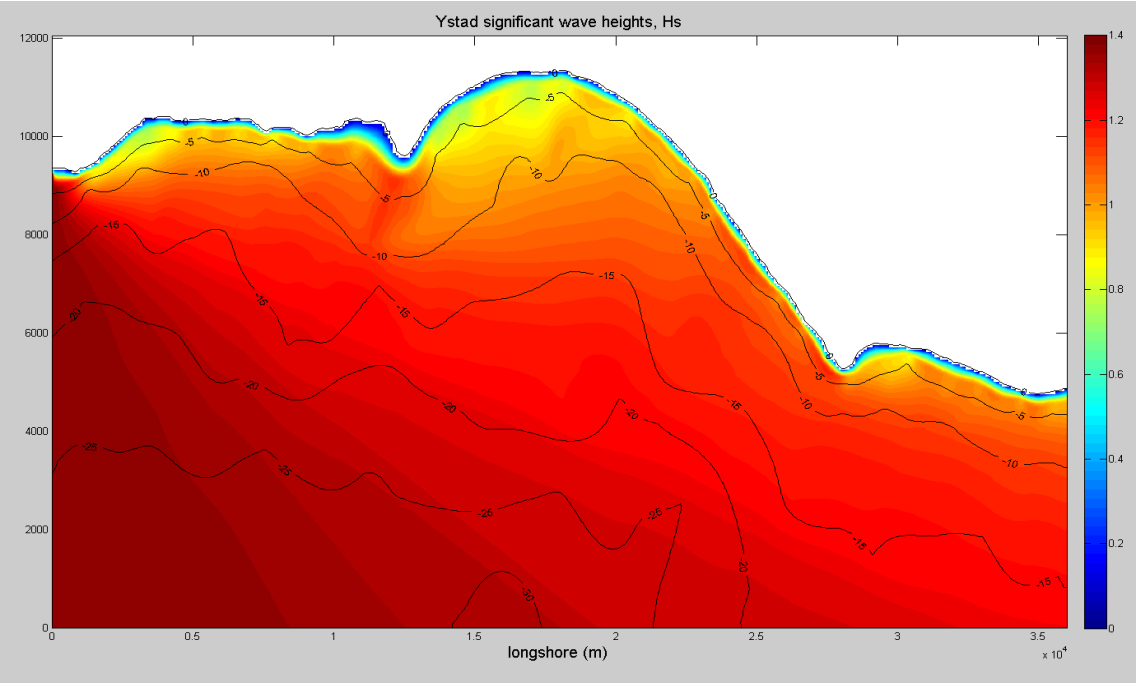

Figure A27. Scenario 16 with the initial Hs=1.36m at offshore

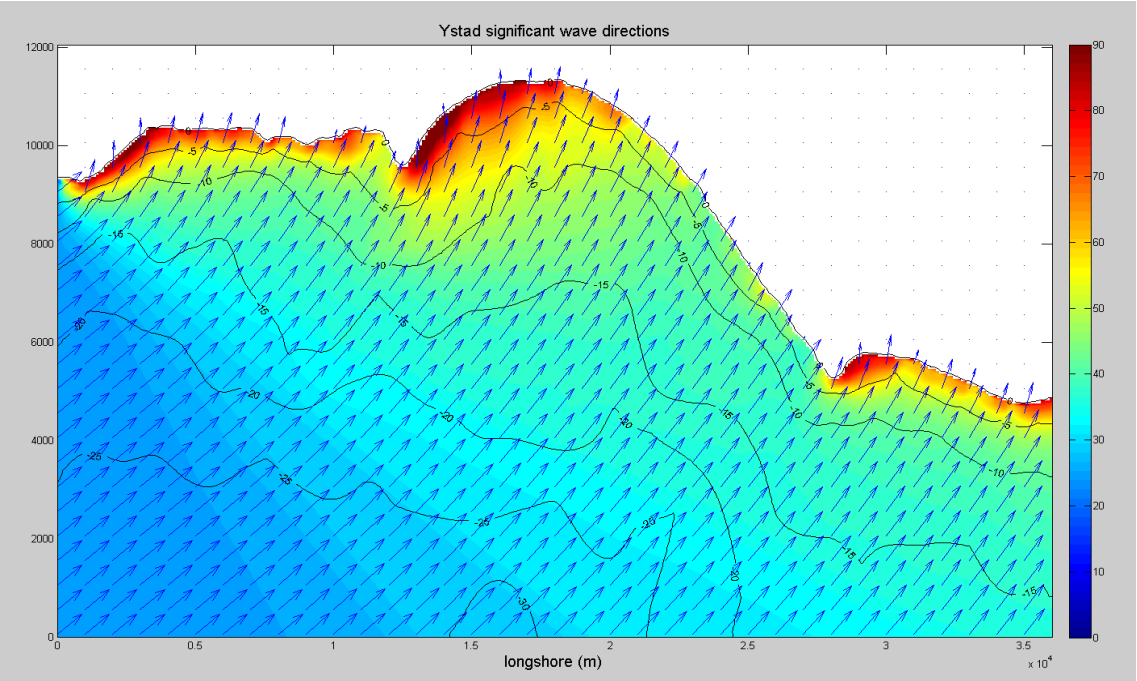

Figure A28. Wave Directions for Ystad Bay, Scenario 16 with the initial direction (θ=25 ^{0}) at offshore

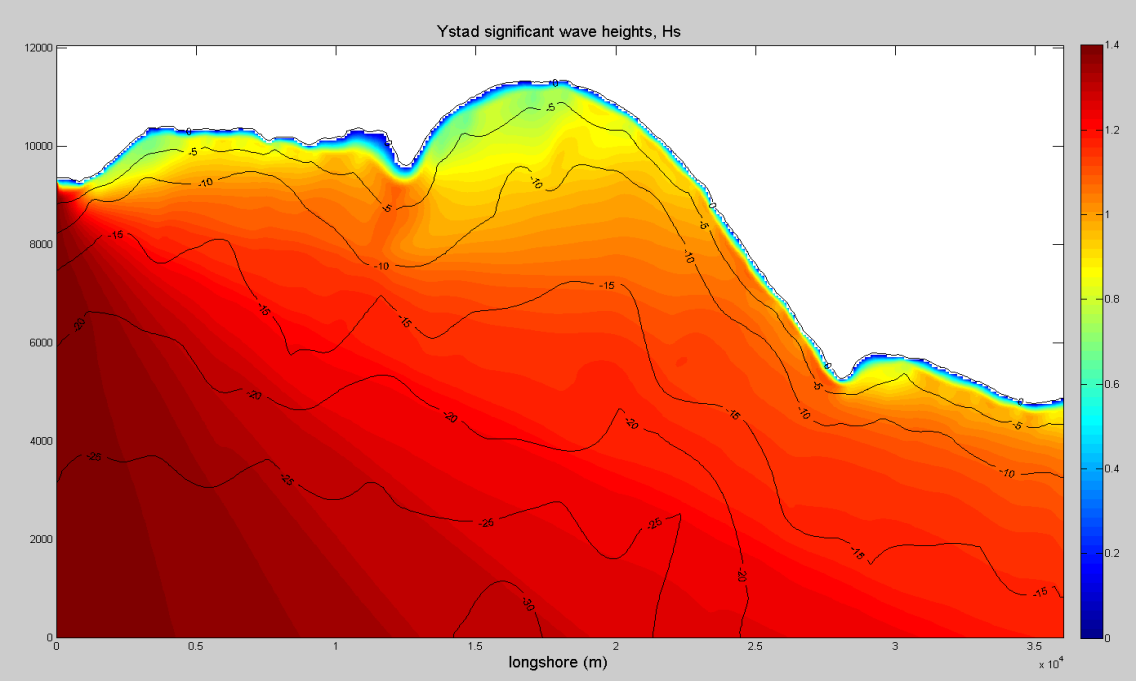

Figure A29. Scenario 17 with the initial Hs=1.38m at offshore

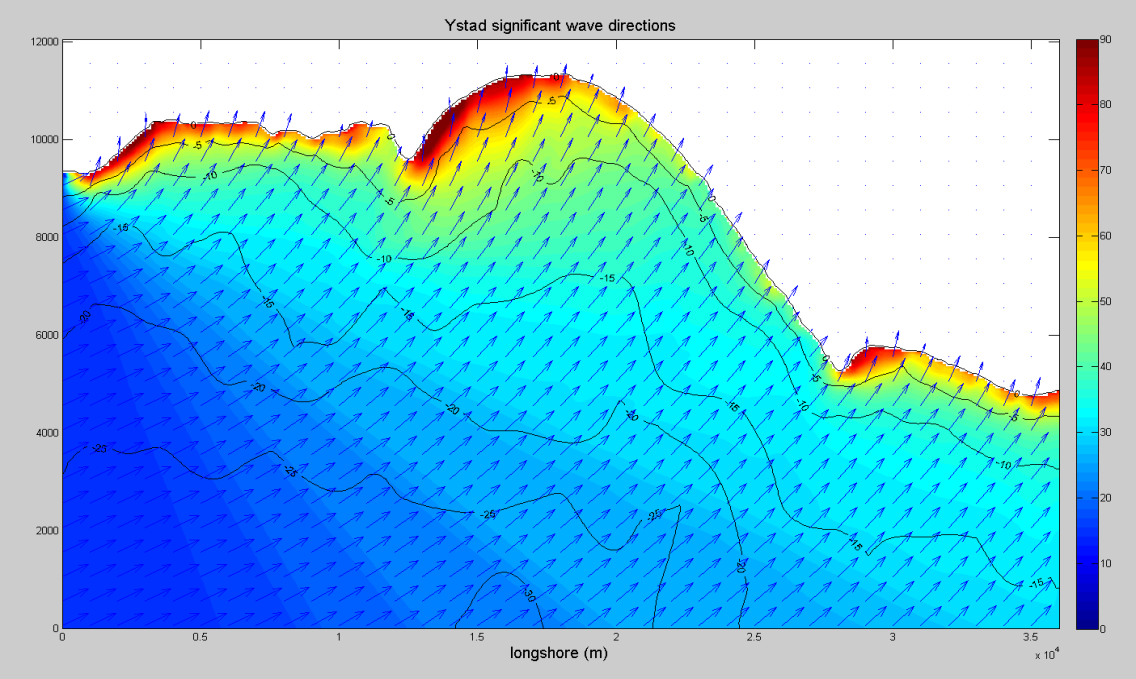

Figure A30. Wave Directions for Ystad Bay, Scenario 18 with the initial direction (θ=15 ^{0}) at offshore

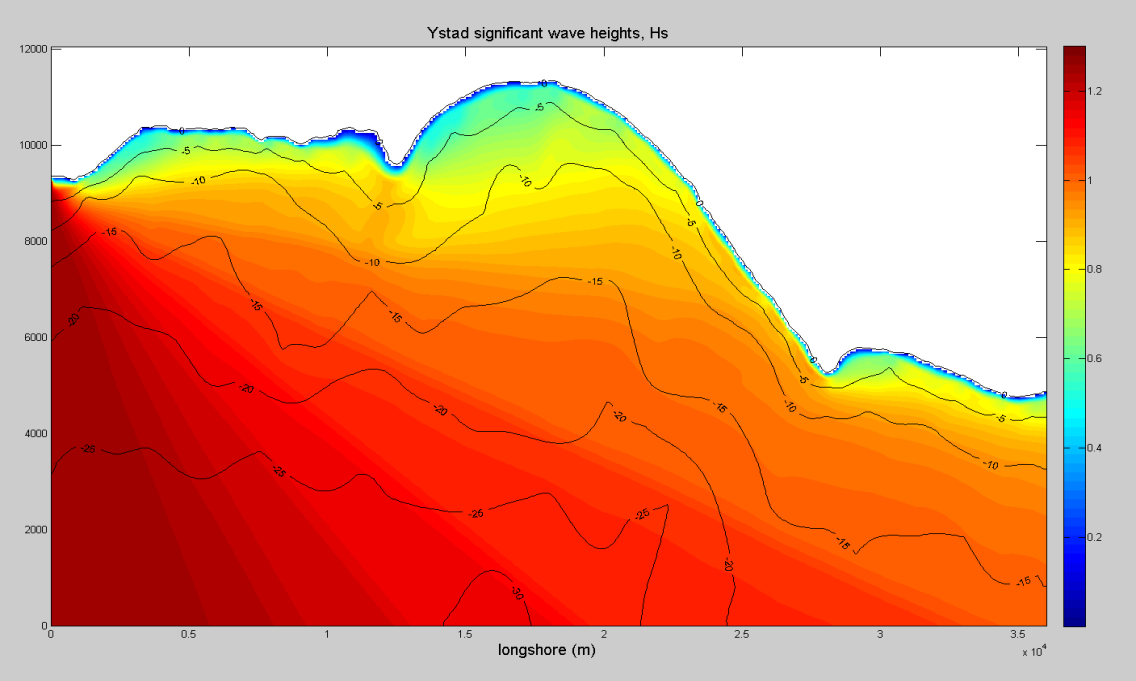

Figure A31. Scenario 18 with the initial Hs=1.24m at offshore

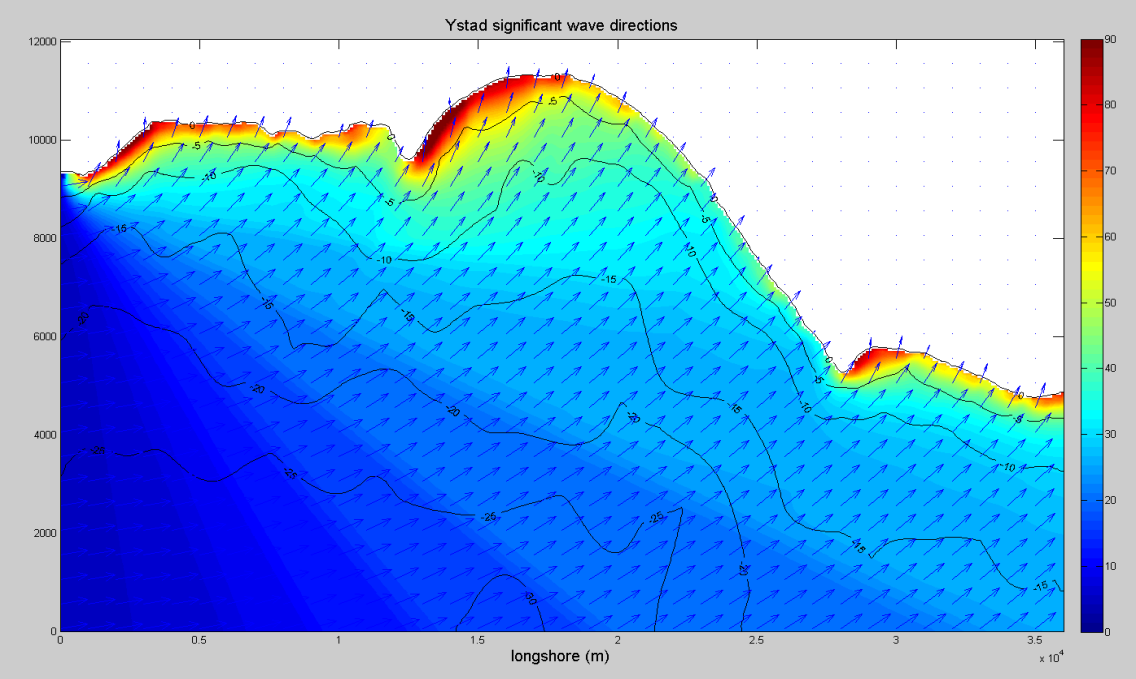

Figure A32. Wave Directions for Ystad Bay, Scenario 18 with the initial direction (θ=5 ^{0}) at offshore

Appendix B

Wave Generation Results from EBED-Modified

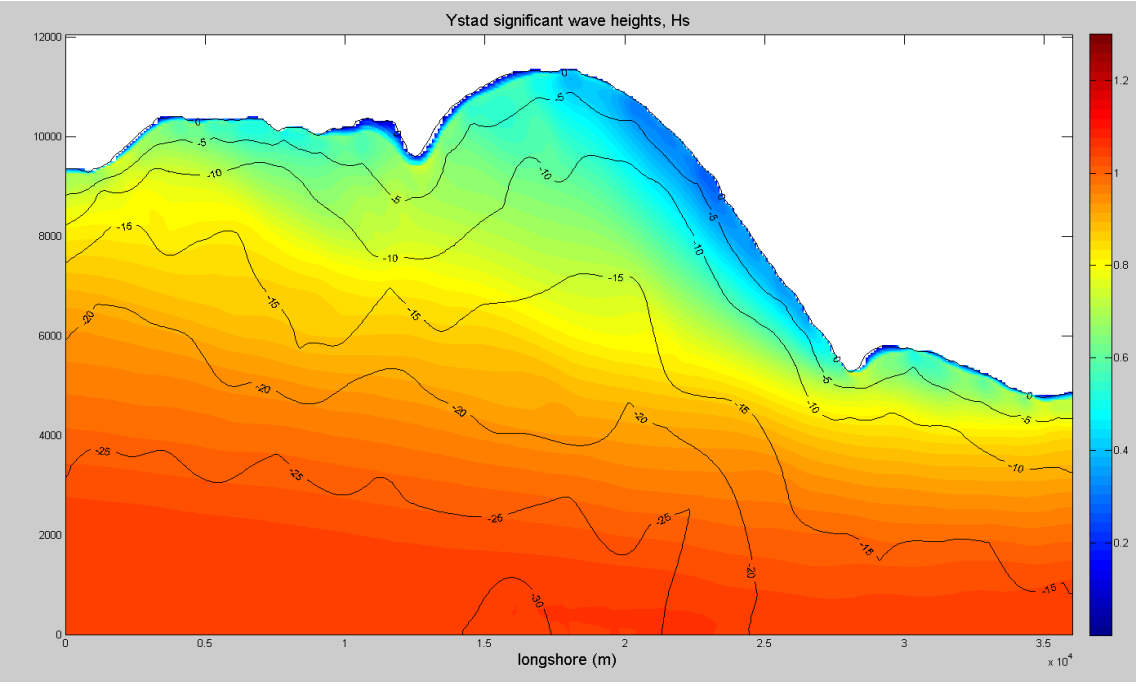

Figure B1. Scenario 1 with the initial Hs=1.06m at offshore

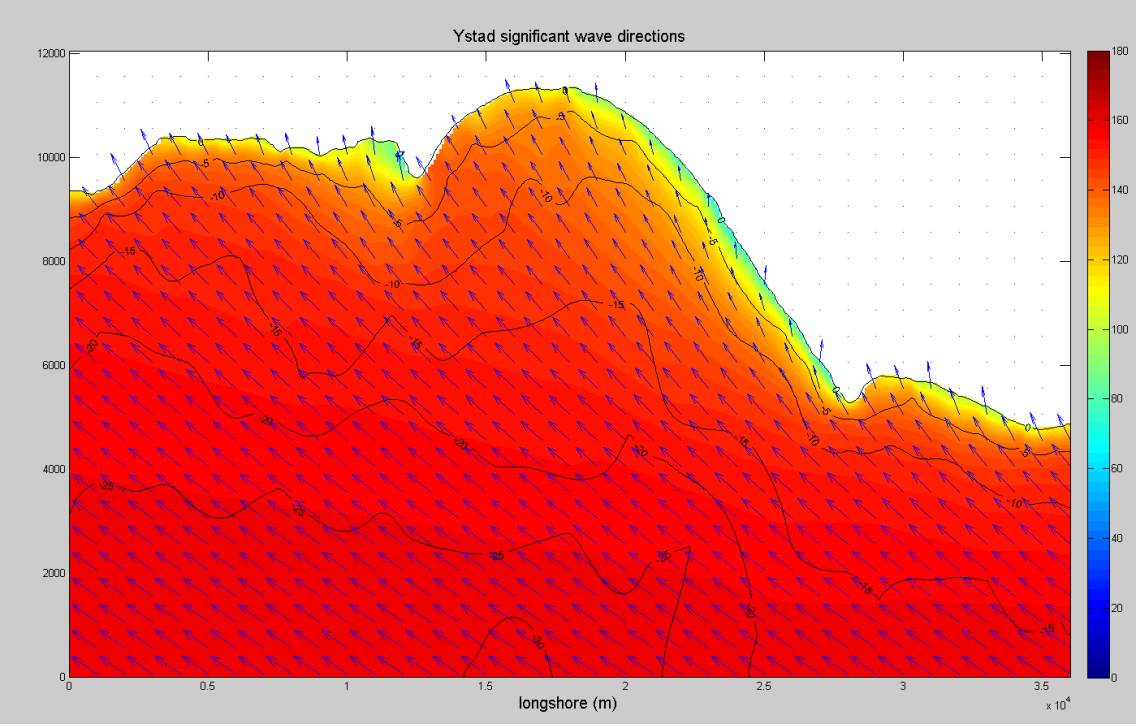

Figure B2. Wave Directions for Ystad Bay, Scenario 1 with the initial direction(θ=175 ^{0}) at offshore

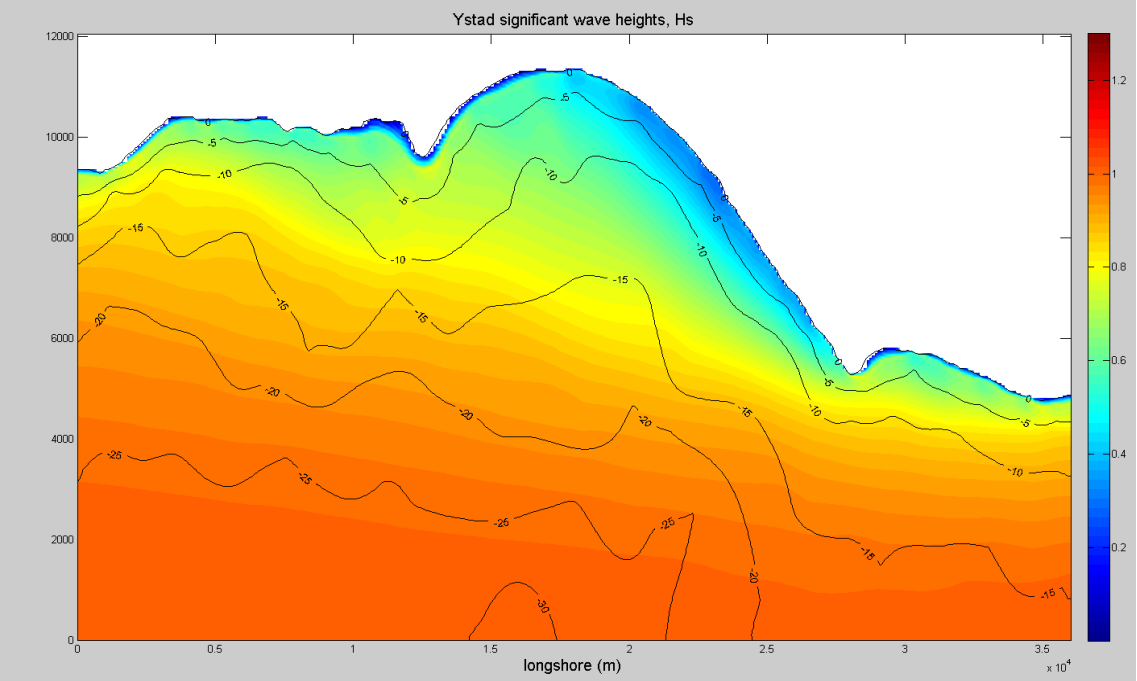

Figure B3. Scenario 2 with the initial Hs=1.01m at offshore

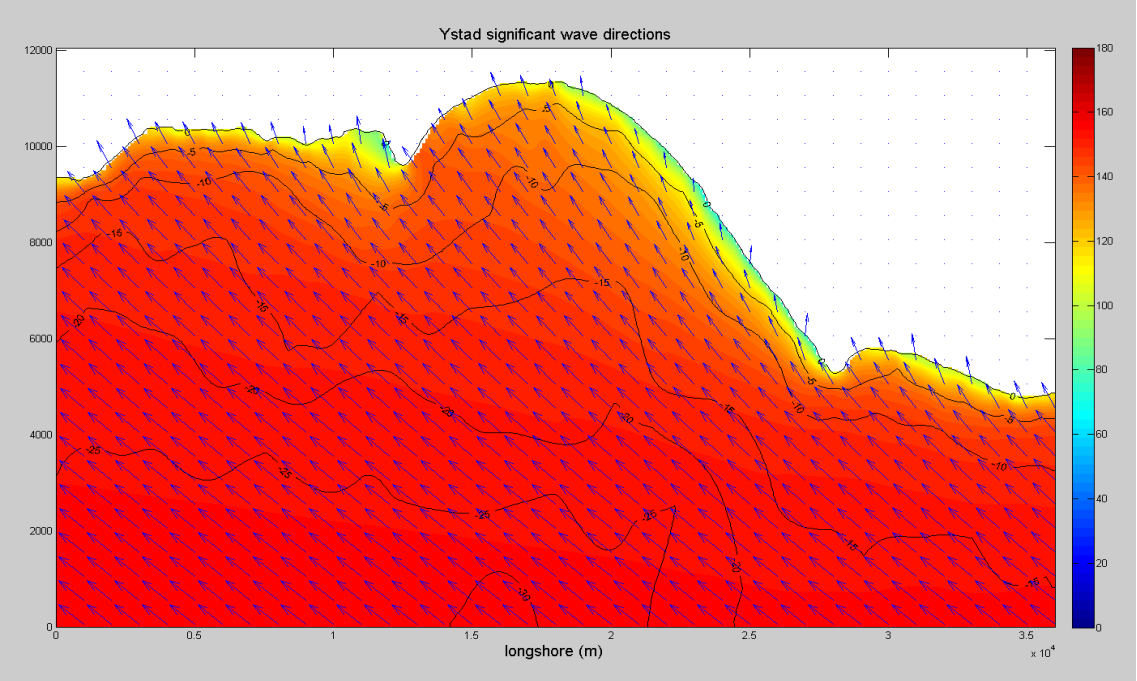

Figure B4. Wave Directions for Ystad Bay, Scenario 2 with the initial direction(θ=166 ^{0}) at offshore

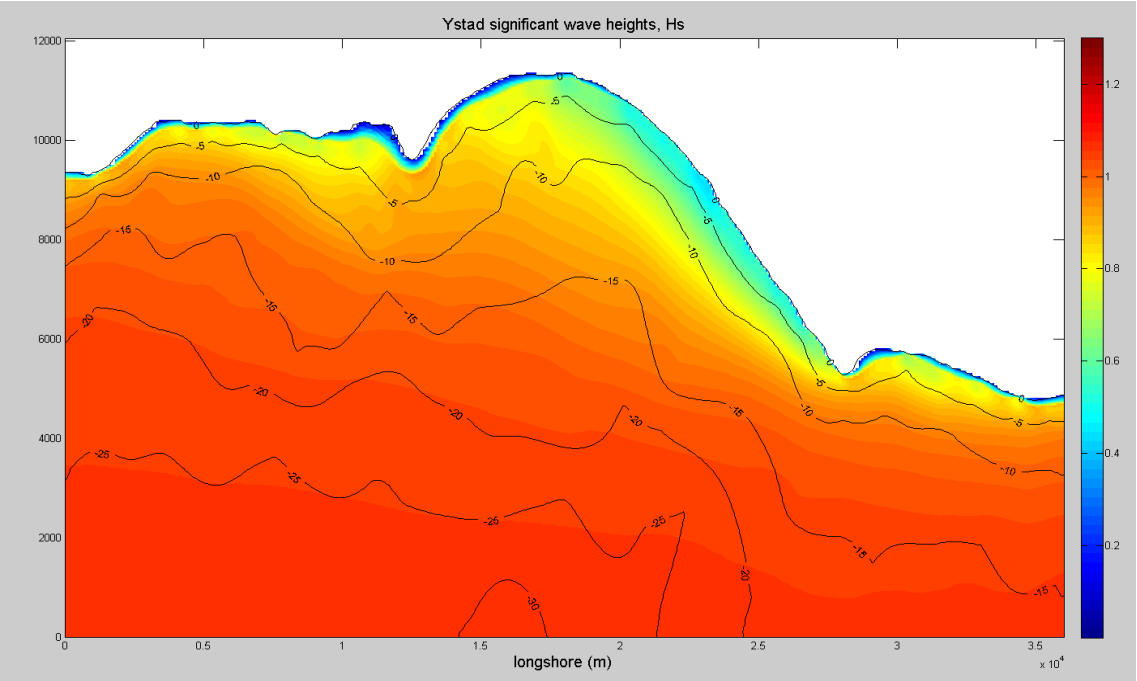

Figure B5. Scenario 4 with the initial Hs=1.07m at offshore

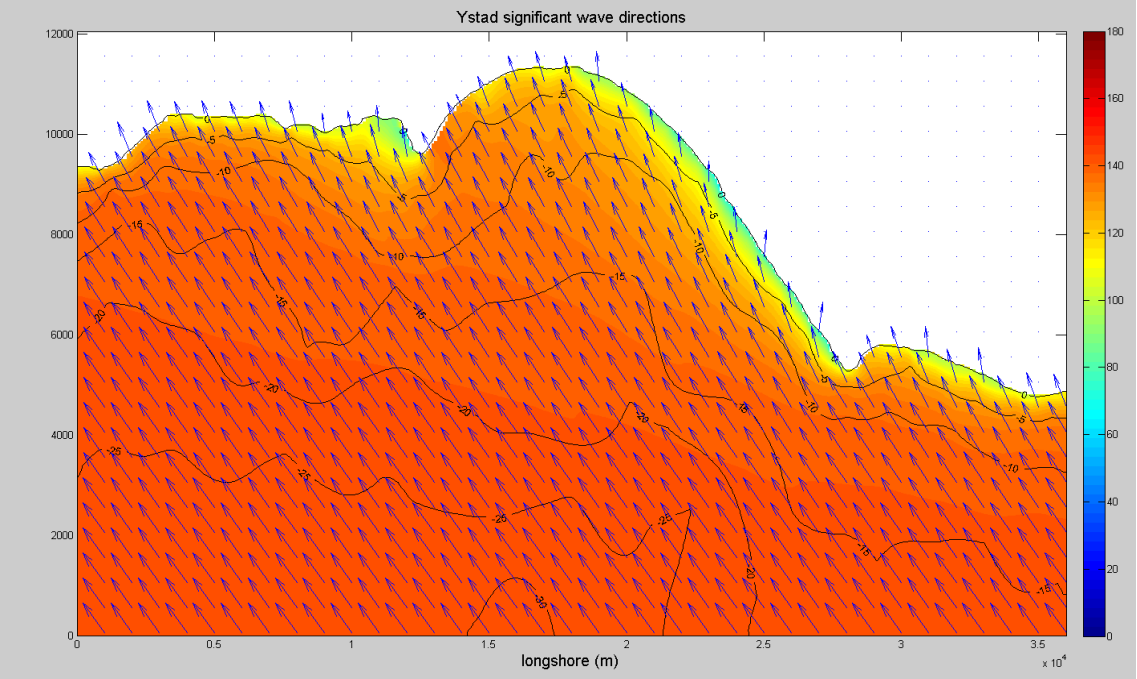

Figure B6. Wave Directions for Ystad Bay, Scenario 4 with the initial direction(θ=145 ^{0}) at offshore

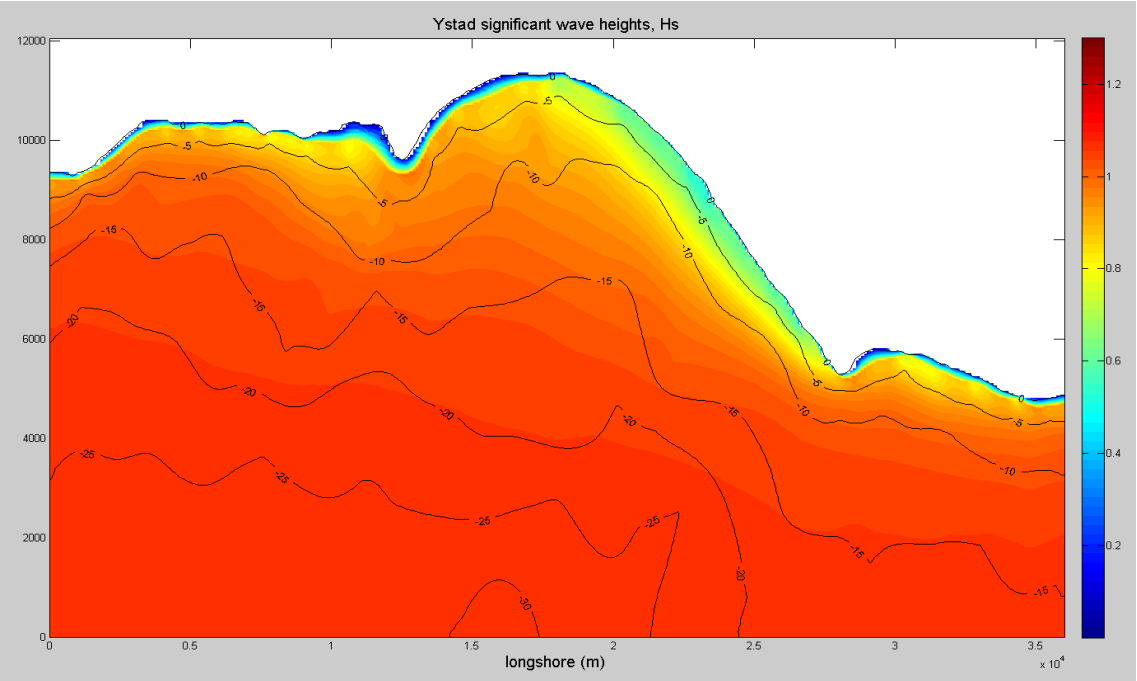

Figure B7. Scenario 5 with the initial Hs=1.07m at offshore

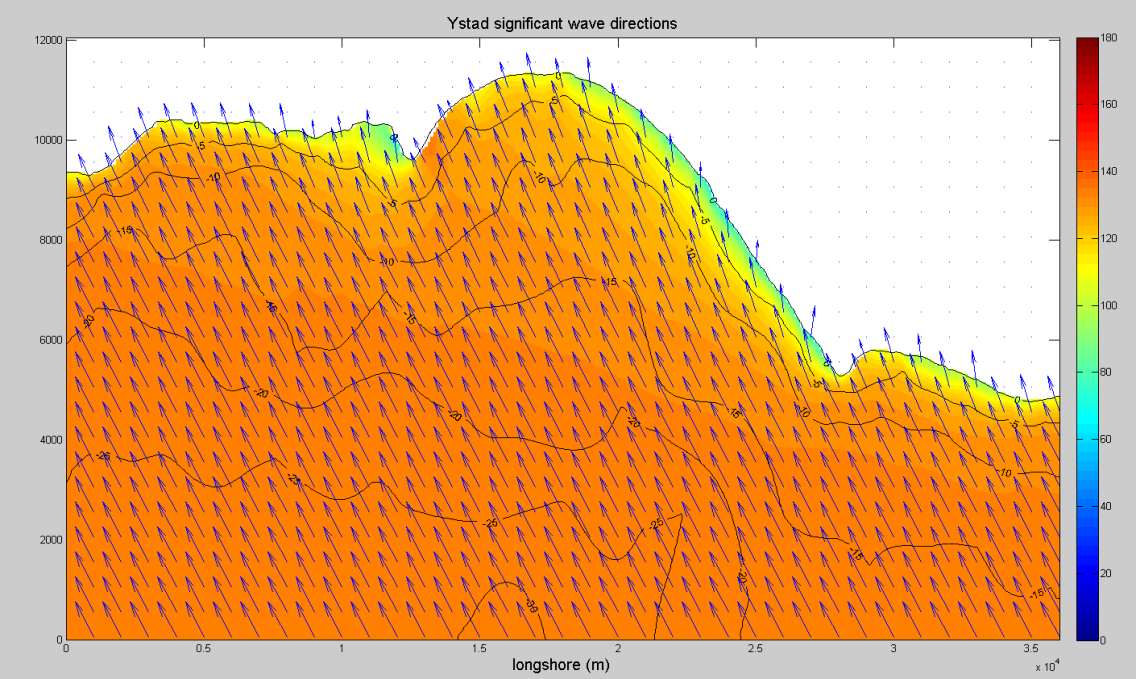

Figure B8. Wave Directions for Ystad Bay, Scenario 5 with the initial direction(θ=136 ^{0}) at offshore

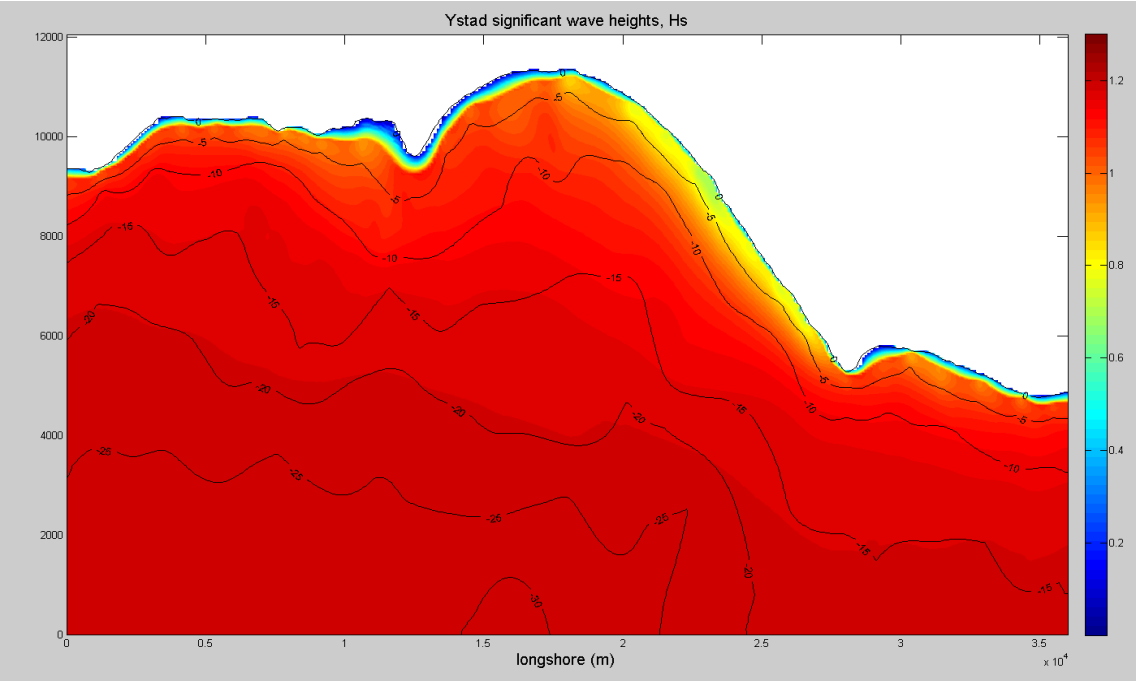

Figure B9. Scenario 6 with the initial Hs=1.19m at offshore

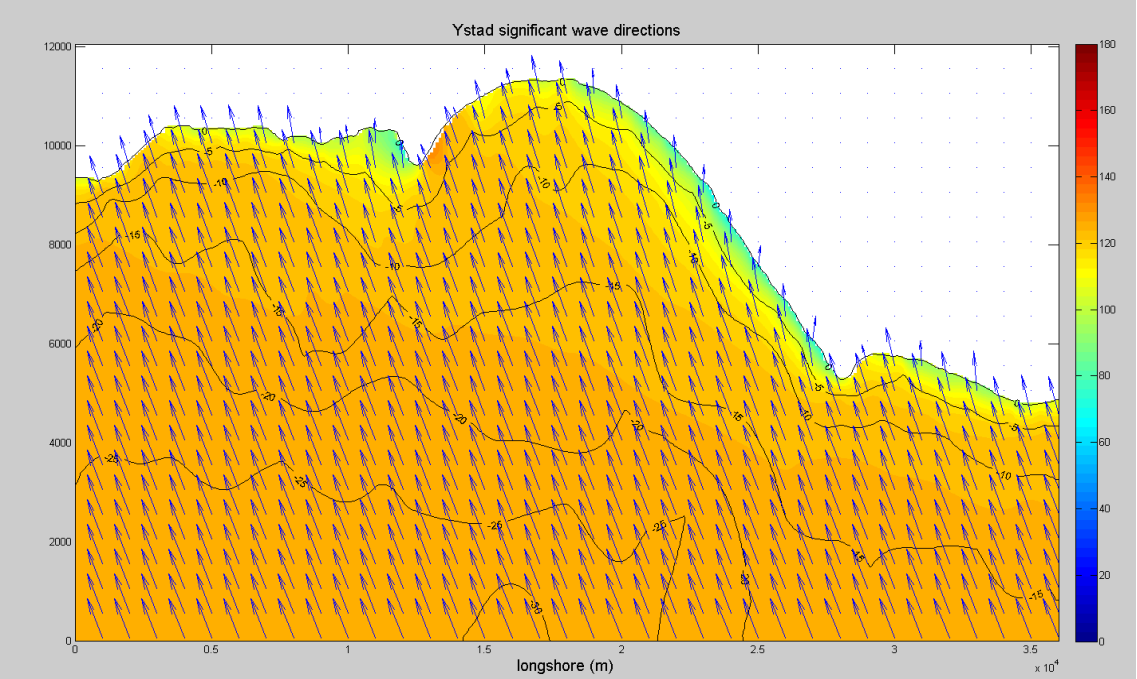

Figure B10. Wave Directions for Ystad Bay, Scenario 6 with the initial direction(θ=126 ^{0}) at offshore

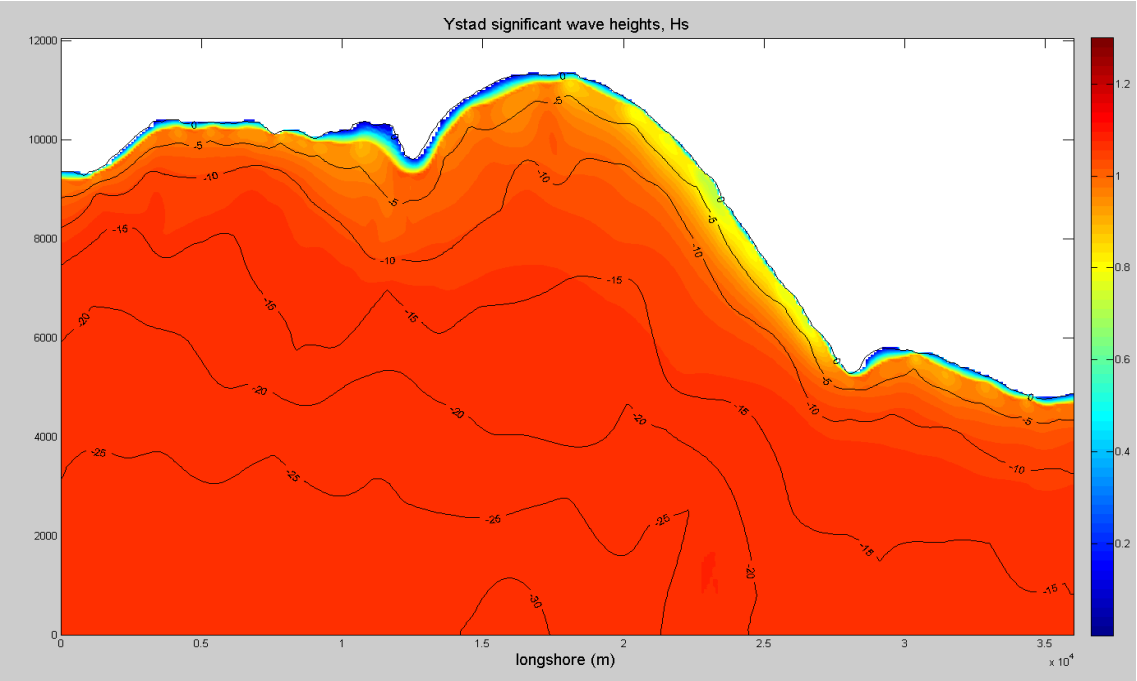

Figure B11. Scenario 7 with the initial Hs=1.08m at offshore

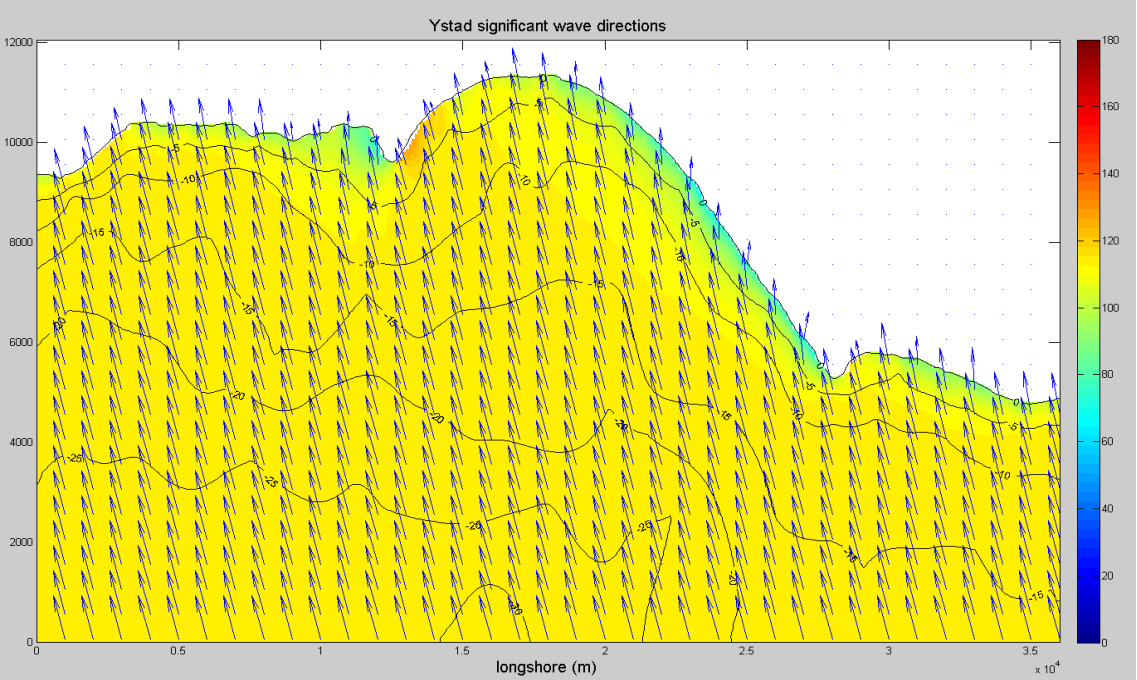

Figure B12. Wave Directions for Ystad Bay, Scenario 7 with the initial direction(θ=115 ^{0}) at offshore

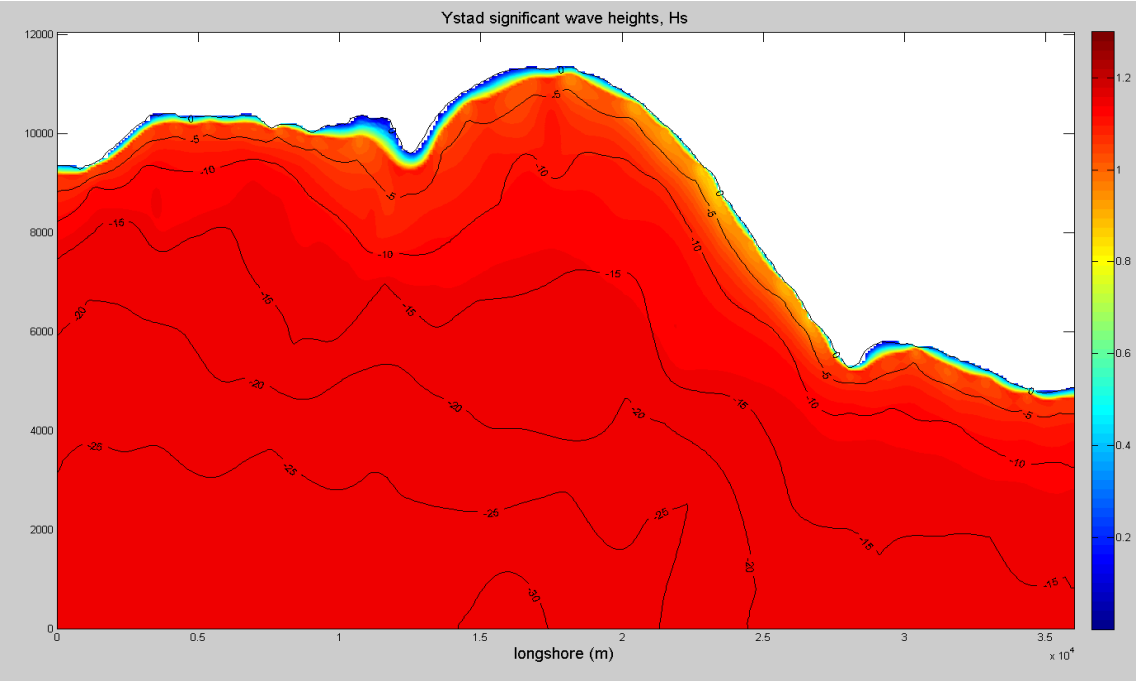

Figure B13. Scenario 8 with the initial Hs=1.16m at offshore

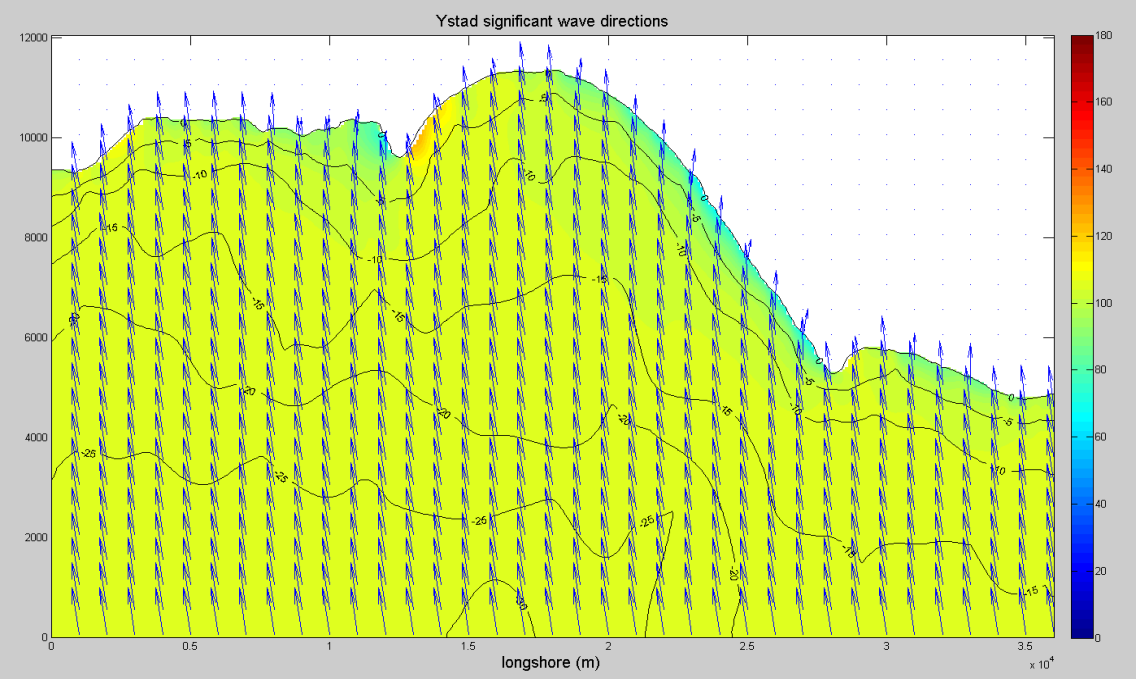

Figure B14. Wave Directions for Ystad Bay, Scenario 8 with the initial direction(θ=105 ^{0}) at offshore

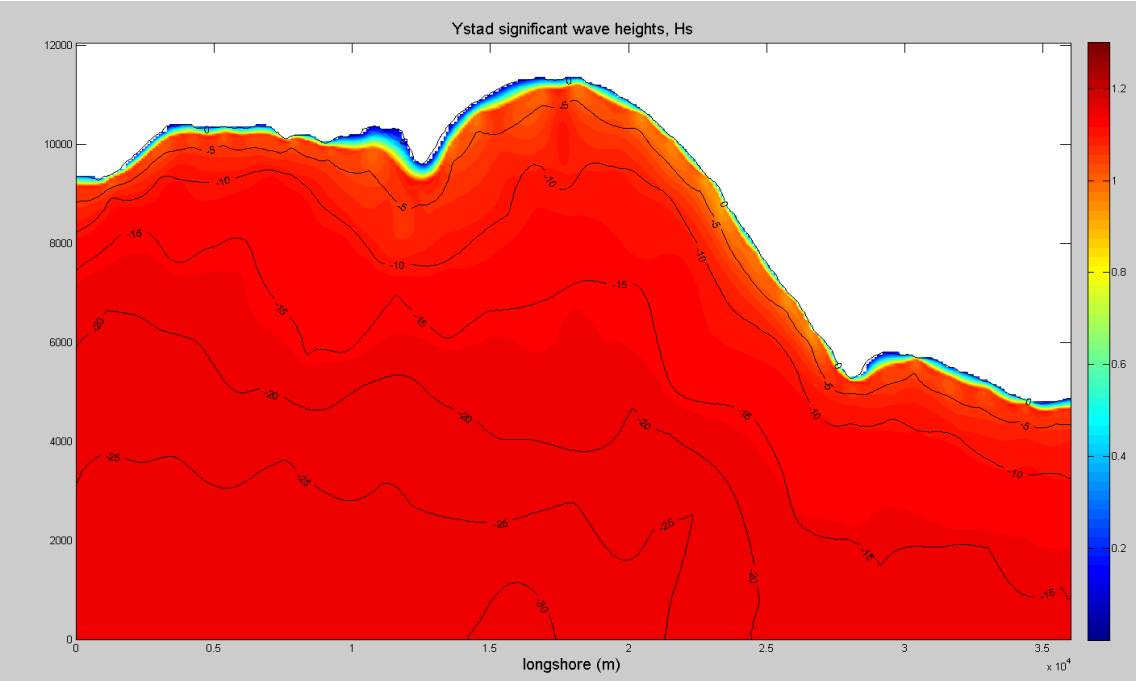

Figure B15. Scenario 9 with the initial Hs=1.15m at offshore

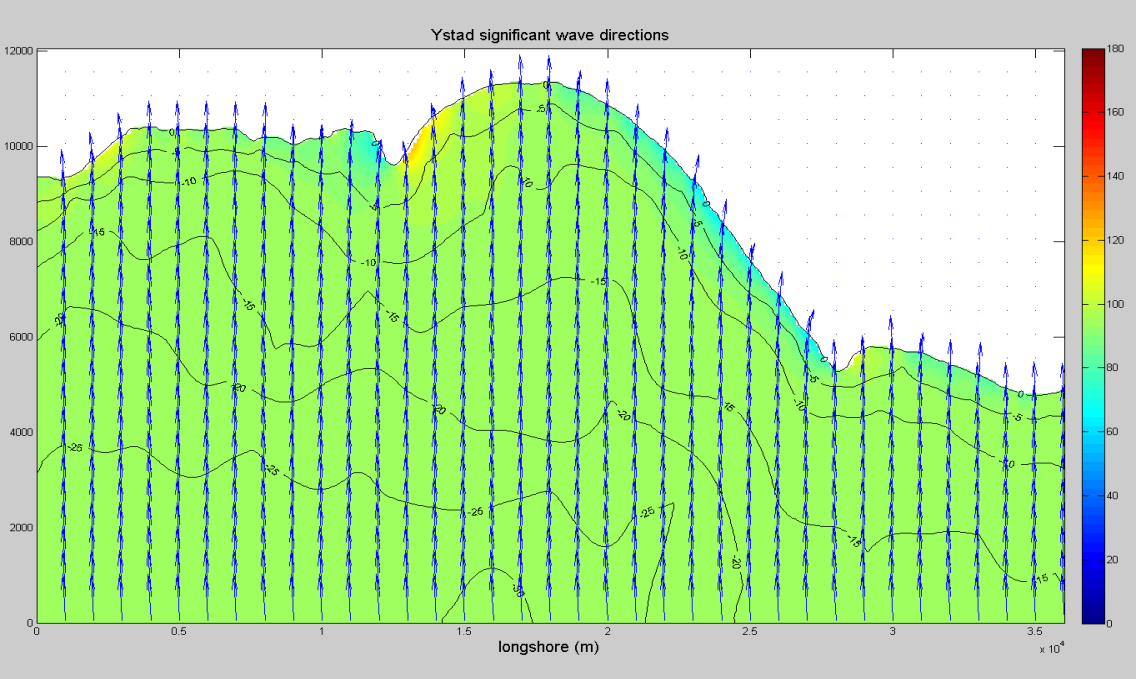

Figure B16. Wave Directions for Ystad Bay, Scenario 9 with the initial direction (θ=95 ^{0}) at offshore

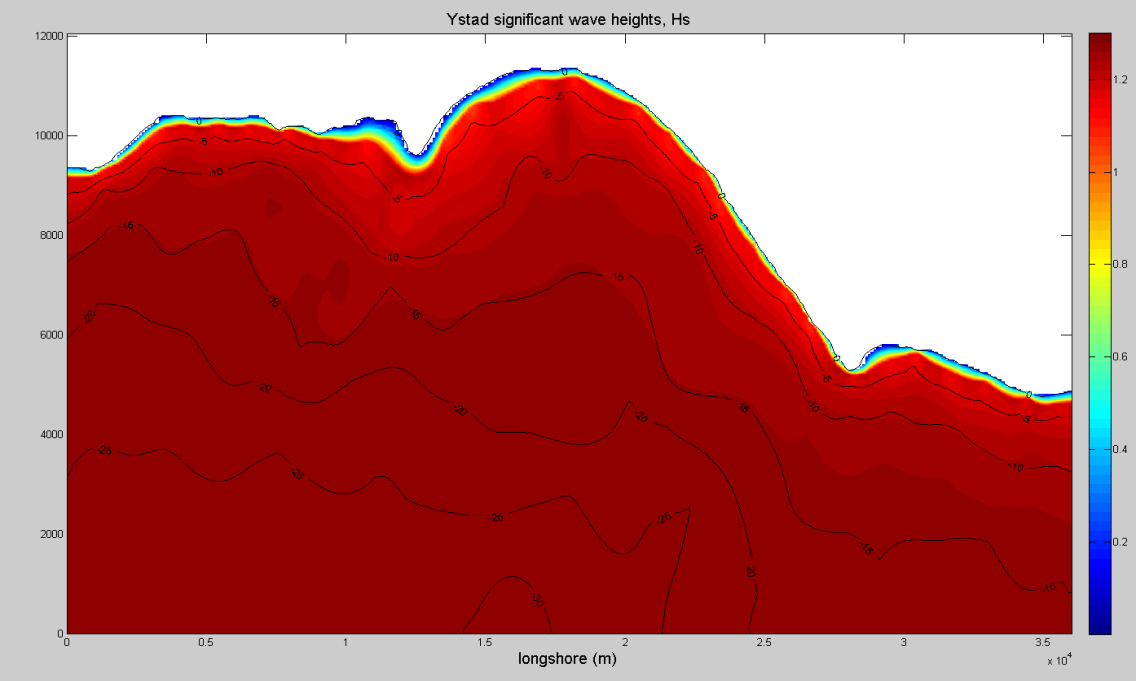

Figure B17. Scenario 10 with the initial Hs=1.28m at offshore

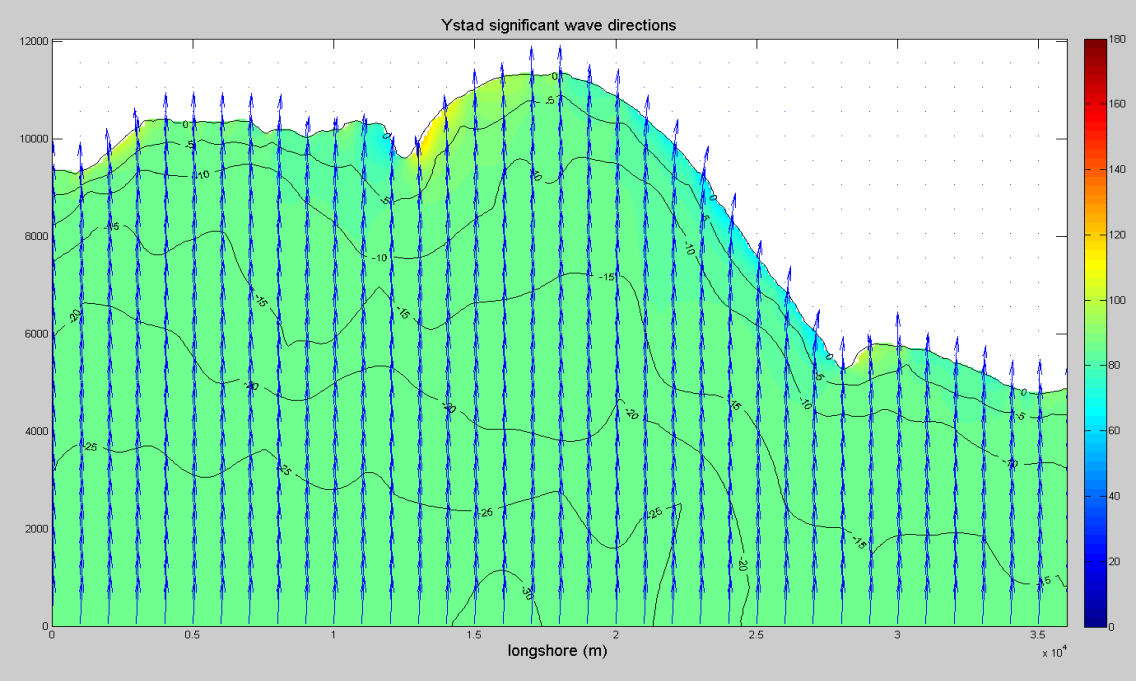

Figure B17. Scenario 10 with the initial Hs=1.28m at offshore

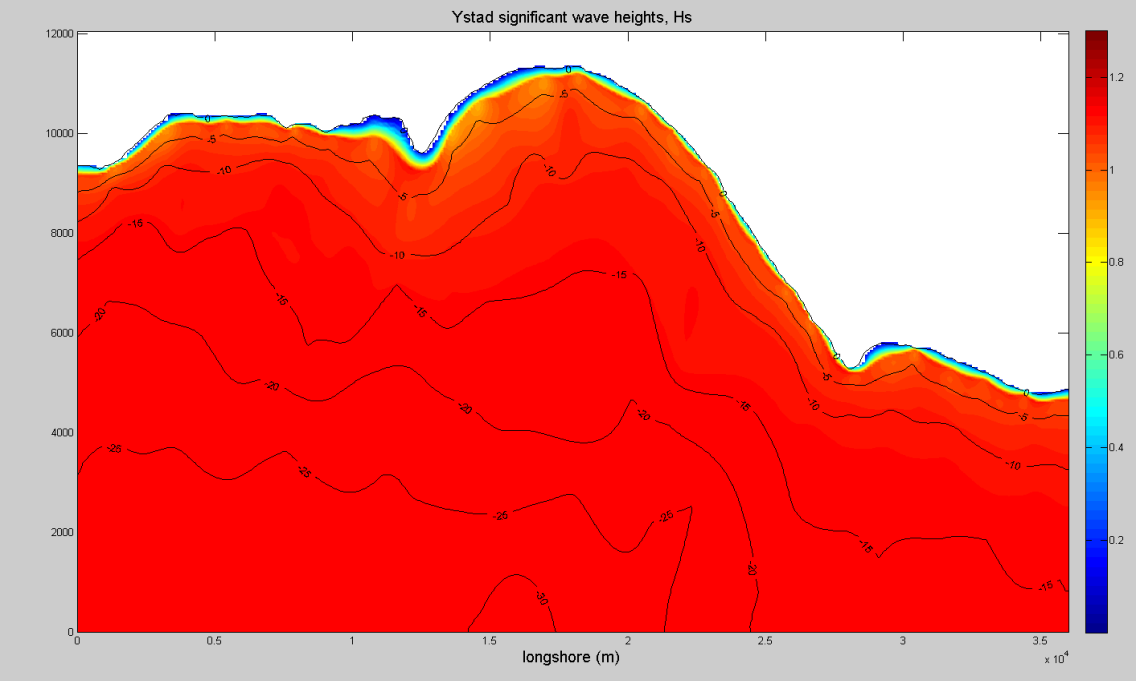

Figure B19. Scenario 11 with the initial Hs=1.14m at offshore

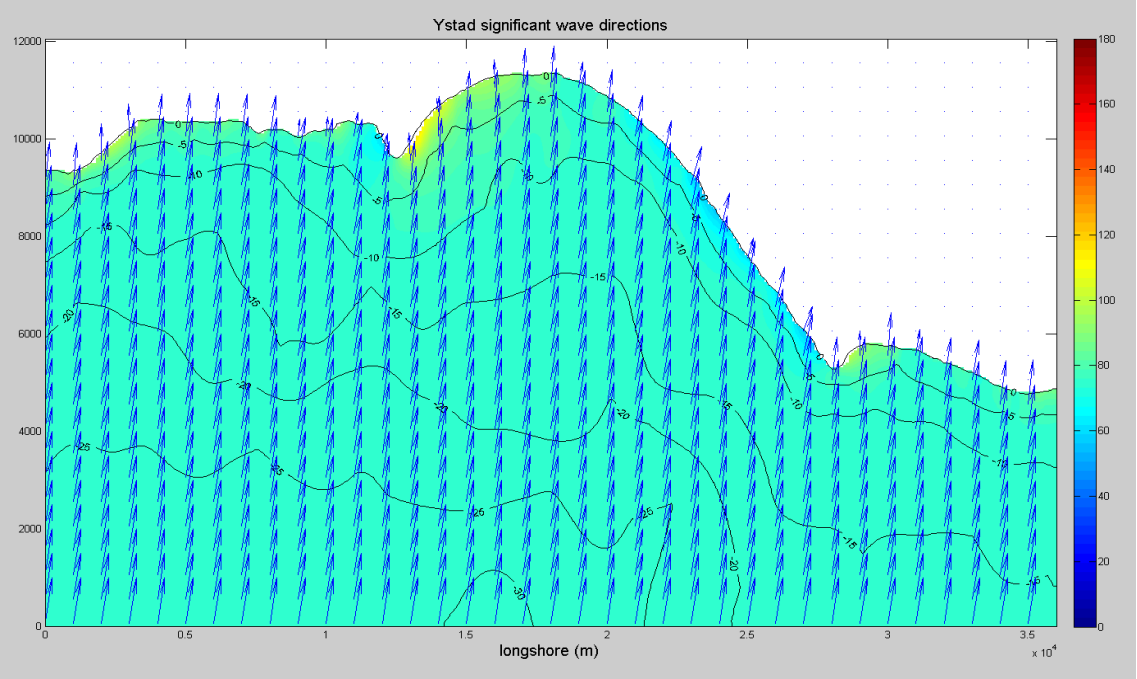

Figure B20. Wave Directions for Ystad Bay, Scenario 11 with the initial direction(θ=74 ^{0}) at offshore

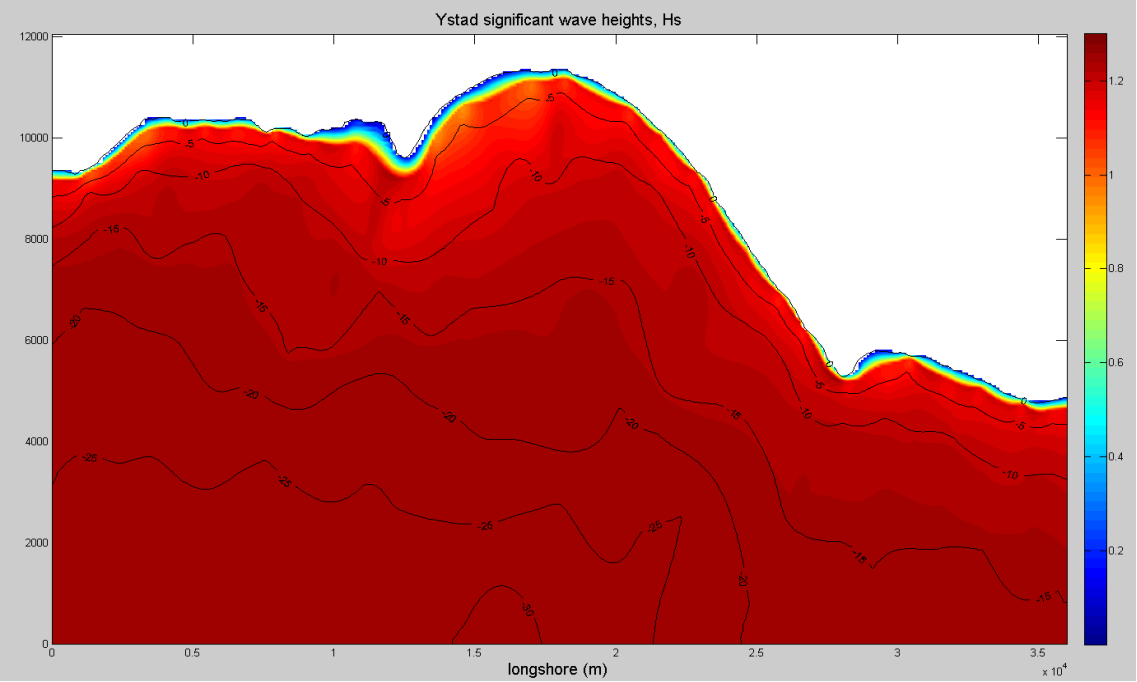

Figure B21. Scenario 12 with the initial Hs=1.26m at offshore

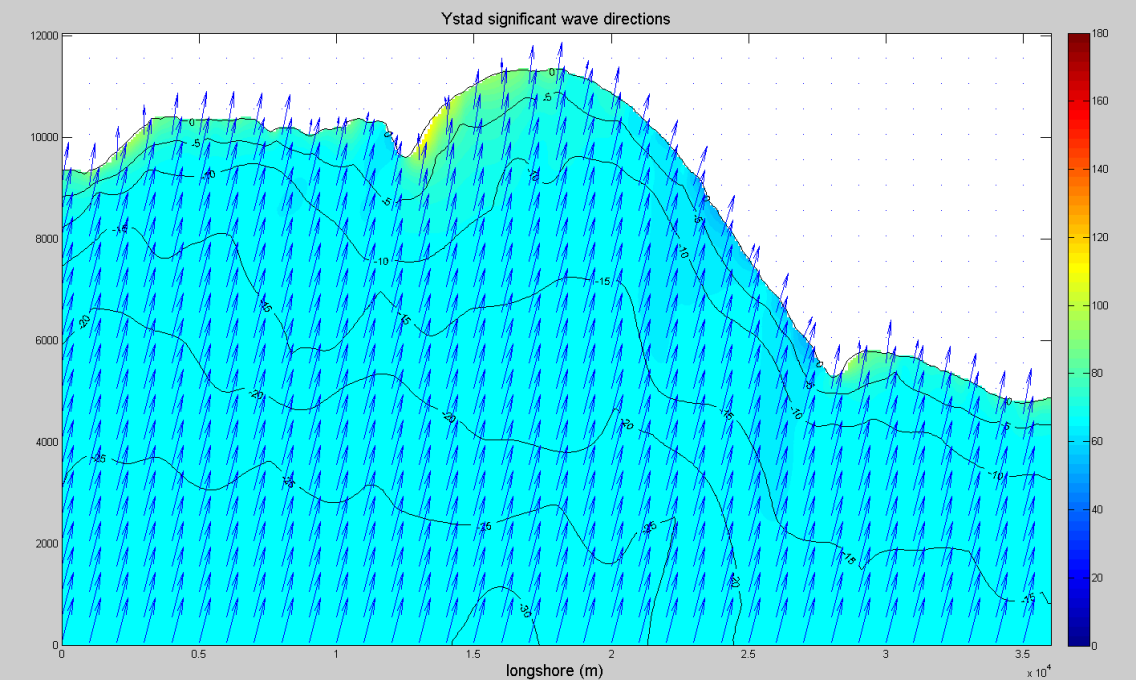

Figure B22. Wave Directions for Ystad Bay, Scenario 12 with the initial direction(θ=64 ^{0}) at offshore

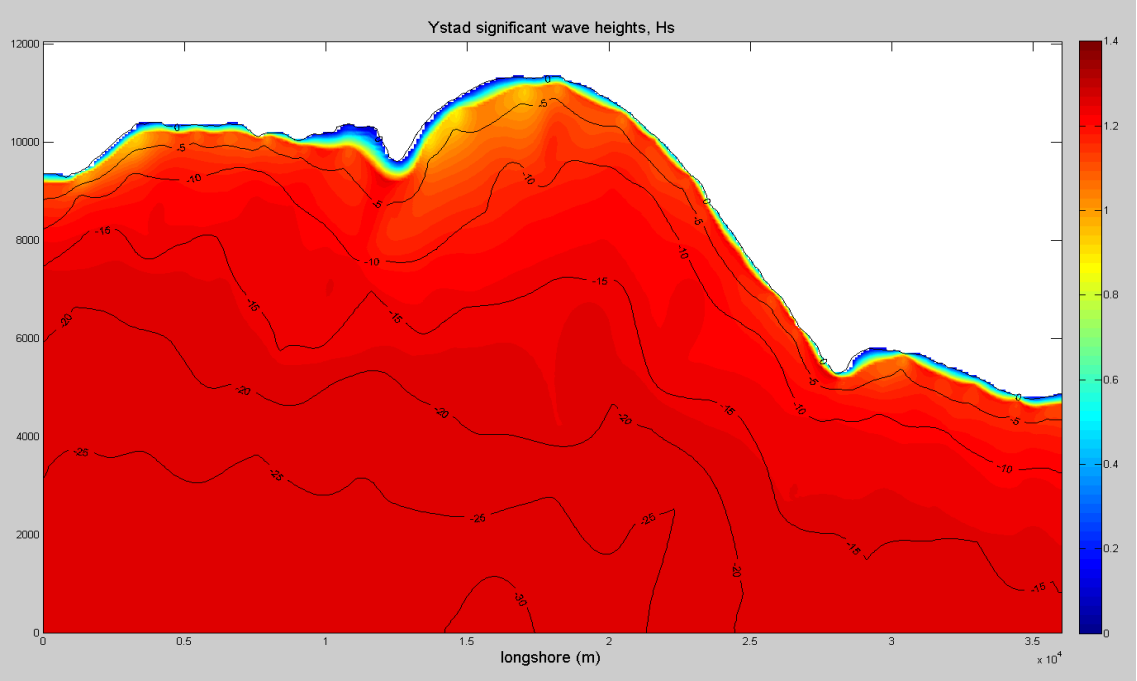

Figure B23. Scenario 13 with the initial Hs=1.27m at offshore

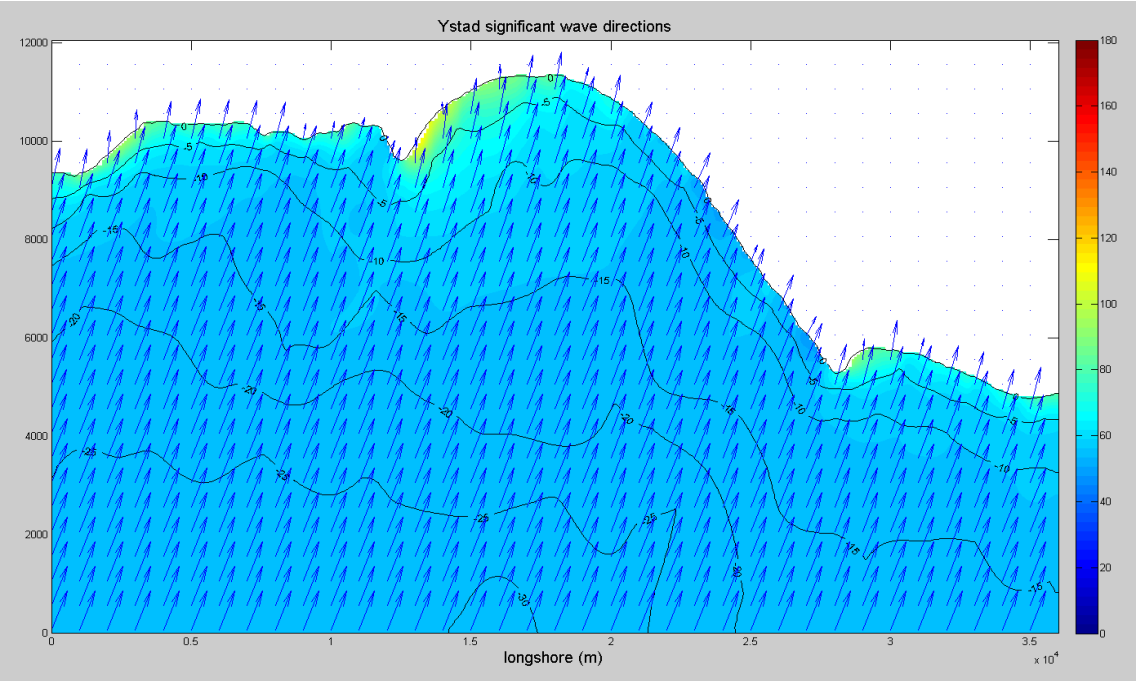

Figure B24. Wave Directions for Ystad Bay, Scenario 13 with the initial direction(θ=54 ^{0}) at offshore

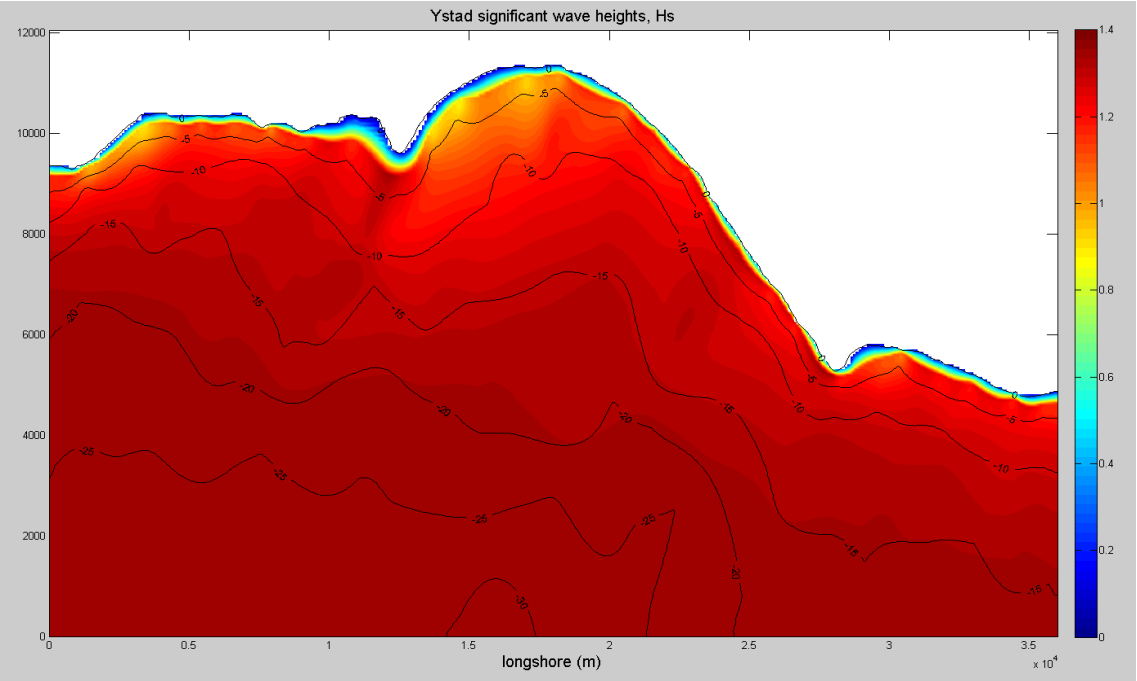

Figure B25. Scenario 14 with the initial Hs=1.36m at offshore

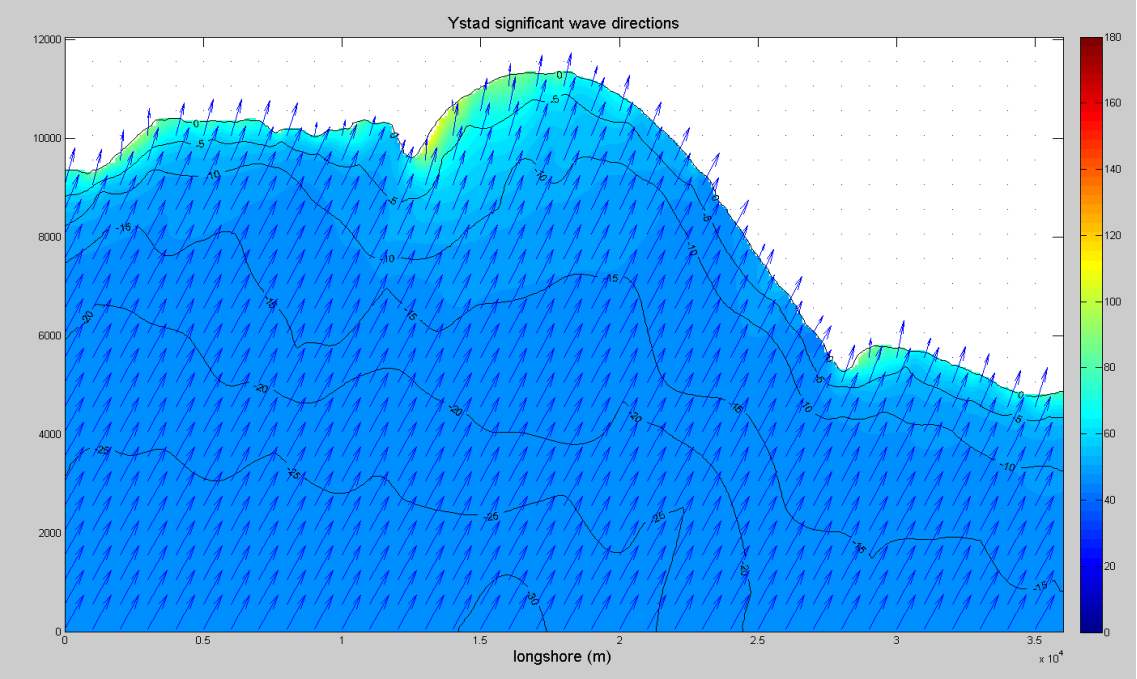

Figure B26. Wave Directions for Ystad Bay, Scenario 14 with the initial direction (θ=44 ^{0}) at offshore

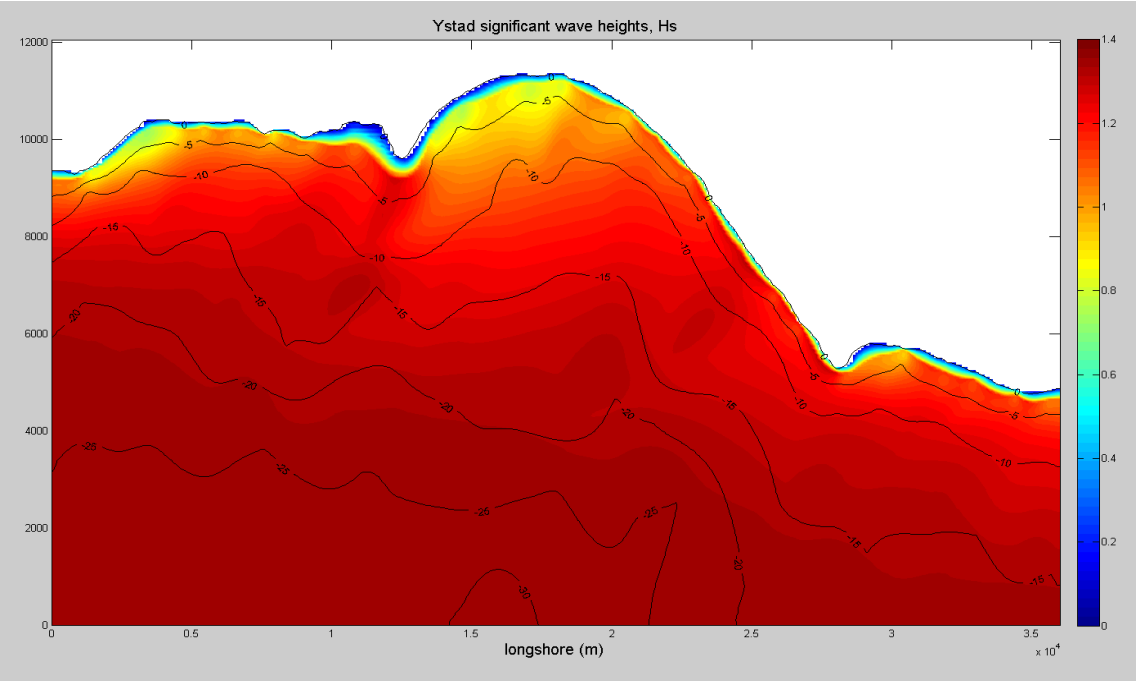

Figure B27. Scenario 16 with the initial Hs=1.36m at offshore

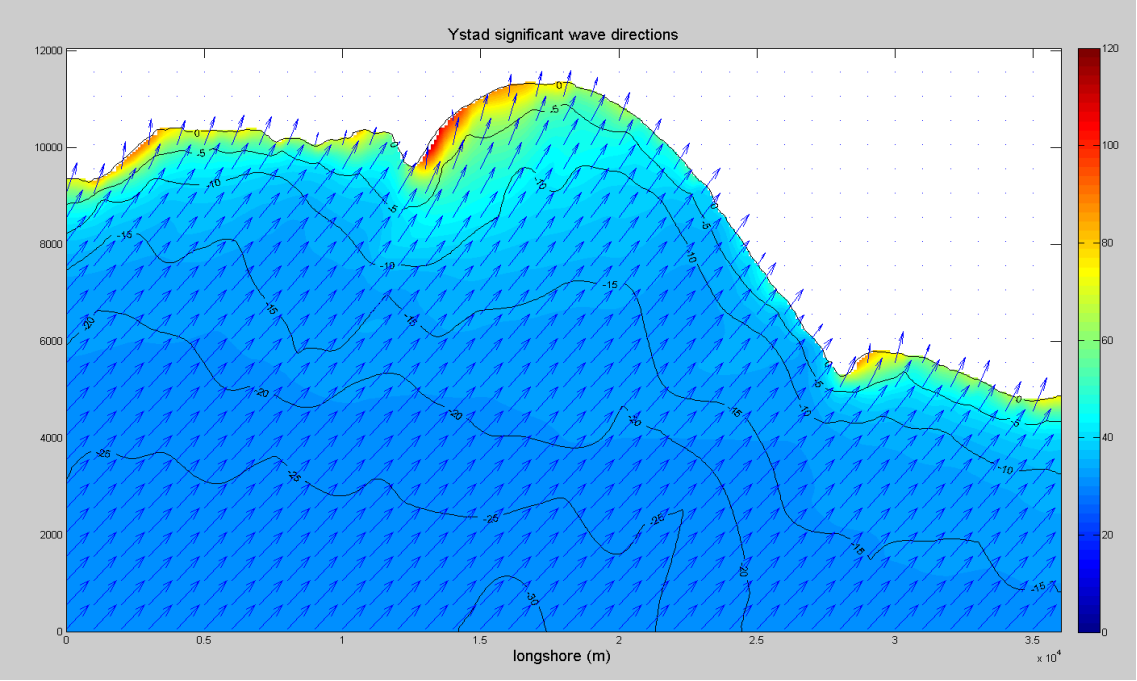

Figure B28. Wave Directions for Ystad Bay, Scenario 16 with the initial direction (θ=25 ^{0}) at offshore

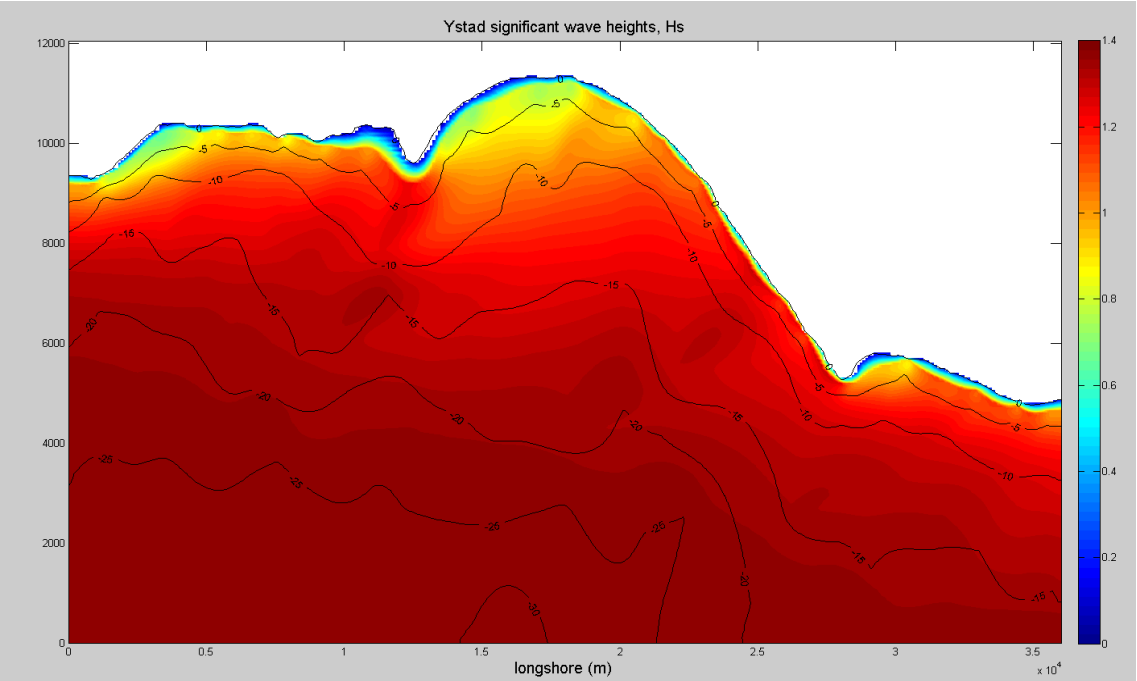

Figure B29. Scenario 17 with the initial Hs=1.38m at offshore

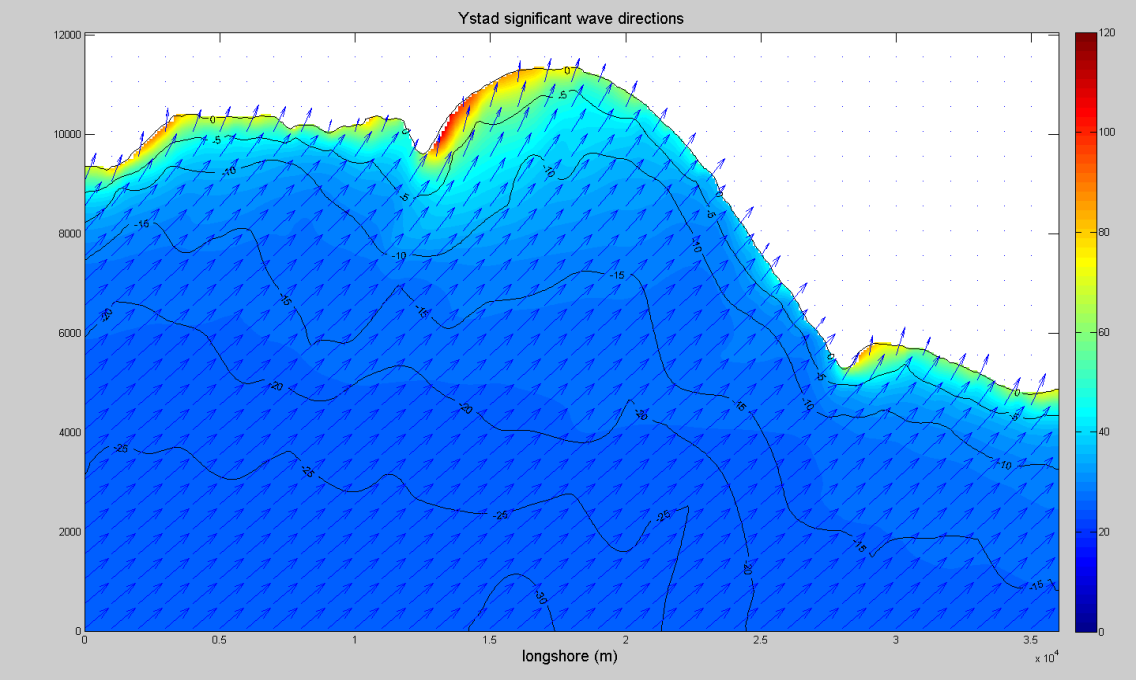

Figure B30. Wave Directions for Ystad Bay, Scenario 18 with the initial direction (θ=15 ^{0}) at offshore

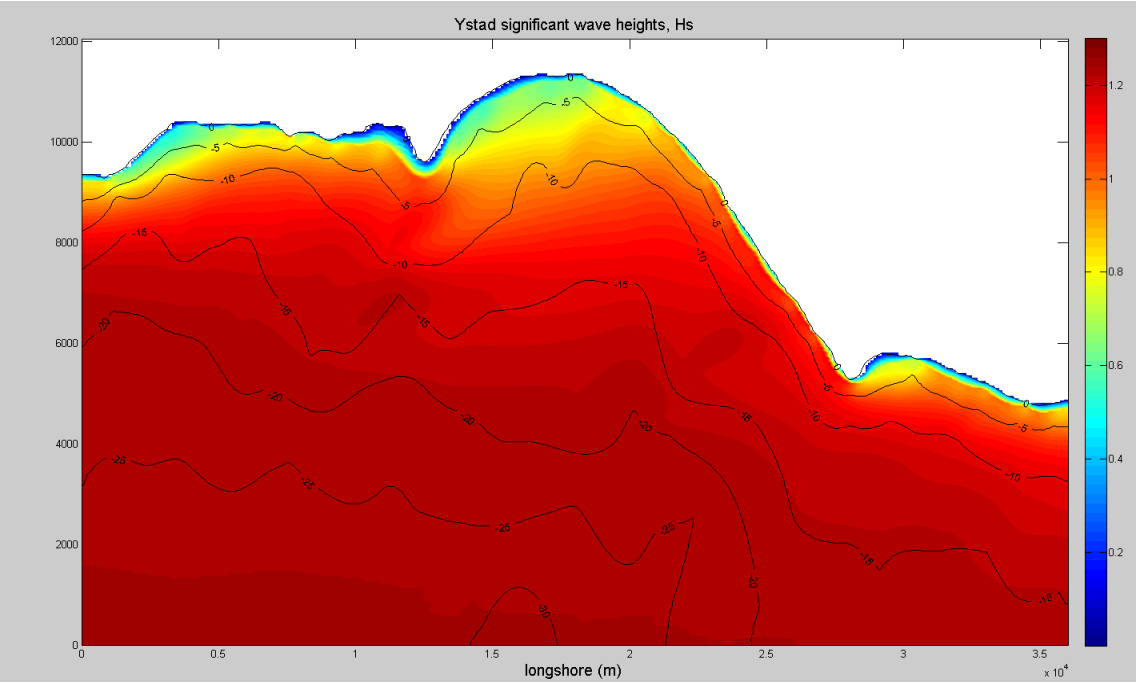

Figure B31. Scenario 18 with the initial Hs=1.24m at offshore

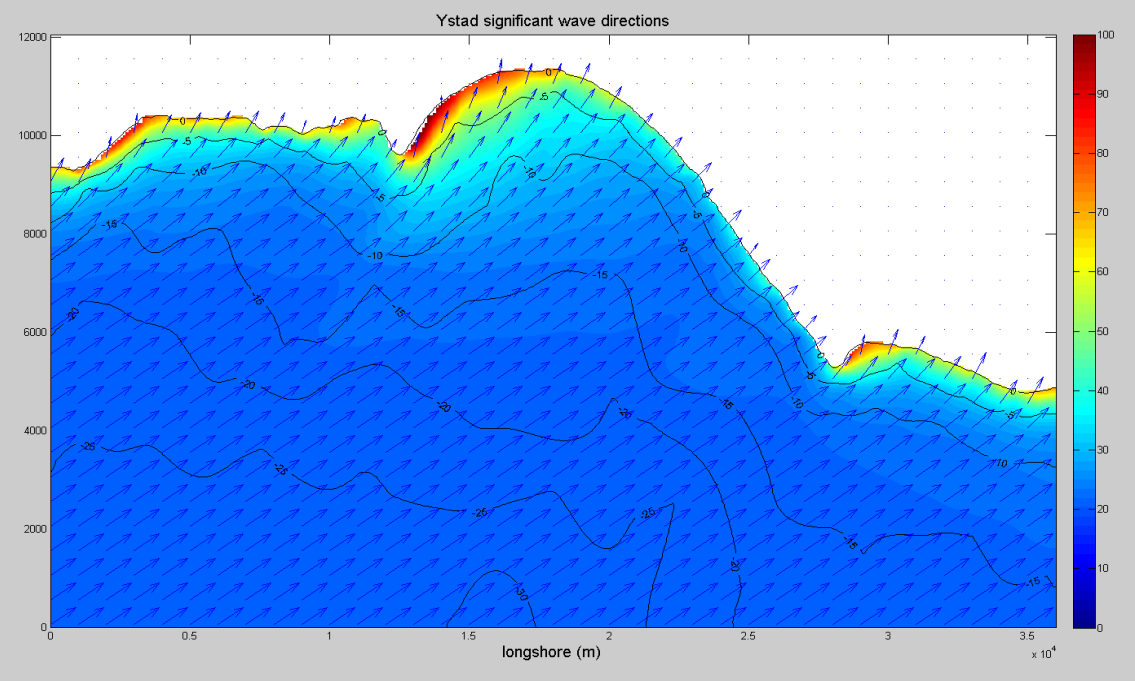

Figure B32. Wave Directions for Ystad Bay, Scenario 18 with the initial direction (θ=5 ^{0}) at offshore